TÉCNICO LISBOA

Towards nanostructured membranes for the artificial kidney

Madalena Pereira Bonifácio Lopes

Thesis to obtain the Master of Science Degree in

Chemical Engineering

Supervisors:
Prof. Dr. Vasco D.B. Bonifácio
Dr. Mónica C. Faria Besteiro

Examination Committee

Supervisor:	Dr. Mónica Faria Besteiro
Members of the Committee:	Prof. Dr. Maria Norberta de Pinho
Members of the Committee:	Dr. Nuno Rodrigues Martinho
Chairperson:	Prof. Carlos Manuel Henriques

November 2021

The work presented in this thesis was partially funded by the project PTDC/MEC-ONC/29327/2017.

Acknowledgements

Firstly, I would like to acknowledge my supervisors, Dr. Mónica Faria, Assistant Researcher in Center of Physics and Engineering of Advanced Materials (CeFEMA), an R&D unit of Instituto Superior Técnico (IST) and an invited lecturer (colaborador docente) of the Chemical Engineering department, at IST, and Prof. Dr. Vasco D. B. Bonifácio, Assistant Professor of the Bioengineering department at IST and a researcher at the Institute of Bioengineering and Biosciences (iBB) and Institute for Health and Bioeconomy (i4HB) at IST. I want to thank both for the opportunity to participate in this project, for the knowledge they gave me, for the guidance and support.

I also would like to thank my colleagues from both membrane and inorganic chemistry laboratory in IST, for all the laboratory guidance and partnership. A special thanks to Adriana Janeca and Flávia Rodrigues for introducing me to the lab and teaching me the membrane synthesis protocol and to Adriana Cruz who made my days easier.

At last, I want to thank my family for giving me this opportunity and for always being by my side. A special thank for my brother, João Pedro Lopes, and my boyfriend, João Matos, for the support, patience, for cheering me up and for the help during all the thesis phases.

Resumo

Foram desenvolvidas novas membranas para hemodiálise, híbridas monofásicas e de matriz mista de acetato de celulose (CA), funcionalizadas com ibuprofeno (IBF), para melhorar a exclusão de toxinas urémicas que se ligam a proteínas por ligação competitiva. Foram fabricadas três membranas híbridas monofásicas com combinação de técnicas de sol-gel e inversão de fases: CA95-SiO_2-$(CH_2)_3NH_2$-MR, CA90-SiO_2-$(CH_2)_3NH_2$-IBF e CA95-IBF-SiO_2-$(CH_2)_3NH_2$; foi também fabricada uma membrana de matriz mista com o dendrímero de poliureia de geração 4 ($PURE_{G4}$), CA99-RB-$PURE_{G4}$, usando a inversão de fases.

Tanto os dendrímeros $PURE_{G4}$ como os precursores de sílica foram funcionalizados com IBF para posterior a incorporação nas membranas de matriz mista e híbridas monofásicas. A estrutura dos novos precursores desenhados para a incorporação de IBF foi confirmada por Ressonância Magnética Nuclear e/ou espectrometria de massa.

Foram igualmente produzidas membranas de controlo, CA95-SiO_2-$(CH_2)_3NH_2$-MR e CA99-RB-$PURE_{G4}$, usando corantes em vez de IBF, de modo a obter uma prova visual da eficiência da conjugação destas moléculas (tendo o IBF como alvo) nesta estratégia de funcionalização química das membranas. Os resultados obtidos mostraram que as membranas mantiveram a coloração inicial, após serem armazenadas por 40 dias em água desionizada, não tido sido observada coloração da solução de armazenamento neste período.

As membranas híbridas monofásicas de ligação competitiva, CA90-SiO_2-$(CH_2)_3NH_2$-IBF e CA95-IBF-SiO_2-$(CH_2)_3NH_2$, foram caracterizadas por estudos de permeação. Os valores de permeabilidade hidráulica para as membranas CA90-SiO_2-$(CH_2)_3NH_2$-IBF e CA95-IBF-SiO_2-$(CH_2)_3NH_2$ de 48.1 e 27.4 $mL^{-1}\ h^{-1}\ m^{-2}\ mmHg^{-1}$, respetivamente. As duas membranas permearam totalmente o ácido úrico e demonstraram elevados coeficientes de rejeição para a BSA. O *molecular weight cut-off* para a membrana CA95-IBF-SiO_2-$(CH_2)_3NH_2$ foi maior do que para a membrana de CA pura (CA100).

Em geral, a performance das novas membranas é promissora, particularmente nas propriedades de permeação as quais revelam total permeação das toxinas urêmicas pequenas e solúveis em água e rejeição total à albumina.

Palavras-chave: membranas híbridas monofásicas; membranas de matriz mista; dendrímeros de poliureia; sol-gel; inversão de fases; ligação de competição; hemodiálise.

Abstract

Novel cellulose acetate (CA)-based monophasic hybrid and mixed matrix membranes functionalized with ibuprofen (IBF) were developed to enhance protein-bound uremic toxins (PBUTs) removal by a competitive binding strategy. Three monophasic hybrid membranes were fabricated coupling phase inversion and sol-gel technologies: CA95-SiO_2-$(CH_2)_3NH_2$-MR, CA90-SiO_2-$(CH_2)_3NH_2$-IBF and CA95-IBF-SiO_2-$(CH_2)_3NH_2$; and one mixed matrix membrane with a $PURE_{G4}$ dendrimer was fabricated using the phase inversion method: CA99-RB-$PURE_{G4}$.

A polyurea dendrimer of fourth generation ($PURE_{G4}$) and silica precursors were functionalized with IBF for further incorporation in mixed matrix membranes and monophasic hybrid membranes. The structure of the novel precursors designed for IBF incorporation was confirmed by Nuclear Magnetic Ressonance (NMR) and/or mass spectrometry.

Control membranes, CA95-SiO_2-$(CH_2)_3NH_2$-MR and CA99-RB-$PURE_{G4}$, with dyes replacing IBF molecules, were prepared to have visual proof of IBF incorporation into the polymer matrix. Results show that the monophasic hybrid and mixed matrix membranes, maintained coloration after being stored for 40 days in deionized water, and no dyes were detected in solution over this time period.

Competitive binding assays with monophasic hybrid CA90-SiO_2-$(CH_2)_3NH_2$-IBF and CA95-IBF-SiO_2-$(CH_2)_3NH_2$ membranes were characterized in terms of permeation properties. Results for CA90-SiO_2-$(CH_2)_3NH_2$-IBF and CA95-IBF-SiO_2-$(CH_2)_3NH_2$ membranes showed hydraulic permeabilities (Lp) values of 48.1 and 27.4 $mL^{-1}\,h^{-1}\,m^{-2}\,mmHg^{-1}$. The molecular weight cut-off (MWCO) for CA95-IBF-SiO_2-$(CH_2)_3NH_2$ showed an increase in average pore sizes in comparison with the pure CA membrane. Both CA90-SiO_2-$(CH_2)_3NH_2$-IBF and CA95-IBF-SiO_2-$(CH_2)_3NH_2$ membranes fully permeated uric acid, and high BSA rejection coefficients were observed (93.6% and 89.5%, respectively).

Overall, the performance of the newly developed membranes is promising, particularly in terms of permeation properties as revealed by competitive binding membranes where the total permeation to small water soluble uremic toxins and complete rejection to albumin.

Keywords: monophasic hybrid membrane; mixed matrix membranes; polyurea dendrimers; sol-gel; phase inversion; competitive binding; hemodialysis

Content

List of Figures

List of Tables

Abbreviations and Symbols

SYMBOL	DESCRIPTION
ABS	Absorbance
AK	Artificial Kidney
APTES	(3-Aminopropyl)triethoxysilane
B	Microchannel half height
BAK	Bioartificial Kidney
BSA	Bovine Serum Albumin
C	Concentration
CA	Cellulose Acetate
CKD	Chronical Kkidney Ddisease
DA	Daltons
EUT_{OX}	European Uremic Toxin Work Group
$F_{REJECTION}$	Rejection coefficients
FUR	Furosemide
HD	Hemodialysis
HDF	Hemodiafiltration
HFHD	High-Fflux Hemodialysis
HSA	Human Serum Albumin
IBF	Ibuprofen
IS	Indoxyl Sulfate
L	Length
LP	Hydrulic Permeability
MMM_S	Mixed Matrix Membranes
MR	Methyl Red
MW	Molecular Weight
MWCO	Molecular Wweight Ccut-Ooff
NMR	Nuclear Magnetic Ressonance
$PBUT_S$	Protein-Bound Uremic Toxins
$_PCS$	*p*-Ccresyl Sulfate
PEG_S	Polyethylene glycol
$PURE_{G4}$	Polyurea dendrimer from of fourth generation
Q_F	Feed flowrate
Q_P	Permeate flowrate
RB	Rose -Bengal
RED	Rapid Equilibrium Dialysis
RKF	Residual Kidney Function
RRT_S OR KRT_S	Renal Rreplacement Ttherapy or Kidney Rreplacement Ttherapy
SHDMM	Single Hemodialysis Membrane Module
T	Shear Stress
TEOS	Tetraethyl orthosilicate
TMP	Transmembrane Pressure
TOC	Total Organic Carbon
TRP	Tryptophan
UT_S	Uremic Toxins
W	Width
ΔP	Pressure drop
μ	Viscosity

Table 1: Acronyms for compounds and membranes synthesized.

Description	Acronym
Synthesized Compounds	
IBF encapsulated in $PURE_{G4}$	IBF@$PURE_{G4}$
IBF conjugated to $PURE_{G4}$	IBF-$PURE_{G4}$
Rose Bengal (RB) conjugated to $PURE_{G4}$	RB-$PURE_{G4}$
Methyl Red (MR) conjugated to $PURE_{G4}$	MR-$PURE_{G4}$
IBF conjugated to TEOS	IBF-TEOS
IBF conjugated to APTES	IBF-APTES
MR conjugated to APTES	MR-APTES
Membranes	
Cellulose Acetate	CA100
Cellulose Acetate with 1% wt of RB-$PURE_{G4}$	CA99-RB-$PURE_{G4}$
Cellulose Acetate with 5% wt of silica	CA95-SiO_2-$(CH_2)_3NH_2$
Cellulose Acetate with 5% wt of silica and IBF-TEOS	CA95-IBF-SiO_2-$(CH_2)_3NH_2$
Cellulose Acetate with 10% wt of silica and IBF-APTES	CA90-SiO_2-$(CH_2)_3NH_2$-IBF
Cellulose Acetate with 5% wt of silica and MR-APTES	CA95-SiO_2-$(CH_2)_3NH_2$-MR
Membrane Sheets Size	
Small Sheet	15x28 cm
Big Sheet	15x45 cm

The membranes synthesized in this work belong to different batches, and each batch can have up to four small or two big sheets. The name given to each membrane has this information in consideration. Sheets are detailed with brackets and batches with a dot after the membrane acronym, as CA95-IBF-SiO_2-$(CH_2)_3NH_2$(*sheet*).*batch*. For example, CA95-IBF-SiO_2-$(CH_2)_3NH_2$(1).2 means cellulose acetate membrane with 5% wt of silica and IBF-TEOS, first sheet made in the second batch.

1 Introduction

Among other functions, the human kidney is responsible for removing water, toxins, drugs, and waste products present in the human blood. The gradual irreversible worsening of the renal function characterizes the chronical kidney disease (CKD) which leads to retention of these harmful compounds in the blood. CKD has a prevalence in the world between 11 and 13% [1] which resulted in 1,2 million deaths in 2017 and it is expected to increase to 2,2 and 4 million deaths in best- and worst-case scenario, respectively, by the year 2040 [2]. Even though transplantation is the best option for CKD patients, the scarcity of organ donors makes renal, or kidney, replacement therapies (RRTs or KRTs) the most used strategies for therapy [3].

Even though RRTs are the most used, the number of patients receiving them are much lower than those needing it as shown in Figure 1. The growth is continuously outpacing the capacity of RRT, defined as maintenance dialysis or kidney transplant, especially in low-income and middle-income countries because of high costs involved [4].

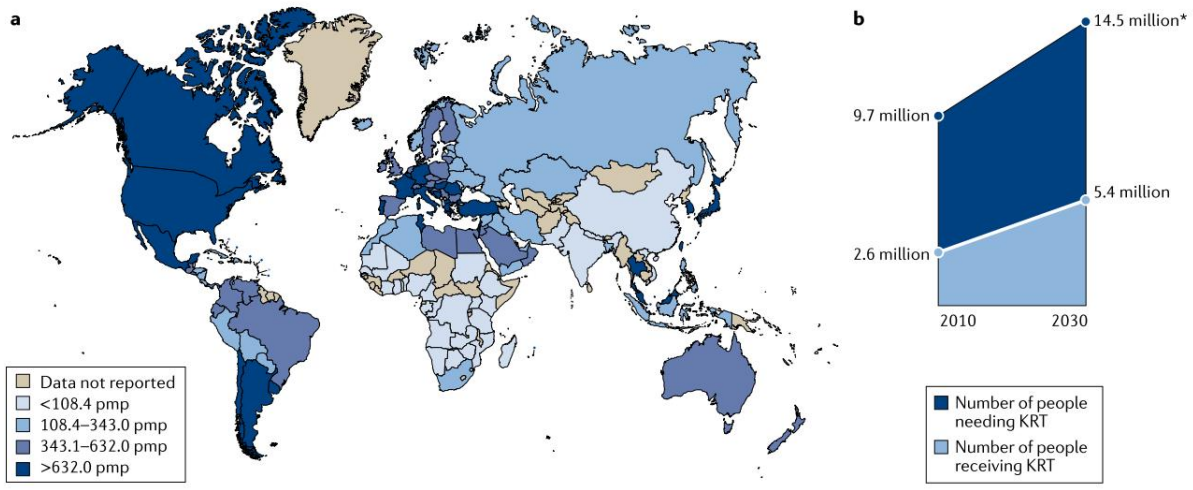

Figure 1: Current and projected prevalence of kidney failure requiring KRT.a) Global prevalence of chronic dialysis, and b) Estimated worldwide need and projected capacity for KRT by 2030, pmp, per million population [4].

Figure 2 shows the schematic representation of Hemodialysis (HD) which is the most widely used RRT for patients with CKD. In general, patients with CKD must travel to a specialized clinic three times a week for HD session which lasts approximately 4 h, a regimen that must continue until either transplantation or death.

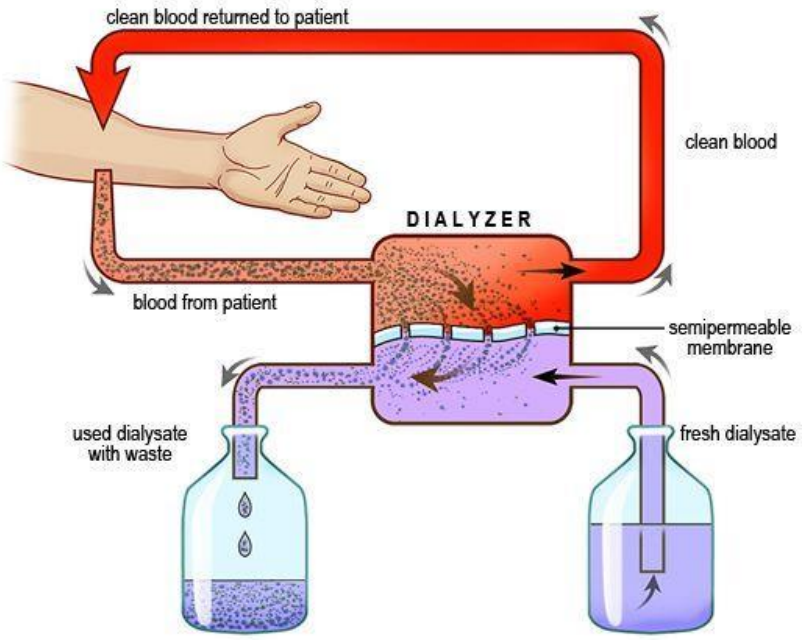

Figure 2: Schematic representation of hemodialysis.

Reproduced from: https://www.tldrpharmacy.com/content/vancomycin-dosing-in-hemodialysis

During each HD session, blood is drawn from the patient via an access device (e.g. fistula, graft, catheter) and is passed through an extracorporeal circuit where it is processed and the returned to the patient. The main component of the extracorporeal circuit is the hemodialyzer also known as the artificial kidney (AK) which is composed of semi-permeable membranes that are responsible for removing accumulated toxins and excess water while retaining vital blood components such as blood cells, platelets, and proteins. While blood flows in one direction, the dialysate flows in counter current direction. The dialysate is a solution of pure water, electrolytes, and salts such as bicarbonate, sodium and potassium, and is used to transport the waste compounds removed from the blood. Also, it maintains the electrolyte balance in patients' blood and enhances the solute removal through diffusion.

The technical and medical progress of the AK depends on two major factors: 1) hemocompatibility, and 2) enhancement of the mass transfer associated with the kidney's metabolic functions. Hemocompatibility refers to the lack of detrimental reactions between the blood and the membrane surfaces and is evaluated following the ISO 10993-4:2002 standard where 3 categories are analyzed: hemolysis, thrombosis and platelet deposition and activation [5]. Enhancement of the mass transfer implies the efficient removal of waste compounds and retention of vital blood components such as proteins, platelets, and cells. All membranes purposed for HD must ensure favorable results for these two factors.

During the first four decades after first being successfully performed by Willem Kolff [6], HD was carried out mainly by diffusion [7]. Diffusive solute removal is driven by the concentration gradient between plasma water and the dialysate and it is enhanced for small molecules that are able to cross through the membranes [8]. However, to overcome the difficulty of removing toxins with higher molecular weights led physicians and scientists to introduce convection leading to new forms of therapy known as

high-flux hemodialysis (HFHD) or hemodiafiltration (HDF). Convective solute removal occurs as a result of water flow through the membrane in response to a hydraulic pressure difference between the two sides of the membrane, process known as ultrafiltration [8]. Solutes with specific sizes and molecular weights are carried with the water and are able to pass through according to their selectivity which is intrinsically related to the pore size and thus the molecular wight cut-off (MWCO).

The European Uremic Toxin Work Group (EUTox) is a research team which focuses essentially on identifying solute retention and removal in CKD patients, and on the deleterious impact of uremic toxins (UT's) on biological systems [9]. The EUTox team classifies UTs in three main groups: small water-soluble compounds, middle molecules, and protein-bound compounds (Table 2).

Table 2: Classification of uremic toxins proposed by EUTox [3,10].

Group	MW range	Protypes	MW (Da)
Small Water-soluble Compounds	< 500 Da	Urea	60
		Creatinine	113
		Uric Acid	168
Middle Molecules	500 – 60000 Da	β_2-Microglobulin	11818
Protein Bound Compounds	< 500 Da	p-Cresyl Sulfate	31
		Indoxyl Sulfate	212

Current HD therapy ensures the efficient removal of small water-soluble compounds characterized by having molecular weights below 500 Da, such as urea, creatinine, and uric acid.

Middle molecules are characterized by having MWs between 500 to 60000 Da [11] and their retention has been linked to cardiovascular complications, such as proinflammatory events, by generating endothelial dysfunction or smooth muscle cell proliferation or by enhancing coagulation. Their removal is enhanced by using high-flux hemodialyzers composed of membranes with larger pore size correlated to the quantity of plasma water removed and replaced in an equivoluminous manner [12].

The third group, the protein bound uremic toxins (PBUT's), are responsible for the most severe CKD complications such as the cardiorenal syndrome [13] and the chronic ischemic heart disease [14]. The two most studied PBUT's are indoxyl sulfate (IS) and *p*-cresyl sulfate (pCS). Levels of pCS in the human body have been highly associated with clinical symptoms of uremia, clinical diseases such as cardiovascular disease, and high hospitalization and mortality rates [12]. Furthermore, high concentrations of IS in the blood have been linked to the increase of oxidative stress, promotion of the production of free radicals, and enhanced expression of inflammatory genes leading to vascular disease and high mortality in CKD patients [15,16].

PBUT's are generally low MW compounds, usually below 500 Da, which in their free form are easily removed by commercial HD membranes. However, these molecules have high affinity towards plasma proteins, especially to human serum albumin (HSA) which has a MW of 66 kDa, so when PBUT's are bound to HSA they form large structures which cannot be removed by current HD membranes. The

two molecules, HSA and PBUTs, are linked by noncovalent bonds, therefore the binding is reversible and obeys the law of mass action where the degree of binding depends, among other things, of the association and dissociation rate constants [17]. PBUTs are, always, in dynamic equilibrium with the carrier protein and when an exogenous compound is introduced, (equation (1) which binds to the same HSA binding site as the one where the PBUT binds to, it results in lower free protein concentration, leading to a shift in dynamic equilibrium (equation (2) to provide more free protein and, consequentely, more free toxin, as per Le Chatelier's law of chemical equilibria. Equations (1), (2) and (3) are displayed below [18].

$$[Protein - Toxin] + [Drug] \leftrightarrow [Protein - Drug] + [Toxin] \quad (1)$$

$$[Protein - Toxin] \leftrightarrow [Protein] + [Toxin] \quad (2)$$

$$[Protein - Drug] \leftrightarrow [Protein] + [Drug] \quad (3)$$

In blood plasma, the fraction of IS and pCS that is bound to HSA is much higher, approximately 90%, than the free, or unbound, fraction approximately 10% of total PBUT concentration [19]. This small percentage is the fraction removed by current HD membranes consequently leaving high quantities of PBUTs circulating in the blood. These complications exemplify the importance of removing these compounds from the blood.

1.1. State of the art

Healthy kidneys clear PBUTs through a series of orchestrated active and regulated cellular processes which depend on a wide range of conditions within the kidneys, such as the composition of urinary filtrate, oxygen concentration, and neuroendocrine signaling. The lack of knowledge of this process and molecules involved makes their removal by artificial approaches arduous [3].

Countless efforts to limit the implications of PBUT retention and enhance their removal have been attempted and six major factors have been considered important: (1) maintenance of residual kidney function (RKF); (2) limitation of PBUTs generated in the colon; (3) administration of oral adsorbents; (4) use of adsorbent technology in current RRTs; (5) development of bioartificial kidney membranes and (6) infusion of HSA binding competitors [3,20].

1.1.1. Maintenance of residual kidney function (RKF)

In patients receiving RRTs, the remaining function of the kidney is referred to as the residual kidney function (RKF) and maintaining RKF serves as a prevention method which has proved to be vital in keeping PBUTs retention low [21]. Numerous studies have shown that the preservation of RKF and, especially, urine production improves the tolerance and management of the water balance in HD patients and has an important contribution to improved clinical outcomes [3]. Furthermore, RKF has been associated with augmented survival in dialysis patients, possibly via preserved PBUT's clearance

[22,23]. However, difficulties and ambiguities still prevail in measuring RKF in individuals with CKD and often most of the patients end up suffering a quick and irreversible total loss of diuresis [3,24].

1.1.2. Limitation of PBUTs generated in the colon

IS and pCS are generated by intestinal bacteria from metabolism of essential amino acids such as tryptophan and tyrosine, respectively [25]. Furthermore, plasma levels of these solutes vary widely among patients with the same degree of renal insufficiency which suggests that their generation is variable and can be controlled [26]. Strategies such as diet modification and intestinal biotic therapies have been analyzed for limiting the production of these PBUTs, however these diets can be cumbersome or even undesirable because protein restriction might enhance malnourishment and the intake of fruits and vegetables as a way to increase fiber intake might result in hyperkalemia [27].

1.1.3. Use of oral absorbents and absorbent technology in current RRTs

The most studied oral absorbent used to stall CKD progression, prolong the time to HD initiation and improve general uremic symptoms experienced in CKD patients is a type of charcoal named the AST-120 [3]. Studies show that total and free levels of IS and pCS have decreased sharply when patients take the AST-120 [28-30]. There are new studies identifying other adsorbents such as DW-7202, a furan-based adsorbent which guarantees the same safety and efficacy and adds adherence and preference from patients due to texture, taste and manipulation compared to AST-120 [31]. However, further randomized clinical trials are necessary to further elucidate the effect of these adsorbents on the prognosis in dialysis patients.

Another approach using absorbent technology has been to directly incorporate absorbents in RRT devices and equipment. Usage of nanoparticles with high adsorbent affinity to PBUTs circulating in the dialysate provokes a deviation in the dynamic equilibrium described in equations (1), (2) and (3) enhancing their removal [32,33]. Direct hemoperfusion through devices containing absorbent such as hexadecyl-immobilized cellulose beads (HICB) [34] and MOF-decorated pollen adsorbents [35] have also shown promising results. Another method is the synthesis of novel mixed matrix membranes (MMMs) where absorbents are imbedded in the polymer matrix of HD membrane. Figure 3 shows an example of these hollow fiber MMMs which are generally composed of polyethersulfone/polyvinylpyrrolidone (PES/PVP) and activated carbon nanoparticles which are known to adsorb several toxins. They show promising results increasing the removal of 49% and 44% for IS and pCS, respectively, comparing with Fresenius F8HPS low flux dialyzer membranes currently used in clinical practice [36,37].

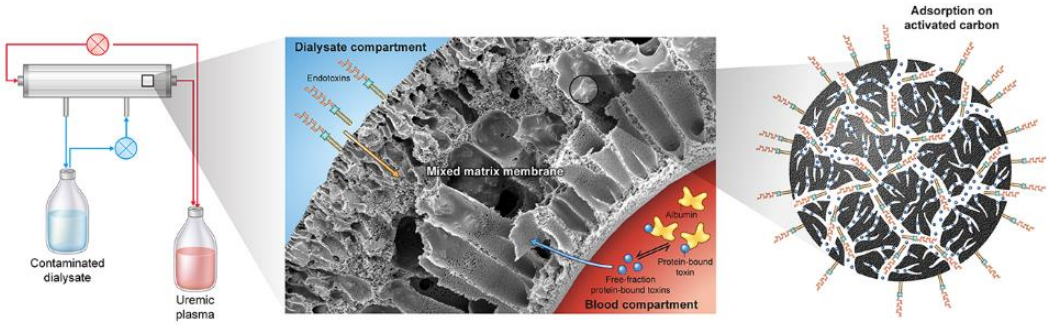

Figure 3: Mixed matrix membrane (MMM) for enhanced removal of PBUT's and endotoxins from the dialysate Reproduced from [37].

1.1.4. Development of bioartificial kidney membranes

Another approach is the development bioartificial kidney (BAK) membranes, also referred to as living membranes. The active transport of PBUTs in the natural healthy kidney is performed by specialized cellular components present in the nephrons, and a group of researchers has been trying to attach and grow these specialized cells on the active layer surface of hollow fiber membranes [20]. Figure 4 shows a recently developed BAK device with proximal tubular cells which are important in the excretion of PBUTs successfully showing attachment of these cells in hollow fiber membranes. Studies show that the BAK device was able to secrete IS in an *in vitro* perfusion system, showing the proof of concept [38,39]. This development is still in preclinical stages but already shows promising perspectives.

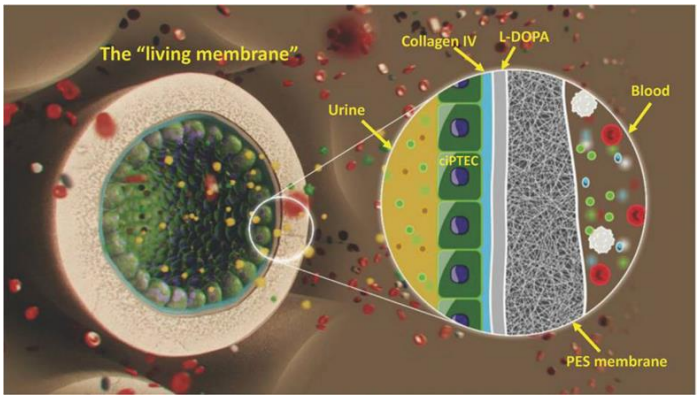

Figure 4: BAK containing kidney proximal tubular cells cultured on polymeric hollow fibers. Reproduced from [39].

1.1.5. Infusion of HSA binding competitors

HSA is the most abundant protein in human plasma, binding not only to PBUTs but also to a wide variety of molecules. Binding competition between different albumin ligands has been reported [40-42] and recent studies have proposed competitive binding as a strategy to remove PBUTs using pharmaceutical drugs as displacers [18,43].

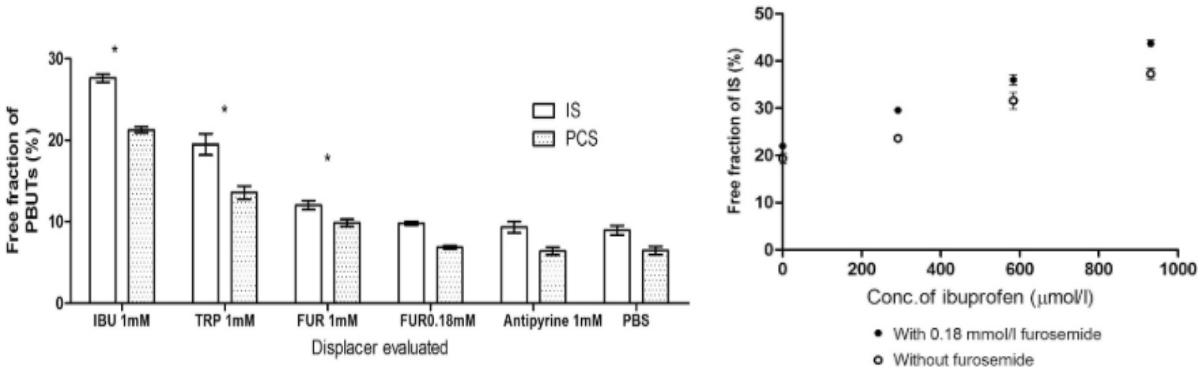

Figure 5: IS and pCS displacement in uremic plasma by furosemide (FUR), tryptophan (TRP) and IBF (left) and IBF and FUR dosage effect in IS displacement (right) both determined in static RED assays [44].

In one study [44], pharmaceutical drugs that compete with IS and pCS binding site were tested in Rapid Equilibrium Dialysis (RED) with human uremic plasma to evaluate their albumin binding with uremic toxins as depicted in Figure 5. Results show that ibuprofen (IBF) possesses the highest binding affinity among the tested displacers. The dosage of IBF followed usual prescription concentrations, being observed a higher removal for higher doses (Figure 5).

With this information, the same study also performed *ex vivo* assays in human whole blood with ibuprofen being infused upstream of the dialyzer into the blood compartment. Results show a proof of concept of enhanced PBUTs removal, particularly a 3-fold increase in IS removal, during HD by infusion of binding competitors, IBF and FUR, upstream in the dialyzer as shown in Figure 6. Also, non-protein-bound toxins, represented by urea, are not affected by the infusion.

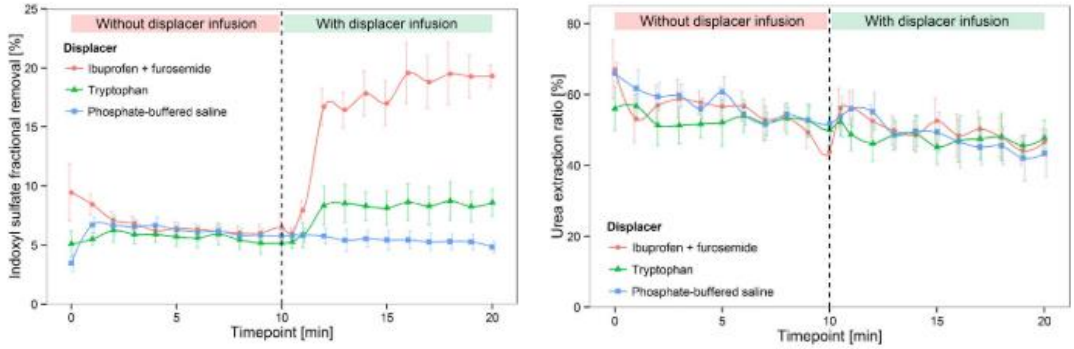

Figure 6: Human whole blood experiments with competitive binding strategy showing IS removal (left) and urea removal (right) [44].

Another clinical study [45], investigated the proof of concept to explore the utility of IBF competitive binding in patients on hemodialysis maintenance. Patients included an age group higher than 18 years old and thrice-weekly HD. The HD treatment included three phases: pre-infusion (1-20 minutes), ibuprofen infusion phase (21-40 minutes) and post-infusion (41-240 minutes). A dose of 800 mg of IBF was infused at a constant rate into the arterial bloodline. Figure 7 shows a schematic concept of the dialyzer referred in this study, where the UTs enter bounded to albumin in blood inflow and

contacts with the displacer (IBF). It was found that IBF displaced the PBUTs, allowing their removal by the dialysis membrane.

The enhanced removal of IS and pCS was effectively observed in all studied patients. The results show a 2,4-fold increase in the concentration of IS and pCS in dialysate outflow during infusion phase reflecting a good efficacy of the competitive binding strategy.

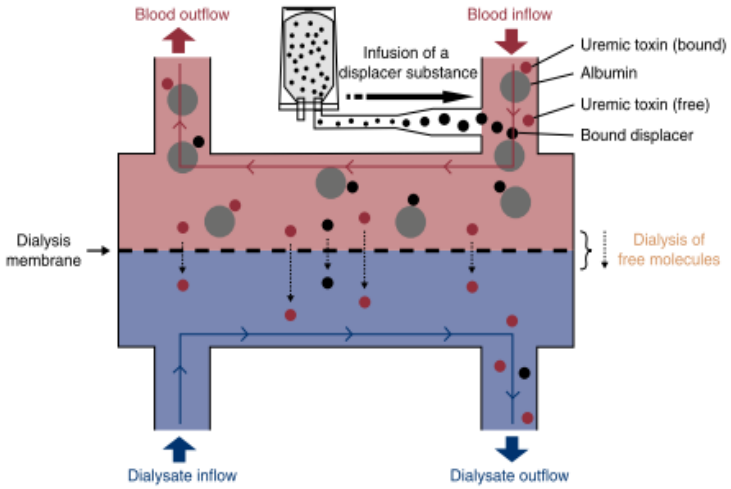

Figure 7: Schematic concept of the dialyzer used in previous work by Madero et al [45].

On another hand, IBF only competes with one of the binding sites in HSA. This could be overcome with the use of more than one drug during infusion, a solution that was analyzed by infusing a mixture of salvianolic acids in Sprague-Dawley rats for 4 h, where the first 2 h served as control. The IS and pCS removal improved by 135,6% and 272%, respectively [46]. This study highlights an important point regarding the use of a binding competitor cocktail that targets multiple binding sites on BSA, which leads to higher PBUTs removal rates during dialysis [18].

Two recent studies also compared other state-of-the-art dialysis methods, hemodiafiltration and adsorption membranes, and validated the outperformance of competitive binding with those strategies [47,48]. This also highlights the potential of combining different approaches to reach better results.

The side effects of long-term administration of pharmaceutical drugs such as IBF, furosemide (FUR) and tryptophan (TRP) are known to have detrimental effects on the patients' health, therefore preventing the administration of these drugs in high doses is highly desirable. The main objective of this thesis is to use HSA binding competitors to enhance PBUT removal without the administration of drugs into the blood circulation. The strategy relies on the direct incorporation of IBF in HD membranes, taking advantage of its high binding affinity to HSA ($2{,}7 \times 10^{6}$ M^{-1}) [18]. Figure 8 depicts the main innovation undertaken in this work when compared to previous strategies found in clinical studies. In this work, the displacer does not circulate freely in the blood, but is strategically incorporated in the surface of the HD

membrane (covalently bonded or physically entrapped), being envisioned a competitive effect without drug metabolization.

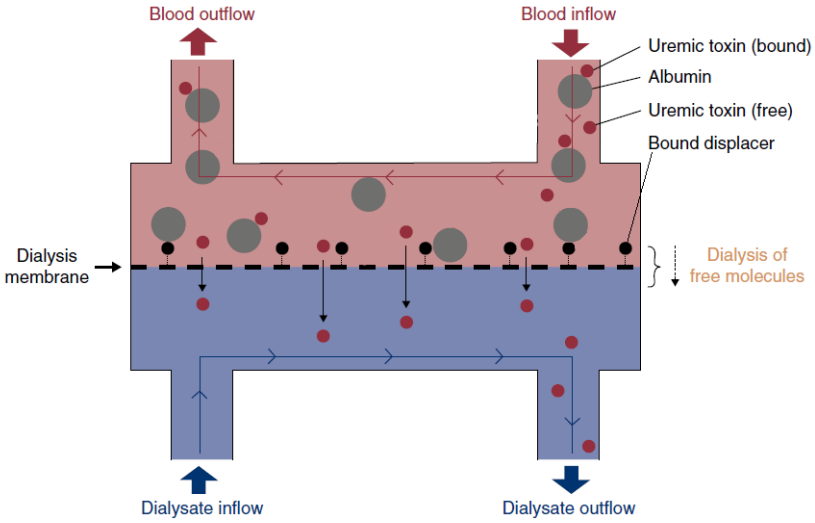

Figure 8: Displacer concept proposed in this thesis.

The HD membranes used in this work are monophasic hybrid cellulose acetate/silica (SiO_2) membranes. Cellulose is an abundant, low-cost polymer with excellent film-forming properties that after functionalization with acetate groups (acetylation) improves average pore size, hydraulic permeability (Lp) and solute removal. Moreover, the replacement of hydroxyl (OH) groups in regenerated cellulose with acetate (CH_3CO_2R) groups in cellulose acetate enhances hemocompatibility by reducing inflammation as well as other immune responses [5].

The disadvantages of using cellulose acetate include low thermal and mechanical properties as well as low shelf-life and resistance to environmental degradation. To overcome these limitations, monophasic hybrid cellulose acetate/silica membranes were developed [5,49,50]. The incorporation of silica is made by coupling phase inversion and sol-gel technologies (see section3) through silica precursors which react with hydroxyl groups present in the cellulose acetate polymer (which always remain after acetylation).

The monophasic hybrid membranes have integral asymmetric cross section structures characterized by a very thin dense active layer and a much thicker and porous layer as shown in Figure 9. The thin dense layer is responsible for the membrane selectivity and presents the highest resistance to permeation while the porous substructure confers mainly mechanical resistance.

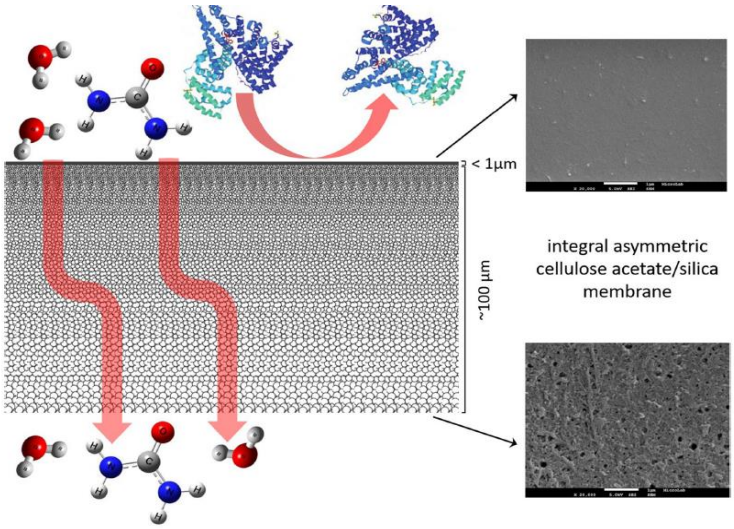

Figure 9: Monophasic hybrid cellulose acetate/silica membranes physical characterization. Reproduced from [5].

1.2. Thesis Structure

This thesis is structured in five main parts:

- Chapter 2 describes the synthesis of silica precursors.
- Chapter 3 shows the fabrication of the membranes studied and a brief discussion of the results expected and achieved is presented.
- Chapter 4 describes the characterization of the membranes fabricated in terms of permeation performance including results and discussion.
- Chapter 5 comprises the overall discussion and conclusion of this thesis and outlook of the results.
- Chapter 6 and 7 show the bibliographic references and annexes, respectively.

2 Synthesis of IBF precursors

Dendrimers are synthetic polymers with a well-defined and highly structured layered three-dimensional architecture with low polydispersity and high functionality.

The polyurea dendrimer used in this work ($PURE_{G4}$, Figure 10) is from a new family of water-soluble blue fluorescent, biocompatible and biodegradable dendrimers. The synthesis is performed in supercritical carbon dioxide by an economic, clean, simple, one-pot divergent-iterative approach [51]. They were proven to show a promising platform for IBF delivery by enhancing its solubility and by reducing its toxic effects [52] making them ideal candidates for this work.

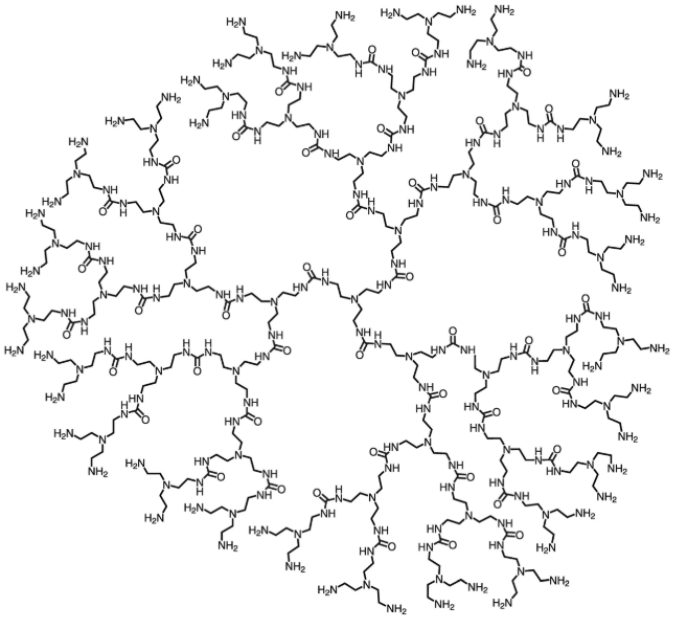

Figure 10: Polyurea dendrimer of fourth generation ($PURE_{G4}$) [51].

The main goal of this work was the incorporation of IBF in the active layer of the membranes with potential use in HD through three approaches described below.

A first approach aimed the incorporation of IBF in the membranes, using dendrimers, by two methods: i) encapsulation in a polyurea dendrimer (IBF@$PURE_{G4}$) and ii) conjugation to the surface of a polyurea dendrimer IBF-$PURE_{G4}$.

A second approach aimed IBF conjugation to the membrane matrix by a covalent linkage to silica of the precursors that are used in membrane synthesis and proven to be incorporated in the polymer matrix [49].

A third approach was designed to validate the previous approaches. Dyes were chosen as model molecules to be encapsulated/conjugated to polyurea dendrimers or incorporated in the membrane matrix, similarly to IBF. Thus, membrane coloration would provide a visual proof that IBF would be incorporated in the membranes. The chosen dyes had a carboxylic acid functional group, like IBF, thus allowing similar reactivity towards functionalization. Initially, rose bengal (RB) was chosen but

at higher pH (>10) it became colorless. Methyl Red (MR) covered all the requirements and turned out to be the best choice.

2.1. Precursors Synthesis

2.1.1. Materials

4-isobutyl-α-methylphenylacetic acid (IBF) (99%, racemic mixture) was purchased from Aldrich.

2.1.2. $PURE_{G4}$ dendrimers

Encapsulation of the ibuprofen (IBF) in a $PURE_{G4}$ dendrimer (IBF@$PURE_{G4}$).

This encapsulation followed a reported protocol [52]. $PURE_{G4}$ dendrimer (100,0 mg, 0,013 mmol) and 4-isobutyl-α-methylphenylacetic acid, 99% (50,0 mg, 0,25 mmol) were added into a glass vial with distilled water (10 mL) at room temperature (≈ 20ºC) and left 24 h under magnetic stirring. The resulting solution was stored in the fridge (4 ºC).

Conjugation of ibuprofen (IBF) with a $PURE_{G4}$ dendrimer (IBF-$PURE_{G4}$).

4-Isobutyl-α-methylphenylacetic acid, 99% (50,0 mg, 0,25 mmol), *N,N'*-dicyclohexylcarbodiimide, 99% (55,0 mg, 0,5 mmol), 1-hydroxypyrrolidine-2,5-dione (55,8 mg, 0,5 mmol) and triethylamine (46,6 mg, 0,46 mmol) were added into a glass vial with dimethyl sulfoxide (5 mL) at room temperature and stayed for 72 h under magnetic stirring. $PURE_{G4}$ dendrimers (191,4 mg, 0,025 mmol) were added to that solution and left or 24 h under magnetic stirring at room temperature. The resulting liquid was washed with water to precipitate the unreacted ibuprofen. After a filtration, the liquid was dialyzed (snakeskin membrane, MWCO 3500 Da) for 24 h under magnetic stirring at room temperature. The product was dried under vacuum (130 mbar, 60 ºC) to give 28,9 mg of a yellow oil in 12% yield.

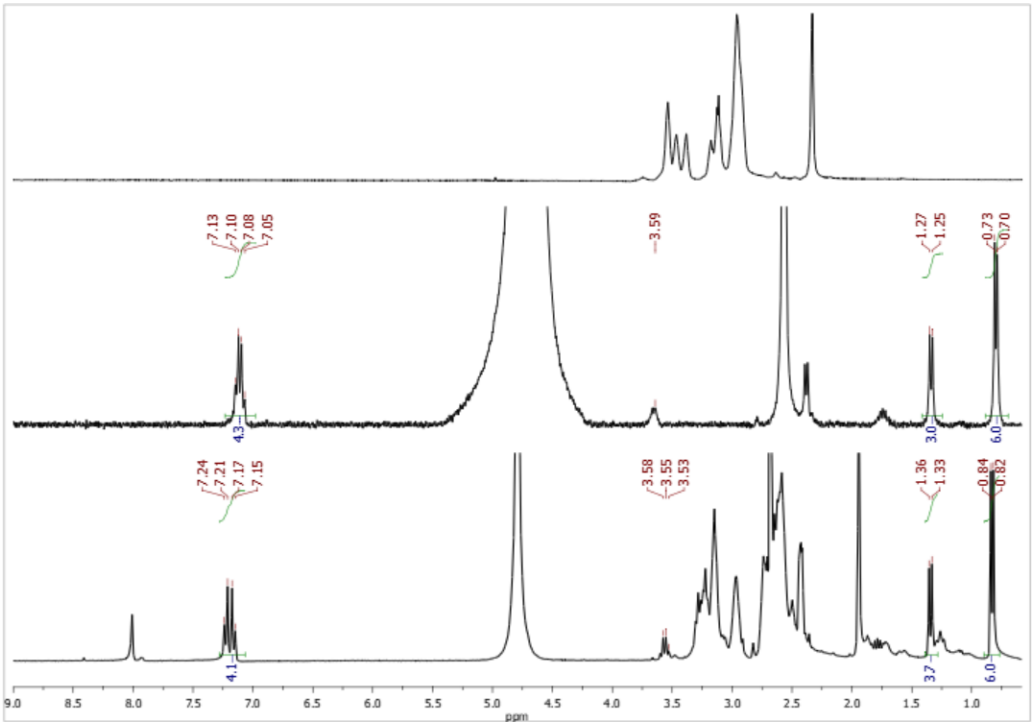

Figure 11: ^{1}H NMR spectra in D_2O of $PURE_{G4}$ (top), ibuprofen (middle) and IBF-$PURE_{G4}$ (bottom).

This conjugation followed a literature protocol [53] and was confirmed by ^{1}H NMR as shown in Figure 11. All peaks are shifted, thus evidencing the success of the reaction.

Conjugation of rose bengal (RB) with a $PURE_{G4}$ dendrimer (RB-$PURE_{G4}$).

N,N'-Dicyclohexylcarbodiimide, 99% (162,5 mg, 0,79 mmol), 1-hydroxypyrrolidine-2,5-dione (90,6 mg, 0,79 mmol) were added to a PBS solution (2 mL) with one drop of hydrochloric acid (1 M) to obtain pH= 6 that was confirmed by a pH paper indicator. This mixture was left for 15 minutes under magnetic stirring at room temperature and then rose bengal (82,5 mg, 0,085 mmol) was added and left for 2 h under magnetic stirring at same temperature. $PURE_{G4}$ (50 mg, 0,006 mmol) was dissolved in PBS with hydrochloric acid (2 mL) and added to the mixture and left for 24 h under magnetic stirring at same temperature with protection from light. The resulting product was purified by a dialysis and dried in vacuum giving 180,9 mg of a pink solid.

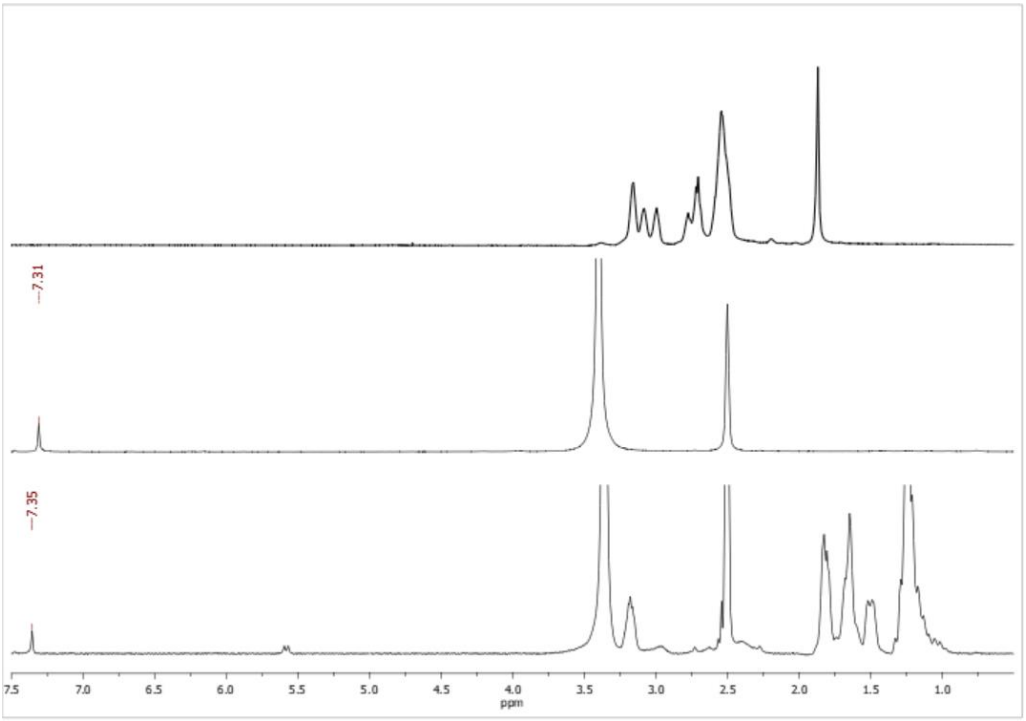

Figure 12: ^{1}H NMR spectra of PURE$_{G4}$ dendrimer in D_2O (top), and rose bengal (middle) and RB-PURE$_{G4}$ (bottom) in DMSO-*d6*.

This reaction followed the same protocol described for IBF-PURE$_{G4}$, but using RB in PBS (pH= 6). The chemical shifts observed for PURE$_{G4}$ peaks (Figure 12) cannot be fully compared because the spectra were recorded in different solvents. However, the presence of the peak from RB evidences a successful reaction.

Conjugation of methyl red (MR) with a PURE$_{G4}$ dendrimer (MR-PURE$_{G4}$).

Method 1: *N,N'*-Dicyclohexylcarbodiimide, 99% (162,5 mg, 0,79 mmol), 1-hydroxypyrrolidine-2,5-dione (90,6 mg, 0,79 mmol) were added to a PBS solution (2 mL) with one drop of hydrochloric acid (1M) to obtain pH= 6 that was confirmed by a pH paper indicator. This mixture was left for 15 minutes under magnetic stirring at room temperature and then methyl red (22,8 mg, 0,085 mmol) was added and left for 2 h under magnetic stirring at same temperature. PURE$_{G4}$ (50 mg, 0,0063 mmol) was dissolved in PBS with hydrochloric acid (2 mL) and added to the mixture and left for 24 h under magnetic stirring at same temperature with protection from light. Using this method, a complex mixture was obtained. Method 2**:** Methyl red (68,1 mg, 0,25 mmol), *N,N'*-dicyclohexylcarbodiimide, 99% (57,4 mg, 0,28 mmol), 1-hydroxypyrrolidine-2,5-dione (58,2 mg, 0,5 mmol), triethylamine (48,6 mg, 0,48 mmol) and PURE$_{G4}$ (50 mg, 0,006 mmol) were added into a glass vial with dimethyl sulfoxide (5 mL) at room temperature and stayed for 24 h under magnetic stirring. The resulting liquid was dialyzed (Snakeskin® membrane, 3500 Da) for one week under magnetic stirring at room temperature.

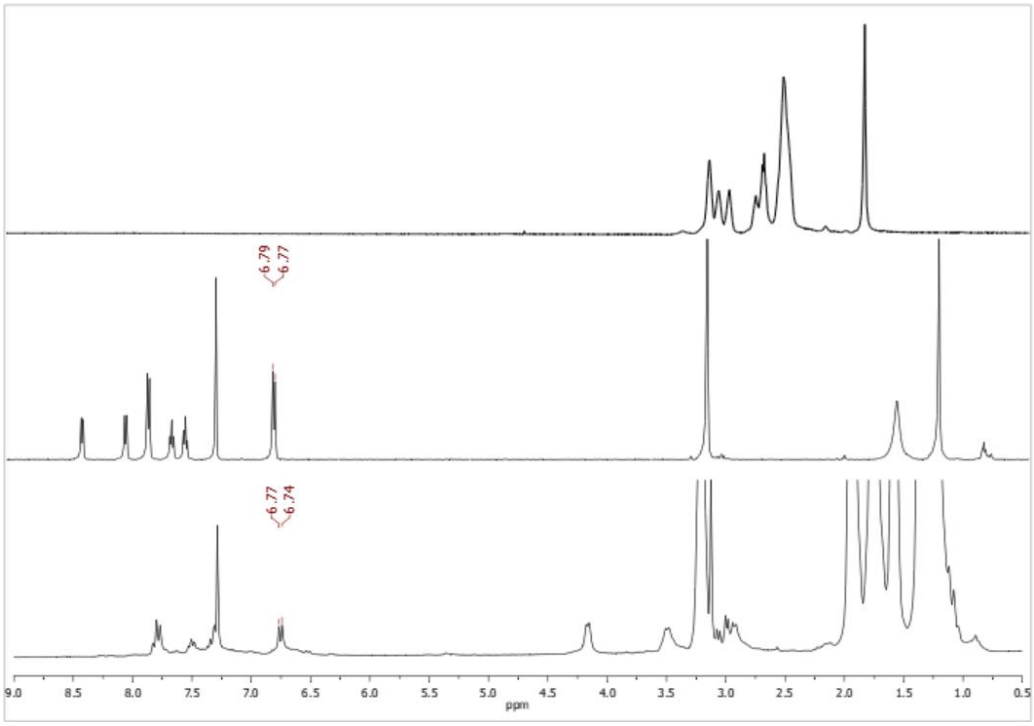

Figure 13: ^{1}H NMR spectra of $PURE_{G4}$ in D_2O (top), and methyl red (middle) and RB-$PURE_{G4}$ (bottom) in $CDCl_3$.

Method one replicated the protocol described for RB-$PURE_{G4}$, but a complex mixture was obtained. This may be attributed to the use of PBS, not adequate in this case. Following the second method the reaction occurred successful, as proofed by NMR analysis (Figure 13).

2.1.3. Silyl derivatives

Conjugation of ibuprofen (IBF) with tetraethyl orthosilicate (TEOS) (IBF-TEOS).

4-Isobutyl-α-methylphenylacetic acid, 99% (200,0 mg, 0,97 mmol), tetraethyl orthosilicate (101,0 mg, 0,48 mmol), triethylamine (49,1 mg, 0,48 mmol) and water (1 drop) were added to a glass vial in acetonitrile (1,6 mL) and left for 1h at room temperature. For crystallization, diethyl ether (3,2 mL) and *n*-hexane (1,6 mL) were added and left undisturbed for 48 h. Several washes with *n*-hexane were made to precipitate the unreacted ibuprofen. The supernatant liquid was dried in vacuum to give 252,2 mg of a colorless oil in 84% yield. MS *m/z*: 528,29 (100,0%), 529,29 (37,8%), 530,29 (6.2%), 530,30 (5,4%), 531,30 (1,2%), 531,29 (1,2%).

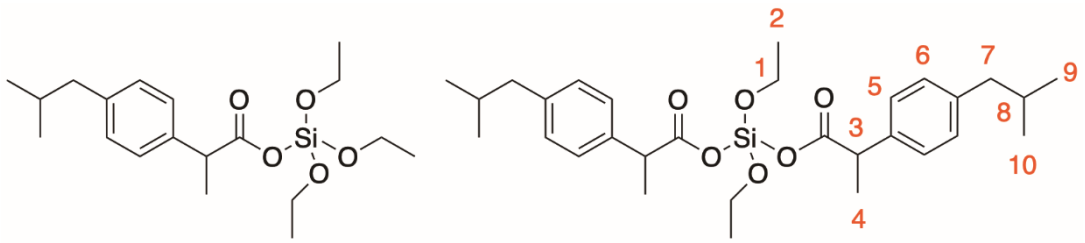

Figure 14: Chemical structure of IBF-TEOS monosubstituted (left) and disubstituted (right).

This reaction followed a literature protocol [54], but only the disubstituted product was isolated (Figure 14 and Table 3). Despite attempts using 1:1 or 2:1 IBF/TEOS ratios, monosubstitution was never achieved as confirmed by NMR and mass spectrometry data analysis.

Table 3: ^{1}H NMR peaks assignment and structural analysis for the IBF-TEOS products (mono- *versus* disubstitution).

Protons	**Chemical shift (ppm)**	**Number of hydrogens**	
		Monosubstitution	Disubstitution
1	3,8 – 3,9	6	4
2	1,1 – 1,3	9	6
3	3,6 – 3,7	1	2
4	1,4 – 1,5	3	6
5 and 6	7,0 – 7,3	2 and 2	4 and 4
7	2,4 – 2,5	2	4
8	1,8 – 1,9	1	2
9 and 10	0,9 – 1,0	3 and 3	6 and 6

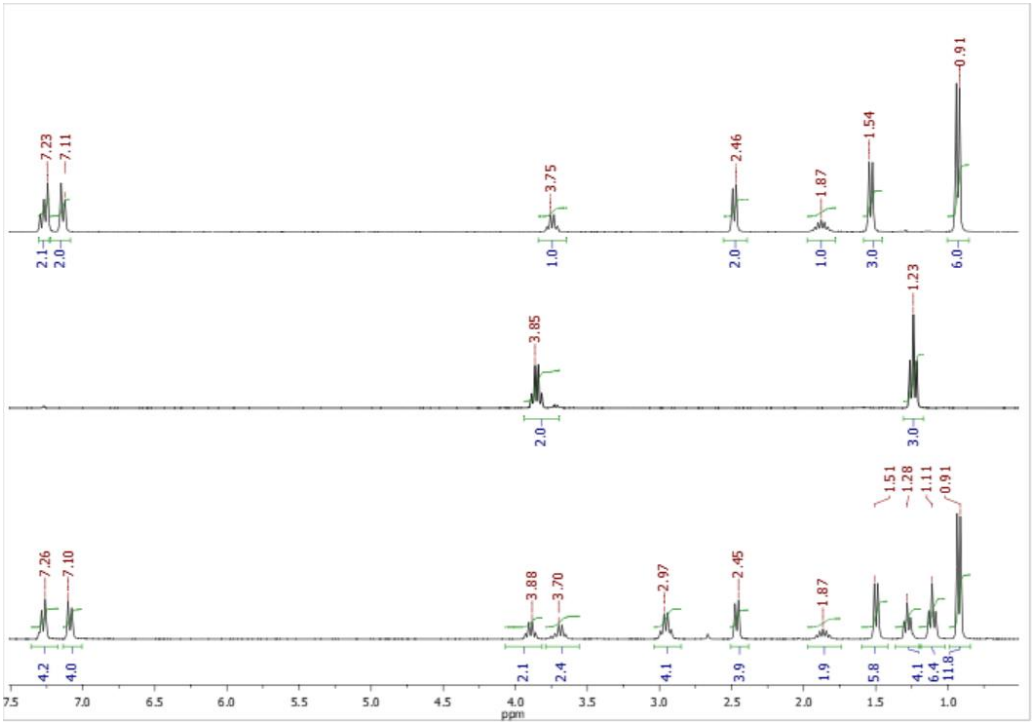

Figure 15: ^{1}H NMR spectra in $CDCl_3$ of ibuprofen (top), TEOS (middle) and IBF-TEOS (bottom).

From Table 3 and Figure 15, we can conclude that two IBF molecule are conjugated to TEOS in IBF-TEOS. This was confirmed by comparing the number of hydrogens with the corresponding peaks integration. The two peaks more shifted are closer to the carbonyl group (H-3 shifted from 3,75 to 3,70 ppm and H-4 from 1,54 to 1,51 ppm). The IBF-TEOS NMR (Figure 15, bottom) shows two-folded peaks for TEOS, for H-1 there is a peak with higher shift (δ= 2,97 ppm) which must correspond to H-2 (δ= 1,11 ppm) comparing with integration (H-4 and H-6, respectively) of hydrogens on Table 3. The other peaks (δ= 3,88 and 1,28 ppm) must correspond to unreacted TEOS, based on the observed lower chemical shifts.

Mass spectrometry also confirmed the isolation of the disubstituted product. Figure 16 predicted the MW and the *m/z* fragmentation data related to the spectrum is shown in Figure 15.

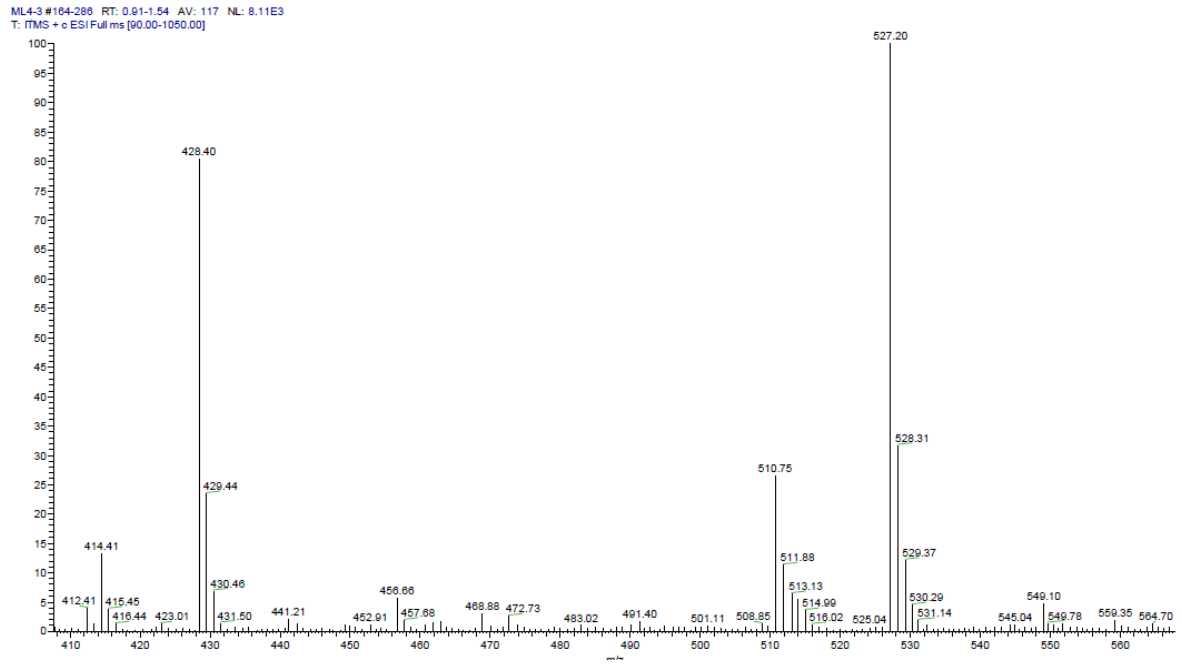

Figure 16: Mass spectrum of IBF-TEOS obtained in positive mode.

Conjugation of methyl red (MR) with (3-aminopropyl)triethoxysilane (APTES) (MR-APTES).

APTES (41,2 mg, 0,186 mmol) was added to methyl red (50,0 mg, 0,186 mmol) in 5 mL of acetonitrile**.** Dicyclohexylcarbodiimide, 99% (57,6 mg, 0,279 mmol), 1-hydroxypyrrolidine-2,5-dione (32,1 mg, 0,279 mmol) and triethylamine (28,2 mg, 0,279 mmol) were added to the mixture and left under magnetic stirring for 8 h. After this period, the mixture was filtrated to remove unreacted methyl red, and the residue was washed several times with acetonitrile. The solvent was evaporated to dryness in a rotavapor giving the product as a red-brown solid.

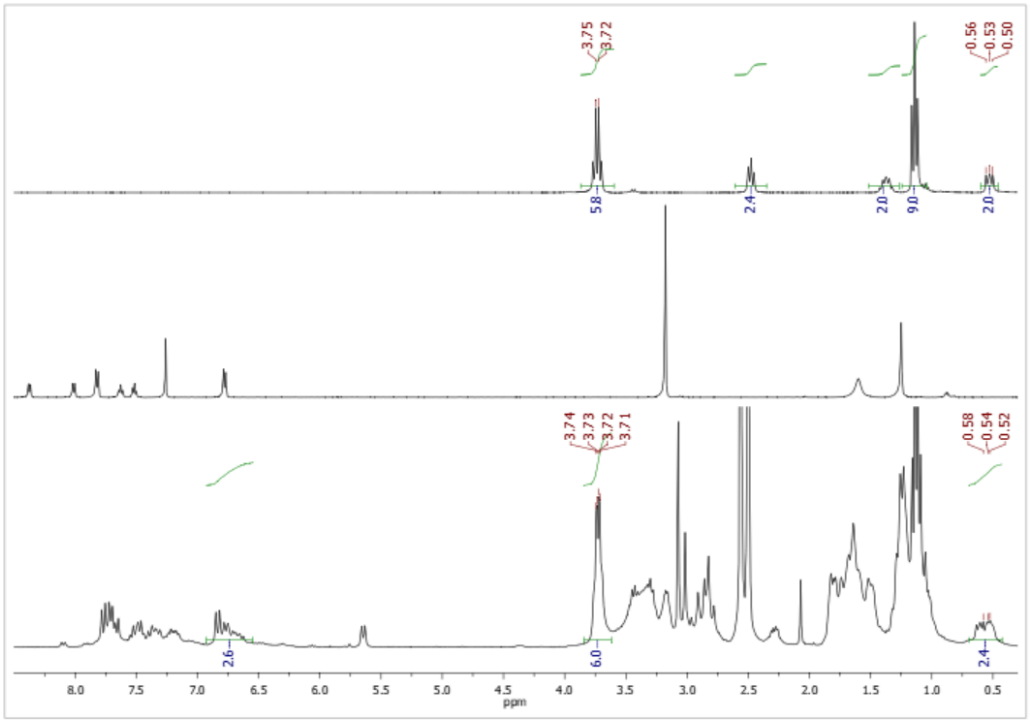

Figure 17: ^{1}H NMR spectra in DMSO-*d6* of APTES (top), methyl red (middle, in $CDCl_3$) and MR-APTES (bottom).

This reaction followed a reported protocol [55]. Since methyl red spectrum was made in $CDCl_3$ and the reaction product in DMSO-*d6*, the chemical shifts from Figure 17 cannot be compared, but the peaks from MR are seen clearly in MR-APTES. APTES chemical shifts and integration can be compared and confirm the conjugation with MR. One of the by-products is dicyclohexylurea (as shown in Annex 7.1) which could not be eliminated and is assigned to broad signals between 3,5 and 1 ppm [56].

Conjugation of ibuprofen (IBF) with (3-aminopropyl)triethoxysilane (APTES) (IBF-APTES).

APTES (53,6 mg, 0,242 mmol) was added to ibuprofen (IBF) (50,0 mg, 0,242 mmol) in 5 mL of acetonitrile**.** Dicyclohexylcarbodiimide, 99% (74,9 mg, 0,363 mmol), 1-hydroxypyrrolidine-2,5-dione (41,8 mg, 0,363 mmol) and triethylamine (36,7 mg, 0,363 mmol) were added to the mixture and left under magnetic stirring for 8 h. Several washes with acetonitrile were done and the solvent was evaporated to dryness in a rotavapor giving the product as a colorless oil.

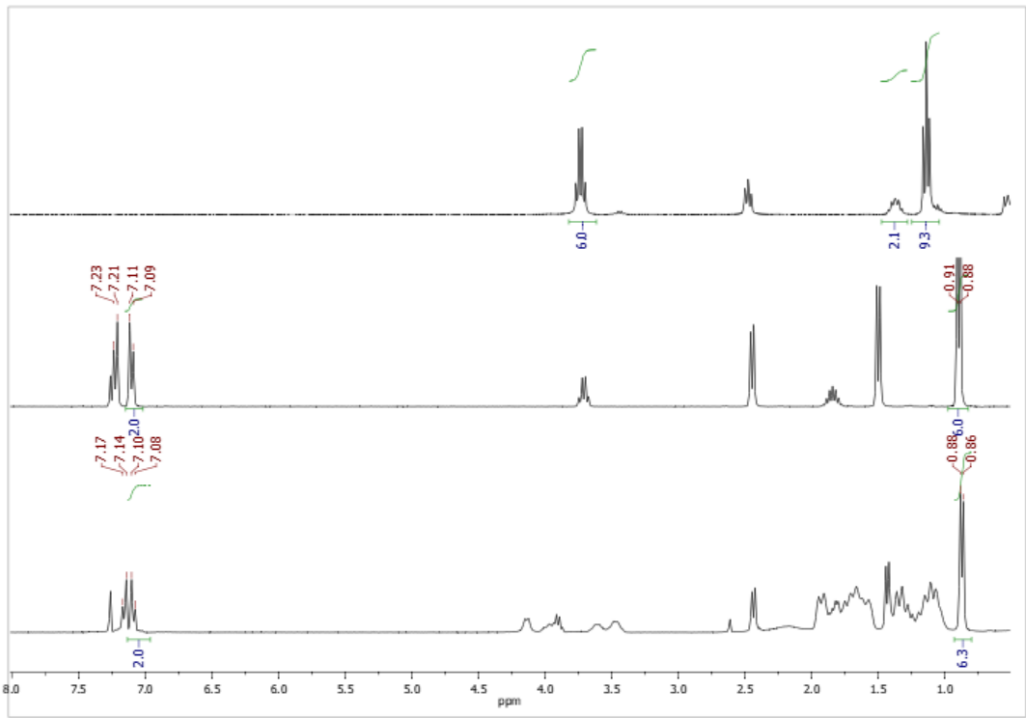

Figure 18: ^{1}H NMR spectra in DMSO-*d6* of APTES (top), ibuprofen (middle) and IBF-APTES (bottom).

This conjugation followed the same protocol as MR-APTES. The spectrum in Figure 18 shows a contamination with dicyclohexylurea (reaction by-product), but IBF conjugation is clearly confirmed by spectral integration. APTES peaks are hard to identify because most of them are overlapped by others but the observed shift in the IBF peaks allows us to conclude that APTES is conjugated.

3 Integral asymmetric cellulose acetate-based membranes: fabrication of monophasic hybrid and mixed matrix membranes

The membranes in this work were fabricated by the phase inversion method resulting in integral asymmetric membranes characterized by a very thin dense active layer and a much thicker, porous substructure. Monophasic hybrid membranes were fabricated by coupling sol-gel and phase inversion technologies and mixed matrix membranes (MMMs) were fabricated by the physical incorporation of $PURE_{G4}$ dendrimer in the polymer (CA) matrix. For comparison purposes, a pure polymer, CA100, membrane was also synthesized.

Table 4 shows the casting solution compositions prepared for the synthesis of the novel membranes.

Table 4: Composition of the casting solutions of the CA100, CA95-SiO_2-$(CH_2)_3NH_2$, CA95-SiO_2-$(CH_2)_3NH_2$-MR, CA90-SiO_2-$(CH_2)_3NH_2$-IBF, CA99-RB-$PURE_{G4}$ and CA95-IBF-SiO_2-$(CH_2)_3NH_2$ membranes.

	Quantity (g)					
	CA100	**CA95-SiO_2-$(CH_2)_3NH_2$**	**CA95-SiO_2-$(CH_2)_3NH_2$-MR**	**CA90-SiO_2-$(CH_2)_3NH_2$-IBF**	**CA99-RB-$PURE_{G4}$**	**CA95-IBF-SiO_2-$(CH_2)_3NH_2$**
CA	4,25	4,10	4,10	3,95	4,25	4,10
Formamide	7,50	7,25	7,25	6,98	7,50	7,25
Acetone	13,25	12,78	12,78	12,30	13,25	12,78
TEOS	-	0,60	0,60	1,20	-	-
APTES	-	0,16	-	-	-	0,16
HNO_3	-	3 drops	3 drops	3 drops	-	3 drops
Synthesized Compound	-	-	MR-APTES	IBF-APTES	RB-$PURE_{G4}$	IBF-TEOS
	-	-	0,16	0,32	0,18	0,60

The casting solutions (described in Table 4) and casting conditions (described in the next section 3.3) resulted in the fabrication of six different membranes named CA100, CA95-SiO_2-$(CH_2)_3NH_2$. CA99-RB-$PURE_{G4}$, CA95-SiO_2-$(CH_2)_3NH_2$-MR, CA90-SiO_2-$(CH_2)_3NH_2$-IBF and CA95-IBF-SiO_2-$(CH_2)_3NH_2$ membranes. Two of these membranes were fabricated with dyes to prove the incorporation of $PURE_{G4}$ dendrimer and modified silyl precursor (MR-APTES) in the CA99-RB-$PURE_{G4}$ and CA95-SiO_2-$(CH_2)_3NH_2$-MR, respectively. Table 5 shows fabricated membranes with weight percentages of precursors added. All monophasic hybrid membranes were synthesized with a SiO_2/NH_2 molar ratio of 80:20.

Table 5: Description of fabricated membranes with wt% of precursors added.

Membrane	**Description**	**CA (wt%)**	**total SiO_2 (wt%)**	**SiO_2 precursor**	**NH_2 precursor**	**IBF precursor**	**Dye (wt%)**
CA100	• Pure CA membrane	100	0	-	-	-	-

CA99- RB-$PURE_{G4}$	• Mixed matrix membrane containing pure CA and $PURE_{G4}$ dendrimer • Pink membrane, the dye is conjugated to $PURE_{G4}$	99	0	-	-	-	1 (same as dendrimer, covalent bond)
CA95-SiO_2-$(CH_2)_3NH_2$	• Monophasic hybrid membrane [57,58]	95	5	TEOS	APTES	-	-
CA95-SiO_2-$(CH_2)_3NH_2$-MR	• Control membrane • Monophasic hybrid membrane • Orange membrane, the dye is conjugated to APTES	95	5	TEOS	MR-APTES	-	MR 1,3wt%
CA90-SiO_2-$(CH_2)_3NH_2$-IBF	• Competitive binding monophasic hybrid membrane • IBF 50wt% conjugated to APTES	90	10	TEOS	IBF-APTES	IBF-APTES	-
CA95-IBF-SiO_2-$(CH_2)_3NH_2$	• Competitive binding monophasic hybrid membrane • IBF 80wt% conjugated to TEOS	95	5	IBF-TEOS	APTES	IBF-TEOS	-

3.1. Fabrication of monophasic hybrid membranes: sol-gel technology and the phase inversion method

The sol-gel process allows the formation of an inorganic framework under mild conditions and the incorporation of minerals, silica in this case, into polymers, thus enhancing chemical, thermal and mechanical properties [59]. Different silica precursors such as tetraethyl orthosilicate (TEOS) and (3-aminopropyl)triethoxysilane (APTES), as shown in Figure 19, can be used to incorporate SiO_2 into the polymer matrix following two reactions: a fast hydrolysis (4) followed by a alcohol or water condensation (5) as showed below.

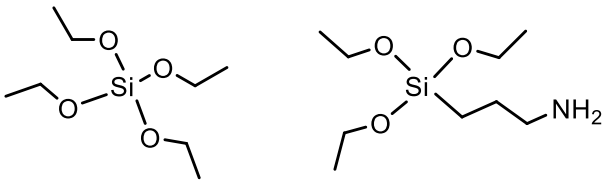

Figure 19: Structures of tetraethyl orthosilicate (TEOS) (left) and (3-aminopropyl)triethoxysilane (APTES) (right).

$$\equiv Si - OR + H_2O \rightarrow \equiv Si - OH + ROH \quad (4)$$

$$\begin{aligned} \equiv Si - OR + HO - Si \equiv &\rightarrow \equiv Si - O - Si \equiv + ROH \\ \equiv Si - OH + HO - Si \equiv &\rightarrow \equiv Si - O - Si \equiv + H_2O \end{aligned} \quad (5)$$

Under acid catalysis (pH 2-7), in the hydrolysis step, the ethoxy group is protonated quickly removing electron density from silicon making it more electrophilic and susceptible for water attack. The water molecule nucleophilic attack on the SiO_2 precursor results in a positive charge that weakens the

protonated ethoxy group. The positively charged ethoxy group becomes a better leaving group, this being displaced from the SiO_2 precursor [60].

The condensation reaction occurs between the silanol groups from the silica precursors or with hydroxyl groups from the polymer, forming $Si - O - Si$ or $Si - O - C$ bonds, respectively, as showed in Figure 20 [61]. The type of structure formed depends considerably on the balance between hydrolysis and condensation reactions which are strongly affected by the pH of the solution. In acid conditions (pH < 5) hydrolysis occurs much faster than condensation, so monomers are rapidly hydrolyzed and most functional groups –OH (close to 4) are available for condensation, resulting in extensive branching and therefore more open, less dense 3D network [50]. The acetylation degree in cellulose acetate used in this work is around 40%.

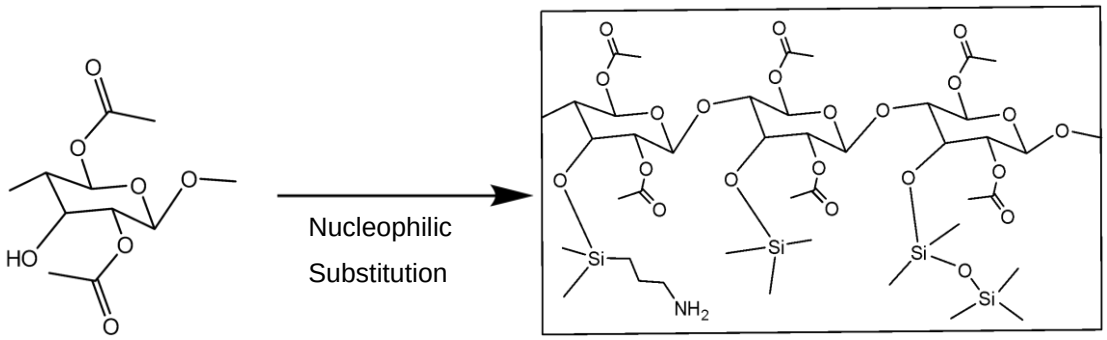

Figure 20: Condensation and incorporation of silica in CA.

The integral asymmetric CA membranes were successfully fabricated through phase inversion technology [62] which is composed by certain steps: casting solution composition, solubilization time, casting and atmosphere temperature, solvent evaporation and immersion precipitation. These steps are crucial to achieve a membrane film with desired pore sizes.

The casting solution composition, specifically the ratio between the solvent and the polymer, ensures the proper viscosity of the casting solution to achieve a membrane film. For the pure CA membrane, a ratio of acetone/CA of 3 is found to be successful [62]. A solubilization time of approximately 24 h is enough for the polymer and other reagents to form a homogeneous mixture.

The temperature of the casting solution and atmospherics are other important parameters which affect the average pore size of the ultrafiltration membranes. Previous studies [63,64] have shown that a higher casting temperature indicates a decrease in average pore sizes which is correlated to a smaller supramolecular polymer aggregation. The increase in the temperature also induces higher evaporation rate constants. Solvent evaporation rate during film formation refers to the rate of solvent removal from the surface which ultimately forms the dense microporous layer in the resulting asymmetric porous membrane; the above rate is a function of solution structure, temperature of casting atmosphere, ambient nature of casting atmosphere including humidity, and solvent evaporation period [64].

The proper time interval between casting and immersion depends on the rate of evaporation of the most volatile solvent from the membrane and hence is a function of the temperature at which the membrane is cast and allowed to remain, prior to immersion. This refers to solvent evaporation period

which was proven to increase average pore size at longer evaporation periods [64] and there is an optimum evaporation period for a maximum membrane productivity [63].

After solvent evaporation, the membrane film is immersed in a nonsolvent bath to precipitate the membrane. When the film is immersed in the nonsolvent bath (water), the solvent leaves the film making space for the precipitant. At the surface, the concentration of nonsolvent soon reaches a value resulting in phase separation. However, in the interior, the concentration is far below the limit for the phase separation resulting a net movement of the polymer in the direction perpendicular to the surface. This leads to a higher concentration of polymer in the surface layer [65].

The integral asymmetric monophasic hybrid CA/SiO_2 membranes in this work are fabricated by a casting solution composed by a solvent system (acetone, 53wt% and formamide, 30wt%) and the polymer (CA, 17wt%) which stays 24 h stirring for solubilization, with the addition of silica precursors in 5 h of stirring. After the 24 h, the membrane is cast in a glass plate with a casting knife of 250 µm thickness at an optimum casting temperature around 20 ºC (room temperature) and left for solvent evaporation time of 30 seconds. The membrane film is immersed in a cooling water bath (0-4 ºC) and left to precipitate from the glass plate. After being detached from the glass, the membrane sheets are stored in deionized water at 4 ºC.

In previous studies [49], the incorporation of silica (SiO_2) was analyzed in membranes containing between 5 and 40wt% and results show that the hydraulic permeability (Lp) was highest for membranes containing 5 and 10wt% silica. Further studies for membranes containing 5wt% silica were made analyzing the functionalization of silica with NH_2 groups (SiO_2-NH_2) [50]. The introduction of 10 molar% of the silica functionalized with an amine group resulted in higher hydraulic permeabilities. Results indicated that a molar ratio of SiO_2/SiO_2-NH_2 of 80:20 would be suitable for hemodialysis membranes, and this composition was chosen in this work.

3.2. Fabrication of mixed matrix membranes

Mixed matrix membrane is the incorporation of a solid phase in a continuous polymer matrix. The application of these membranes is a good way to reach contributory effects between the polymeric matrix and solid particles. In MMMs, solid particles are added to the polymer dope and the flat sheet membranes are formed by the phase inversion method [66].

In this case, $PURE_{G4}$ dendrimer nanoparticles are the solid phase which will be added to the continuous CA polymer matrix.

3.3. Fabrication of pure CA100, mixed matrix CA99-RB-$PURE_{G4}$ membrane, monophasic hybrid CA-SiO_2-$(CH_2)_3NH_2$ membrane and competitive binding of CA-SiO_2-$(CH_2)_3NH_2$ based membranes

3.3.1. Materials

All the membranes were prepared with cellulose acetate (CA) with MW~30000 g/mol purchased from Aldrich; formamide from AppliChem; acetone from José Manuel Gomes dos Santos; tetraethyl

orthosilicate (98%) from Alfa Aesar; (3-aminopropyl)triethoxysilane (≥98%) from Sigma-Aldrich, nitric acid (65%) from Chem-Lab. Modified silica precursors, IBF-TEOS, IBF-APTES and MR-APTES were synthesized in the laboratory (see section 2.1.3). The $PURE_{G4}$ dendrimer was available in the host lab at iBB/IST, and the precursors containing IBF were obtained as described in section 2.1.2.

Mechanical agitation in membrane synthesis was improved by the Shaker S50 purchased from CAT.

3.3.2. Fabrication of pure cellulose acetate, (CA100) membrane

The casting solution was prepared by adding CA (4,25 g, 0,142 mmol) to formamide (7,50 g, 166,5 mmol) in a glass vial and stirred with a glass rod. Acetone (13,25g, 228,1 mmol) was added to the mixture and the final casting solution was mixed by magnetic stirring for 24 hours at room temperature (20 ºC). After 24 h, the casting solution was cast on a glass plate using a 250 µm casting knife. A solvent evaporation time of 30 seconds preceded the immersion of the glass plate into an iced water bath (0-5 ºC). The membranes were left in the bath for at least 30-60 minutes, until the membranes detached from the glass. The resulting membranes are stored in deionized water at 4 ºC. The pure CA membranes are referred as CA100.

3.3.3. Fabrication of mixed matrix CA99-RB-$PURE_{G4}$ membrane

The casting solution was prepared by adding CA (4,25 g, 0,142 mmol) to formamide (7,50 g, 166,5 mmol) in a glass vial and stirred with a glass rod. Acetone (13,25g, 228,1 mmol) was added to the mixture and the final casting solution was mixed by magnetic stirring for 24 h at room temperature (20 ºC). After 5 h, RB-$PURE_{G4}$ (0,18 g, 0,02 mmol) was added to the casting solution. After 24 h, since the casting solution was put under stirring, the casting solution was cast on a glass plate using a 250 µm casting knife. A solvent evaporation time of 30 seconds preceded the immersion of the glass plate into an iced water bath (0-5 ºC). The membranes were left in the bath for at least 30-60 minutes, until the membranes detached from the glass. The resulting pink membranes (4 small sheets, see sheet size described in Table 1) are stored in deionized water at 4 ºC. The pink-colored CA mixed matrix membranes functionalized with RB-$PURE_{G4}$ are referred as CA99-RB-$PURE_{G4}$.

3.3.4. Synthesis of Monophasic Hybrid, CA-SiO_2-$(CH_2)_3NH_2$, membranes

The casting solution was prepared by adding CA (4,10 g, 0,137 mmol) to formamide (7,25 g, 161,0 mmol) in a glass vial and stirred with a glass rod. Acetone (12,78 g, 220,0 mmol) was added to the mixture and the final casting solution was mixed by magnetic stirring for 24 h at room temperature (20ºC). After 4 h of stirring, TEOS (0,60 g, 2,88 mmol) and APTES (0,16 g, 0,723 mmol) were added to the casting solution. After 1 h of the silica percursors addition, three drops of nitric acid were slowly added to the mixture. After the 24 h since the casting solution was put under stirring, the casting solution was cast on a glass plate using a 250 µm casting knife. A solvent evaporation time of 30 seconds preceded the immersion of the glass plate into an iced water bath (0-5 ºC). The membranes were left in the bath for at least 30-60 minutes, until the membranes detached from the glass. The resulting

membranes are stored in deionized water at 4 ºC. The monophasic hybrid cellulose acetate/silica functionalized with amine groups membranes are referred as CA-SiO_2-$(CH_2)_3NH_2$.

3.3.5. Synthesis of competitive binding CA-SiO_2-$(CH_2)_3NH_2$ based membranes

Competitive binding CA-SiO_2-$(CH_2)_3NH_2$ based membranes with the silica precursors synthesized and described in chapter 2 (Synthesis of IBF precursors) were fabricated. Three novel monophasic hybrid membranes were produced (in chronological synthesis order):

3.3.5.1. CA95-SiO_2-$(CH_2)_3NH_2$-MR membranes

In order to evaluate if IBF can effectively conjugate to the monophasic CA-SiO_2-$(CH_2)_3NH_2$ based membrane, by incorporation of the novel silica precursor IBF-APTES in the casting solution, a control membrane, named CA95-SiO_2-$(CH_2)_3NH_2$-MR membrane was produced. To do so, methyl red (MR), a pH indicator (red, low pH/orange, neutral-high pH) was used to prepare a MR-APTES intermediate. This dye was selected since possess a carboxylic acid group with similar chemical reactivity of IBF, thus resulting in an IBF-APTES analogue. Since MR-APTES is colored (in contrast with colorless IBF-APTES) the addition of this intermediate to the CA matrix allow a visual proof of MR (and IBF later on) membrane incorporation.

The casting solution was prepared by adding CA (4,10 g, 0,137 mmol) to formamide (7,25 g, 161,0 mmol) in a glass vial and stirred with a glass rod. Acetone (12,78 g, 220,0 mmol) was added to the mixture and the final casting solution was mixed by magnetic stirring for 24 h at room temperature (20 ºC). After 4 h of stirring, TEOS (0,60 g, 2,88 mmol) and MR-APTES (0,16 g, 0,339 mmol) were added to the casting solution. After 1 h of the silica precursor addition, three drops of nitric acid were slowly added to the mixture. After the 24 h, since the casting solution was put under stirring, the casting solution was cast on a glass plate using a 250 µm casting knife. A solvent evaporation time of 30 seconds preceded the immersion of the glass plate into an iced water bath (0-5 ºC). The membranes were left in the bath for at least 30-60 minutes, until the membranes detached from the glass. The resulting membranes are stored in deionized water at 4 ºC. The orange colored membranes (4 small sheets, see sheet size described in Table 1) are referred to CA95-SiO_2-$(CH_2)_3NH_2$-MR.

3.3.5.2. CA90-SiO_2-$(CH_2)_3NH_2$-IBF membranes

The casting solution was prepared by adding CA (3,95 g, 0,132 mmol) to formamide (6,98 g, 155,0 mmol) in a glass vial and stirred with a glass rod. Acetone (12,30 g, 211,8 mmol) was added to the mixture and the final casting solution was mixed by magnetic stirring for 24 h at room temperature (20ºC). After 4 hours of stirring, TEOS (1,20 g, 5,76 mmol) and IBF-APTES (0,32 g, 0,781 mmol) were added to the casting solution. After 1 hour of the silica precursors addition, three drops of nitric acid were slowly added to the mixture. After the 24 h, since the casting solution was put under stirring, the casting solution was cast on a glass plate using a 250 µm casting knife. A solvent evaporation time of 30 seconds preceded the immersion of the glass plate into an iced water bath (0-5 ºC). The membranes were left in the bath for at least 30-60 minutes, until the membranes detached from the glass. The

resulting membranes are stored in deionized water at 4 ºC. The competitive binding monophasic hybrid membranes (2 big sheets, see sheet size described in Table 1) functionalized with IBF-APTES are referred as CA90-SiO_2-$(CH_2)_3NH_2$-IBF, whose the first sheet is CA90-SiO_2-$(CH_2)_3NH_2$-IBF(1) characterized by clusters spread throughout the membrane and a solvent evaporation time of 30 seconds and the second sheet, CA90-SiO_2-$(CH_2)_3NH_2$-IBF(2), characterized by an homogeneous opaque white membrane and a solvent evaporation of 15 seconds.

3.3.5.3. CA95-IBF-SiO_2-$(CH_2)_3NH_2$ membranes

The casting solution was prepared by adding CA (4,10 g, 0,137 mmol) to formamide (7,25 g, 161,0 mmol) in a glass vial and stirred with a glass rod. Acetone (12,78 g, 220,0 mmol) was added to the mixture and the final casting solution was mixed by magnetic stirring for 24 h at room temperature (20 ºC). After 4 hours of stirring, IBF-TEOS (0,60 g, 1,14 mmol) and APTES (0,16 g, 0,723 mmol) were added to the casting solution. After 1 h of the silica precursors addition, three drops of nitric acid were slowly added to the mixture. After the 24 h, since the casting solution was put under stirring, the casting solution was cast on a glass plate using a 250 µm casting knife. A solvent evaporation time of 30 seconds preceded the immersion of the glass plate into an iced water bath (0-5 ºC). The membranes were left in the bath for at least 30-60 minutes, until the membranes detached from the glass. The resulting membranes are stored in deionized water at 4 ºC.

Two batches of membranes were made for this composition. The first batch, named CA95-IBF-SiO_2-$(CH_2)_3NH_2$.1 was fabricated by adding IBF-TEOS directly to the casting solution, but the compound did not dissolve well, resulting in the two big sheets (see sheet size described in Table 1) with many dots spread throughout the entire surface. Permeation experiments revealed that these membranes presented low hydraulic permeabilities values ranging 32,1 and 33,8 mL min^{-1} m^{-2} $mmHg^{-1}$. The second batch of membranes CA95-IBF-SiO_2-$(CH_2)_3NH_2$.2 was fabricated by dissolving the IBF-TEOS and APTES in a fraction of the acetone of the initial casting solution prior to adding the precursor to the other components (CA, formamide and the rest of acetone. IBF-TEOS and APTES were solubilized in a fraction of the total volume of acetone of the casting solution with magnetic stirring and at a temperature of 40 ºC. CA, formamide and the other portion of acetone was solubilized under mechanical stirring in another recipient. After solubilization of both solutes the solutions were left to reach room temperature and after 4 h of constant stirring were added to one another with constant mechanical stirring. After 1 h, nitric acid was added to complete the final casting solution. Membranes were cast under the same condition as described in section 3.3.4. Two big membrane sheets were produced, and no visible dots could be seen. One sheet, CA95-IBF-SiO_2-$(CH_2)_3NH_2$(1).2 membrane, was produced after a solvent evaporation time of 10 seconds and the other sheet CA95-IBF-SiO_2-$(CH_2)_3NH_2$(2).2 membrane was produced with a solvent evaporation of 30 s.

3.4. Results and discussion

3.4.1. CA99-RB-PURE$_{G4}$ membranes

Figure 21 shows a photo of the CA99-RB-PURE$_{G4}$ membrane. The pink color confirms the physical incorporation of highly branched RB-PURE$_{G4}$ in the CA matrix. Permeation performance and further chemical structure studies were not performed due to time constrains but are planned.

Figure 21: CA99-RB-PURE$_{G4}$ pink membrane.

3.4.2. CA95-SiO_2-$(CH_2)_3NH_2$-MR , CA90-SiO_2-$(CH_2)_3NH_2$-IBF and CA95-IBF-SiO_2-$(CH_2)_3NH_2$ membranes

For the silica precursors, the differences between TEOS/APTES and the newly synthesized precursors rely on steric constrains introduced by from IBF or the selected dyes. In a previous work [49] using TEOS, where the TEOS silicon atom has four ethoxy groups, it was possible to incorporate up to 40% of silica in a CA membrane. In another study [50] using APTES, where the APTES silicon atom has 3 ethoxy groups and one propylamine group, the experiments made were always with 5% weight of silica and changing the molar composition of TEOS:APTES.

The results showed a great increase in hydraulic permeability (Lp) until 10% molar of APTES, suggesting the interference of the APTES extra steric hindrance (compared to TEOS) that forces the polymer network to open, thus producing a more porous matrix. Above 10% the opposite happens, and the Lp values drop significantly thus showing that when APTES content is high enough the propylamine chains start to interact more with the CA matrix, making it more compact and a decrease in the Lp values is observed [50].

The compound IBF-TEOS has only two available ethoxy groups and the other two groups are IBF molecules, three times bigger. In the other two precursors, MR-APTES and IBF-APTES, the dye (MR or IBF) is conjugated to the propylamine. And, in sol-gel technique [60], the hydrolysis rate is decreased by substituents that increase steric crowding around silicon which is what happens in these systems. Thereupon, from this point of view, APTES derivatives have less steric hindrance and should give better hydrolysis yields.

In another perspective, the IBF-TEOS synthesis was confirmed both by NMR and mass spectrometry, showing to be very pure. On the other hand, IBF-APTES and MR-APTES were less pure, as shown by NMR (Figure 17 and Figure 18). So, in this case, the results from IBF-TEOS membrane would be more “reliable” because possible interferences from residual contaminants may occur.

The membrane with MR-APTES was successfully synthesized which also corroborates the bound between silicon and CA matrix, producing an orange membrane as shown in Figure 22. The orange color is a result from the intermediate pH of the solution (between 2 and 7).

Figure 22: CA95-SiO_2-$(CH_2)_3NH_2$-MR orange membrane.

One of the sheet membranes was stored separately in deionized water and samples of the storage solution (water) were collected periodically to quantify the dye wash out from the membrane. This samples were read later in a UV-visible spectrophotometer at 410 nm [67] and are listed in Table 6. The results (Table 6) show that after more than one month of storage in water, the maximum dye release was 0,80 mg/L, which is a residual value.

Table 6: MR concentration in storage water from CA95-SiO_2-$(CH_2)_3NH_2$-MR in a 37 days period.

Day	ABS_{410}	C (mg/L)
1	0,0023	0,066
2	0,0127	0,363
3	0,0221	0,631
4	0,0193	0,551
5	0,0150	0,429
6	0,0182	0,520
7	0,0160	0,457
8	0,0170	0,486
9	0,0265	0,757
10	0,0184	0,526
20	0,0184	0,526
37	0,0280	0,800

This visual proof is an indication that the synthesis of membranes using IBF-TEOS or IBF-APTES silica precursors (in replacement of dye-silica precursors) could be successfully accomplished. The IBF-APTES membranes were made with higher percentage of silica (10%), based on previous

work. Even though the 5% silica was chosen to be the best option, it is from 10% silica that the identification of $Si - O - C$ bond is clearer. So, as the first membrane synthesized, the silica content is higher to promote bonding identification.

Since there was an ongoing characterization work for CA95-SiO_2-$(CH_2)_3NH_2$ membrane in parallel to this work [57,58], the membrane with IBF-TEOS is equal to CA95-SiO_2-$(CH_2)_3NH_2$ but instead of pure TEOS, IBF-TEOS was added. So, the difference of results would be specifically targeted for this replacement. The second sheet from second batch (CA95-IBF-SiO_2-$(CH_2)_3NH_2$(2).2) was used to compare results because the procedure was equal with CA95-SiO_2-$(CH_2)_3NH_2$ (30 seconds of evaporation).

4 Permeation Studies: experimental set-up, materials and methods

To evaluate the mass transfer properties associated to the metabolic functions of the kidney several parameters have to be studied, namely, the hydraulic permeability (Lp), molecular weight cut-off (MWCO), rejection coefficient to small water soluble UTs, and long-term albumin filtration. Table 7 shows the permeation parameters evaluated for the different membranes fabricated in this work. All experiments were made for the CA100 and CA95-SiO_2-$(CH_2)_3NH_2$ membranes. For the CA95-SiO_2-$(CH_2)_3NH_2$-MR, the Lp was evaluated and samples of the collected permeate were further analyzed by UV-visible spectroscopy at wavenumber 410 nm to see if the MR-APTES precursor was leached from the membrane. The CA90-SiO_2-$(CH_2)_3NH_2$-IBF membrane was evaluated in terms of Lp, rejection to uric acid and BSA filtration. The CA95-IBF-SiO_2-$(CH_2)_3NH_2$ membrane was evaluated in terms of Lp, MWCO, rejection to uric acid and BSA filtration. Due to limited time, it was not possible to evaluate all the parameters for all of the fabricated membranes.

It is important to note that, for the CA90-SiO_2-$(CH_2)_3NH_2$-IBF membrane, two different sheets were characterized, CA90-SiO_2-$(CH_2)_3NH_2$-IBF(1) and CA90-SiO_2-$(CH_2)_3NH_2$-IBF(2). The casting solution were the same but the casting conditions differed by the solvent evaporation time being 15 s for the CA90-SiO_2-$(CH_2)_3NH_2$-IBF(2) and 30s for the CA90-SiO_2-$(CH_2)_3NH_2$-IBF(1) membrane. As for the CA95-IBF-SiO_2-$(CH_2)_3NH_2$ membranes, three sheets were analyzed, The casting solution was the same for the first two, CA95-IBF-SiO_2-$(CH_2)_3NH_2$(1).1 and CA95-IBF-SiO_2-$(CH_2)_3NH_2$(2).1, which had poor solubilization of IBF-TEOS resulting in membranes with clusters spread all over the membranes surface. The observed problem of solubilization was solved by a new casting solution, described in section 3.3.5.3, which produced CA95-IBF-SiO_2-$(CH_2)_3NH_2$(1).2 and CA95-IBF-SiO_2-$(CH_2)_3NH_2$(2).2 membranes sheets. The casting condition for these membranes differ by the solvent evaporation time being 10s for CA95-IBF-SiO_2-$(CH_2)_3NH_2$(1).2 membrane and 30s for the CA95-IBF-SiO_2-$(CH_2)_3NH_2$(2).2 membrane.

Table 7: Permeation experiments carried out for each membrane synthesized.

Membrane	Description			Characterization			
		Lp	MWCO	urea rejectio*	creatinine rejection**	uric acid rejection ***	BSA rejection ****
CA100	• Pure CA membrane	x	x	x	x	x	x
CA99-$PURE_{G4}$-RB	• Mixed matrix membrane containing pure CA and $PURE_{G4}$ dendrimer • Pink membrane, the dye is covalently bound to $PURE_{G4}$ (RB-$PURE_{G4}$)						
CA95-SiO_2-$(CH_2)_3NH_2$	• Monophasic hybrid membrane	x	x	x	x	x	x
CA95-SiO_2-$(CH_2)_3NH_2$-MR	• Monophasic hybrid membrane • Orange membrane, the dye is covalently bound to APTES (MR-APTES)	x					

CA90-SiO_2-$(CH_2)_3NH_2$-IBF(1)	• Competitive binding monophasic hybrid membrane • IBF conjugated to APTES (IBF-APTES) • Solvent evaporation time 30 s • Dots spread throughout membrane surface due to poor solubilization of IBF-APTES	x			x	x	x
CA90-SiO_2-$(CH_2)_3NH_2$-IBF(2)	• Competitive binding monophasic hybrid membrane • IBF conjugated to APTES (IBF-APTES) • Solvent time evaporation of 15 s (lower to other membranes)	x					
CA95-IBF-SiO_2-$(CH_2)_3NH_2$(1).1	• Competitive binding monophasic hybrid membrane • Two IBF molecules conjugated to each TEOS • Solvent time evaporation of 30 s	x					
CA95-IBF-SiO_2-$(CH_2)_3NH_2$(2).1	• Competitive binding monophasic hybrid membrane • Two IBF molecules conjugated to each TEOS • Dots spread throughout membrane surface due to poor solubilization of IBF-TEOS • Solvent time evaporation of 30 s	x					
CA95-IBF-SiO_2-$(CH_2)_3NH_2$(1).2	• Competitive binding monophasic hybrid membrane • Two IBF molecules conjugated to each TEOS • Improved solubilization of IBF-TEOS in casting solution • Solvent times evaporation of 15 s						
CA95-IBF-SiO_2-$(CH_2)_3NH_2$(2).2	• Competitive Binding Monophasic hybrid membrane • Two IBF molecules bounded to each TEOS • Improved solubilization of IBF-TEOS in casting solution • Solvent times evaporation of 30 s	x	x			x	x

*4600 mgL^{-1}; **240 mgL^{-1}; ***60 mgL^{-1} **** 900 mgL^{-1}.

4.1. Experimental set-up

The laboratory experimental set-up used for the permeation studies [68] is detailed in Figure 23. The set-up has been described in previous work [57]. Briefly, the feed solutions are stored in a reservoir inside a bath at 37 ºC which mimics the blood temperature in human body. The solution is pumped and smoothed by a damper then, passes through the first pressure sensor (S1) before entering

the single hemodialysis membrane module. The portion that crosses the membrane passes by another sensor (S3) before is collected as permeate sample. The other part also passes by a sensor (S2) and can be collected as feed sample or can be recirculated to the reservoir.

The pressure sensors are connected to a computer where pressures and corresponding time are recorded for posterior use. It is important to highlight that between these pressure sensors there is several accidents as an expansion in the module entrance, a slit in the permeation area, contraction in the outlet, etc. which adds error to the collected data.

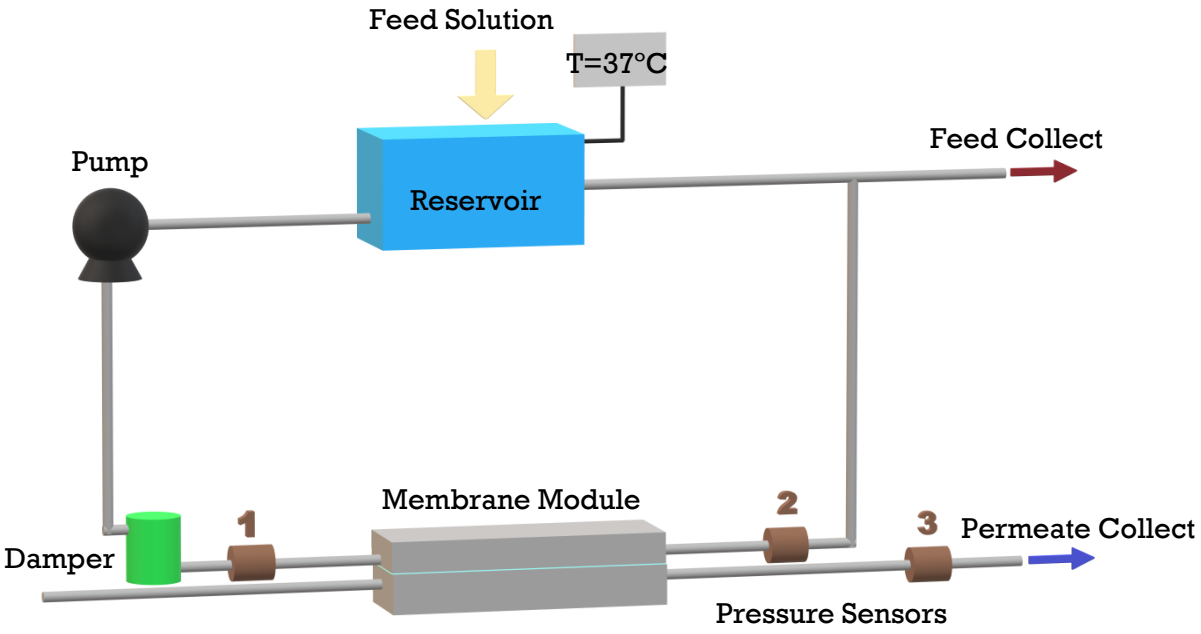

Figure 23: Laboratory setup for permeation studies. *Created in Paint 3D.*

The single hemodialysis membrane module (SHDMM) consists in five parts as drawn in Figure 24. Pieces I and V function as support for the other parts. The second piece (II) is the feed, or blood, compartment which the upper part of the membrane is connected. The third part (III) is the membrane support where has a porous layer and splits the blood and dialysate compartment. Above this layer, paper filter is placed before the membrane to support and avoid damaging from the module. The thickness of this piece provides transport only by convection and not by diffusion. The fourth piece is the permeate, or dialysate, compartment that stays below the porous layer.

The dimensions (length x width) of the pieces and the porous layer are 35x3 and 25x3 cm, respectively. Two sheet sizes can be produced, detailed in Table 1, however, small membranes sheets (15x28 cm^2) cannot fit in this SHDMM. To overcome this complication, between unit II and III, before the membrane is laid, a transparent non permeable acetate sheet is placed with the same dimensions was SHDMM but with a hole cut inside with the dimensions of the small membrane sheet. This method is used to study the possible leaching from the CA95-SiO_2-$(CH_2)_3NH_2$-MR further described in section 4.2.

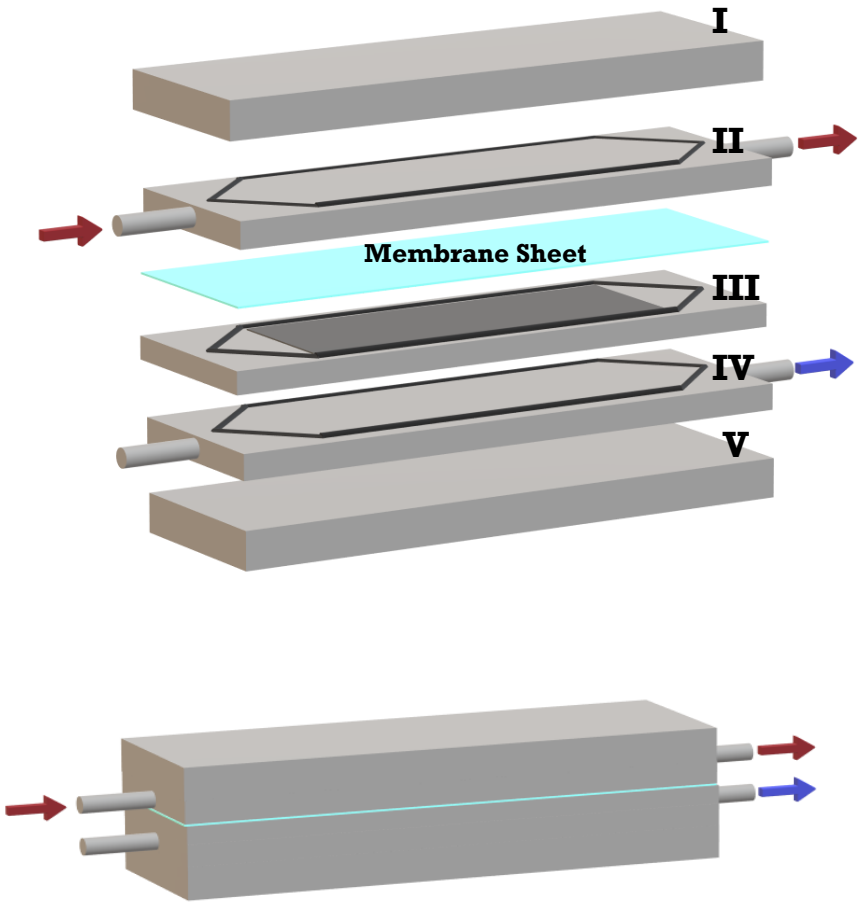

Figure 24**:** Single membrane module in laboratory setup. *Created in Paint 3D*.

Some parameters are collected from the installation that are very important for further characterization and monitoring experiments of the membranes.

Transmembrane pressure (TMP) is calculated as average pressures in blood compartment minus average pressure in the dialysate compartment. It is defined as the hydrostatic pressure gradient which allows for ultrafiltration or convection across a dialyzer membrane i.e. describes the force needed to make the water circulate through the membrane. [68,69] In this case, TMP given by Equation (6):

$$TMP = \frac{P_{S1} + P_{S2}}{2} - P_{S3} \tag{6}$$

Rejection factor is a percentage of how much solute, after reaching steady state in feed solution, and after usually 90 minutes,, passes through the membrane to the permeate. This parameter tends to zero in molecules that the membrane is permeable or to 100% to molecules retained by the membrane. Rejection factor (f_t) at time t is defined in equation (7) where C equals to solute concentration.

$$f_{rejection} = 1 - \frac{\bar{C}_{permeate,t}}{\bar{C}_{feed,0}} \quad (7)$$

The pressure drop (ΔP) is the difference of pressures from blood compartment inlet and outlet from the membrane module. This parameter helps to monitor the membrane performance because if flow rate and temperature are constant, pressure drop should not change, unless there is fouling or some physical block. This value is a result from the fluid friction on the walls of membrane installation and it is calculated by equation (8).

$$\Delta P = P_{S1} - P_{S2} \quad (8)$$

In membrane module, when all parts are assembled, the liquids flow through the microchannels of feed or permeate compartments. The thickness of these microchannels is an important indicator of membrane fouling. This value varies with the thickness of the membrane and the paper filter and, also, with possible molecule deposition from the experiments. In literature [70,71], the parameter half-thickness, B, is estimated using laminar flow in a narrow slit and assuming the flow Newtonian, laminar and fully developed giving equation (9). It is important to notice that this estimation assumes impermeable walls which in this case, do not happen giving this value a qualitative interpretation.

$$B = \sqrt[3]{\frac{Q_F * \mu * L}{\Delta P * W} * \frac{3}{2}} \quad (9)$$

Where Q_F is the volumetric feed flow rate collected by pump calibration (Annex 7.3.1), W and L is width and length of the porous part (piece III) and μ is the viscosity of the fluid, in this case, water ($\mu_{w,37ºC} = 0{,}0007\ Pa.s$). When fouling happens, B reduces and increases ΔP.

Shear stress (τ) is a fluid dynamics parameter and is very important to avoid blood damaging as platelet activation and hemolysis. A healthy human vessel (vein or artery) has an approximate shear stress of 0,1 to 20 Pascal (Pa). Studies have proven that platelet activation increases significantly when exposed to shear stress higher than 20 Pa and mechanical cell damage, hemolysis, at 30 Pa [72,73]. Hence, it is essential to operate artificial devices in a safe mode to ensure the maximum shear stress is below the threshold stress of hemolysis and platelet activation.

This parameter is defined as the frictional force exerted by blood flow on the vessel wall, as in an artery wall or of a medical device, assumed to be impermeable wall [74]. It is calculated by balancing the shear force profile at the wall against the pressure gradient (interface blood-membrane) for a slit channel at steady state [71] giving the equation (10) which can be simplified with half-thickness, B, equation (9).

$$\tau\ [Pa] = \frac{3 * \mu * Q_F}{2 * W * B^2} = \frac{B * \Delta P}{L} \quad (10)$$

4.2. Quantification of MR-APTES leaching from the CA95-SiO_2-$(CH_2)_3NH_2$-MR membrane.

Further pure water permeation experiments were performed with the CA95-SiO_2-$(CH_2)_3NH_2$-MR membrane to understand if any dye would be leached from the membrane. The experiment lasted 4 h of passing deionized water at 37 ºC through the membrane at a feed flowrate of 321 mL/min and TMP of 134 mmHg. This membrane was synthesized into four small sheets and these sheets are smaller than the membrane module. So, to overcome this problem, a transparent non permeable acetate sheet was cut with membrane module size (35x3 cm^2) and cut a hole inside with the space for the small membrane sheet (21x3 cm^2) to be installed. With this fitting, the permeation only happens through the hole where the colored membrane is placed as shown in Figure 25. The orange sheet is the membrane, the red rectangle is the non-permeable acetate sheet, and the black lines are the O-rings which seal the module.

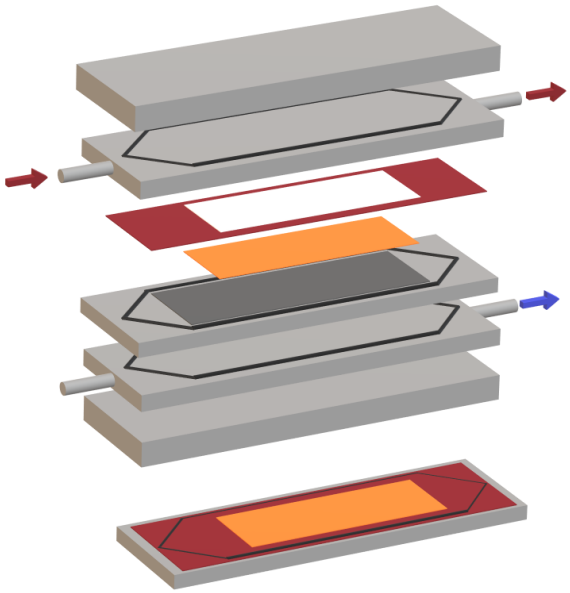

Figure 25: Fitting for experiments with orange-colored CA95-SiO_2-$(CH_2)_3NH_2$-MR membrane.

Permeate samples were collected at each pump position and read in spectrophotometer to convert into dye concentrations. A calibration curve for MR was made in UV-visible spectrophotometer (UV-1700 PharmaSpec from Shimadzu) at 410 nm and is described in Annex 7.3.5.

4.3. Evaluation of Hydraulic Permeability

The hydraulic permeability (Lp) provides information on the diffusive or convective transport of components through a membrane under a hydrostatic pressure driving force [75]. It indicates the water flux per unit are per unit time per unit of pressure applied. The higher the permeability, more porous the membrane [76]. The permeate water flux is calculated dividing permeate flowrate measured, Q_P, by effective filtration area (A= 105 cm^2 except for CA95-SiO_2-$(CH_2)_3NH_2$-MR membrane detailed in section 4.2; schematized in Figure 24) as shown in equation (11).

$$J_w(\frac{mL}{min.cm^2}) = \frac{Q_P}{A_{eff}} \quad (11)$$

A plot of permeate flux *versus* TMP passing through the origin gives a straight line which the resulting slope yield the hydraulic permeability of the membrane.

Other standard parameters such as permeate flowrate, TMP and shear stress are used to help choosing a feed flow rate which approximates to HD values as much as possible. In order to assure efficient excess fluid removal from CKD patients, an ultrafiltrate or permeate flow rate of 1 mL/min is considered to be good. TMP and shear stress values of approximately 70 mmHg and 20 Pa, respectively are also considered to be reasonable and therefore the operating parameters used in the permeation experiments were chosen in these ranges. Table 8 shows the operating conditions for each experiment and the corresponding channel height which is calculated as double of B.

Table 8: Feed flow rate, TMP, shear stress and channel height parameters associated to each permeation experiment which each membrane placed inside the SHDMM.

Membrane	Feed flowrate (mL/min)	TMP (mmHg)	Shear stress (Pa)	Channel height (μm)
CA100	98,98	45,79	3,53	255
CA95-SiO_2-$(CH_2)_3NH_2$	98,64	70,72	5,38	205
CA90-SiO_2-$(CH_2)_3NH_2$-IBF(1)	146,72	74,10	6,18	235
CA90-SiO_2-$(CH_2)_3NH_2$-IBF (2)	194,01	97,19	6,60	227
CA95-IBF-SiO_2-$(CH_2)_3NH_2$(1).1	146,72	89,36	8,01	206
CA95-IBF-SiO_2-$(CH_2)_3NH_2$(2).1		78,66	6,64	227
CA95-IBF-SiO_2-$(CH_2)_3NH_2$(2).2		75,25	6,37	231

*CA95-SiO_2-$(CH_2)_3NH_2$ was characterized in other installation with a different pump [57,58].

The permeability experiments were made with deionized water at 37 ºC. Permeate is collected over 120 seconds, weighed, and transformed in volume by water density at 37 ºC (ρ= 0,993 g/mL). These values were obtained in triplicate for each feed flow rate (from 28,4 to 214,2 mL/min) and TMP values from and 10 to 150 mmHg. Full Lp data and the pump calibration curve are described in Annex's 7.2 and 7.3.1, respectively.

4.4. Molecular Weight Cut-Off (MWCO)

The molecular weight cut-off of a membrane is generally used to characterize a membrane in terms of pore size distribution and retention [77]. It refers to the lowest *molecular weight* solute (in Daltons) in which 90% of the solute is retained by the membrane.

Linear polymers such as polyethylenglycol (PEG) or dextran are used for MWCO determination. In this study, six PEGs with increasing MWs were used: 3000, 6000, 10000, 20000 and 35000 Da. When or if the rejection factor did not reach 90%, dextran T40 and T70, with MWs of 40000 and 70000 Da, respectively, were used.

Quantification was achieved with a Total Organic Carbon (TOC) analyzer (TOC-V CSH from Shimadzu). The TOC analyzer reports the concentration of organic carbon in the sample analyzed. Calibration curves were made for all polymers and are shown in Annex 7.3.3.

Since the rejection factor *versus* molecular weight usually doesn't give a straight line, equation (12) is used to generate a linear dependence for polymers with the highest rejection factor. Thus, the intersection between the rejection factor of 90% and the line which connect all rejection factors gives the MWCO value and the minimum is given by the intersection of the straight line produced by linearization and linearized 90% value.

$$y = log\left(\frac{f}{1-f}\right) \quad (12)$$

Before starting the experiments, the SHDMM is washed for approximately 30 minutes with ultrapure MiliQ water. The initial solution of each polymer was prepared with a concentration of 600 mg/L and is placed in reservoir at 37ºC and recirculated for 10 minutes. The priming volume was estimated at 40 mL and, to avoid dilution, this volume is collected in feed before starting the assay.

Permeate and feed samples are collected at 0, 10, 50 and 90 minutes and the concentration of the polymer in the permeate at time zero is considered to be zero. For comparison purposes, this assay was performed for the pure CA100 membrane and for the CA95-IBF-SiO_2-$(CH_2)_3NH_2$(2).2 membrane.

4.5. Evaluation of rejection coefficients to small water-soluble uremic toxins

Small water-soluble toxins have the lowest molecular weight (MW< 500 Da) and are generally easily removed by current hemodialysis membrane. Therefore, the novel membranes must be efficient in their removal, *i.e.* must exhibit low rejection factors.

Creatinine (anhydrous, ≥98%, purchased from Sigma-Aldrich), urea (purchased from MERCK), and uric acid (99%, purchased from Alfa Aesar) were the small water-soluble UT's studies in this work. A healthy person with good kidney performance has lower blood concentrations of these UTs while CKD patients, have much higher concentrations. Thus, for each of these three toxins experiments were performed with two different feed solutions concentrations to reproduce the values found in healthy and unhealthy patients. These values can be found in Table 9 [10,78]

The quantification of each toxin was obtained by spectrophotometry. Each toxin has a maximum absorption peak and calibration curves were obtained for each one using a UV-visible spectrophotometer (UV-1700 PharmaSpec from Shimadzu) using deionized water as the blank. The correspondent concentrations and absorption peaks are detailed in Table 9.

Table 9: Concentration and absorption wavelength of small water-soluble toxins.

Toxin	Normal Concentration	Pathological Concentration	Wavelength (nm)
Creatinine	12 mg/L	240 mg/L	230
Urea	0,4 g/L	4,6 g/L	200
Uric Acid	40,5 mg/L	83 mg/L*	293

*Uric acid solubility in water is lower than 83 mg/L. The experiments were done using the solubility limit (60 mg/L).

These experiments were performed as described in section 4.4. Instead of ultrapure MiliQ water, the deionized water was used.

Feed and permeate samples are collected at every 15 minutes for a total of 90 minutes. Absorbance values were read in a UV-visible spectrophotometer (UV-1700 PharmaSpec from Shimadzu) at the wavelength mentioned in Table 9. Concentrations were calculated using the calibration curve presented in Annex 7.3.2, and the rejection factor was calculated using equation (7).

4.6. Long-term BSA filtration

Albumin in one of the most important and abundant protein in our blood and it is responsible, among other things, of carrying substances such as enzymes, hormones, toxins and pharmaceutical drugs throughout our body. For this reason, it is vital that albumin does not pass through the hemodialysis membranes from the blood to the ultrafiltrate. Furthermore, it's important to know how much time HD membranes can endure without suffering extensive protein deposition and adhesion which may result in membrane fouling.

Bovine serum albumin (BSA), purchased from Aldrich, was the albumin used in this assay and an initial solution with a concentration of 900 mg/L was prepared. During the first 90 minutes, samples from feed and permeate streams were collected at intervals of 15 minutes, and after that, at intervals of 30 minutes until a total of 8 hours of filtration was achieved.

The Blue Coomassie reagent, also called Bradford reagent, used for the detection of proteins, was prepared as described [79]. The detection is made by UV spectrophotometry. Concentrations higher than 100 mg/L have a linear behavior in 595 nm with a proportion of 1:50 of sample and Bradford reagent. In this case, in a 3 mL quartz cell, the volumes of sample and the Bradford reagent are 0,059 and 2,941 mL, respectively.

For lower concentrations (< 100 mg/L), linearization is made with different peaks and proportions [80]. The ratio of two peaks, 590 and 450 nm, and a proportion of 1:4 sample/Bradford are described to give a calibration line. Since the blank used only deionized water, the BSA zero concentration is not at the origin.

High concentrations of protein are expected in the feed solutions while low concentrations are expected in the samples collected from the permeate stream. Absorbance values are converted to BSA concentrations by the calibration curves shown in Annex 7.3.4.

4.7. Permeation Forecast

The permeation performance of the membranes fabricated with the compounds synthesized in this work, CA99-RB-PURE$_{G4}$, CA95-SiO_2-$(CH_2)_3NH_2$-MR, CA90-SiO_2-$(CH_2)_3NH_2$-IBF and CA95-IBF-SiO_2-$(CH_2)_3NH_2$ membranes, will be compared to those obtained for the pure CA100 and monophasic hybrid CA95-SiO_2-$(CH_2)_3NH_2$ membranes which have already been studies in previous works [5,49], [50,57]. Next are some considerations about the results expected considering the novel materials and the respective membrane behavior.

Data found in literature [49], reveals that the incorporation of up to 10wt% of silica (SiO_2) by the sol gel reaction between TEOS and CA, enhances the hydrophilicity and increases the Lp of monophasic hybrid CA/SiO_2 membranes. For higher silica content (20 and 40wt%) the Lp value decreases and this behavior was attributed to the fact that water molecules become strongly bonded to the molecules of the hybrid matrix hindering water permeation [49].

In another work, monophasic hybrid CA95-SiO_2-$(CH_2)_3NH_2$ membranes were prepared with the incorporation of two silica precursors, TEOS and APTES. Characterization and permeation studies reveal that the introduction of 20mol% of the propylamine group results in more hydrophobic membranes and higher steric hindrance when compared to CASiO_2 membranes prepared with only TEOS. [50].

The competitive binding monophasic hybrid CA90-SiO_2-$(CH_2)_3NH_2$-IBF membrane fabricated in this work has 10wt% silica content and 20mol% IBF-APTES. The competitive binding monophasic hybrid CA95-IBF-SiO_2-$(CH_2)_3NH_2$ membrane has 5wt% of silica and IBF is conjugated to TEOS in the proportion of 80mol% of IBF-TEOS to 20mol% of APTES. It is expected that the CA90-SiO_2-$(CH_2)_3NH_2$-IBF membrane will have a higher permeability value than the CA95-IBF-SiO_2-$(CH_2)_3NH_2$ membrane because it seems that IBF-APTES (which accounts for 320 mg) is associated to IBF steric hindrance and hydrophobicity. It is also envisioned that the 5wt% of silica (corresponding to 760 mg) present in the CA95-IBF-SiO_2-$(CH_2)_3NH_2$ membrane will contribute to a lower hydraulic permeability because TEOS is covalently bound to two IBF molecules.

In terms of MWCO, it is estimated that the introduction of IBF-APTES and IBF-TEOS in the monophasic hybrid membranes will result in larger spaces between the CA polymer chains as these silica precurors are larger than unconjugated TEOS and APTES.

In terms of long-term BSA filtration experiments, we estimate that there could be an increase in protein adhesion/deposition at the surface of the competitive binding membranes because BSA has a high affinity towards IBF. IF this occurs at an extensive level, long-term BSA studies should reveal some evidence of membrane fouling.

5 Permeation Studies: results and discussion

5.1. Quantification of MR-APTES leaching from the CA95-SiO_2-$(CH_2)_3NH_2$-MR membrane.

The hydraulic permeability of the CA95-SiO_2-$(CH_2)_3NH_2$-MR membrane was found by measuring the permeate fluxes as a function of TMP which ranged from 16,1 mmHg to 133,6 mmHg. During the experiment, samples of the permeate were analyzed by UV-visible spectroscopy to detect the presence of MR dye that may have been leached from the membrane using the calibration curve obtained in Annex 7.3.5. For comparison purpose, the values used to calculate the hydraulic permeability started from feed flow rate of 231,2 until 321,7 mL/min and TMPs from 81,0 to 133,6 mmHg. The resulting Lp for CA95-SiO_2-$(CH_2)_3NH_2$-MR was 92,4 mL h^{-1} m^{-2} $mmHg^{-1}$ (or 68,9 kg h^{-1} m^{-2} bar^{-1}).

Table 10 shows the results obtained when determining the concentration of MR in the permeate samples collected during the experiment to determine the Lp. This was performed over a time of 240 minutes. The highest concentration of MR, 0,30 mg/L, was detected at the beginning of the experiment for a feed flow rate of 28,4 mL/min and a TMP of 16,1 mmHg. After this, the concentration of MR decreased reaching a value of 0,08 mg/L after 240 minutes. The mass of MR added to the casting solution was 160 mg and therefore results indicate that there is a good incorporation of the compounds in the membrane and that leaching is negligible.

Table 10: Hydraulic permeability values and concentration of methyl red in permeate samples.

Feed flowrate (mL/min)	Permeate flux (mL $min^{-1}cm^{-2}$)	TMP (mmHg)	ΔP (mmHg)	C (mg/L)
28,4	0,0140	16,1	4,4	0,30
51,7	0,0139	16,8	7,7	0,12
76,1	0,0157	22,3	13,6	0,16
99,0	0,0159	26,9	18,0	0,10
122,5	0,0159	34,5	24,9	0,10
130,8	0,0159	40,4	30,1	0,11
146,7	0,0134	47,8	38,7	0,16
177,7	0,0124	55,6	47,2	0,09
194,0	0,0153	61,8	52,1	0,05
214,2	0,0133	74,0	62,7	0,16
231,2	0,0129	81,0	68,5	0,00
255,7	0,0139	91,3	77,9	0,08
269,4	0,0153	98,6	84,6	0,09
283,5	0,0177	113,5	94,0	0,08
1,158	0,0186	118,8	102,1	0,06
1,235	0,0199	133,6	107,9	0,01

5.2. Hydraulic Permeability

The pure water permeation fluxes obtained for the CA100, CA90-SiO_2-$(CH_2)_3NH_2$-IBF and CA95-IBF-SiO_2-$(CH_2)_3NH_2$ membranes were measured at flow rates between 28,4 and 133,6 mL/min and TMP values between 5,1 and 137,6 mmHg. The pure water permeation fluxes obtained for the

CA95-SiO_2-$(CH_2)_3NH_2$-MR membrane were measured at flow rates between 231,2 and 321,7 mL/min and TMP values between 81,0 and 133,6 mmHg. Results of the permeation fluxes *versus* TMP are shown in Table 11 and Figure 26. Equal batches are represented by the same colors in the graph of Figure 26 and Figure 27. The Lp was obtained from the slope of the straight line drawn across all points and intersecting the origin and the values obtained are shown in Table 11. The most obvious result Is that the Lp of the dyed monophasic hybrid CA95-SiO_2-$(CH_2)_3NH_2$-MR (control) membrane is much higher than all the other membranes. This may be because the compound MR-APTES was not completely pure. The contaminants presence could have interfered in the membrane structure, and, eventually, with Lp results. The second obvious result is that the competitive binding CA90-SiO_2-$(CH_2)_3NH_2$-IBF membrane containing IBF in the same position that was occupied by MR in the membrane described previously shows two different results for Lp, each of which corresponds to two different fabricated membrane sheets (light and dark green data in Figure 26 and Figure 27). One of the membranes CA90-SiO_2-$(CH_2)_3NH_2$-IBF(1) has a Lp value 48,1 mL h^{-1} m^{-2} $mmHg^{-1}$ very close to the pure CA membrane while the second CA90-SiO_2-$(CH_2)_3NH_2$-IBF(2) membrane has a value of 2,8 times lower, 16,9 mL h^{-1} m^{-2} $mmHg^{-1}$.

This behavior can be justified by the discrepancies in the synthesis method described in section 3.3.5.2. The CA90-SiO_2-$(CH_2)_3NH_2$-IBF(1) membrane (dark green) which was fabricated with a solvent evaporation time of 30 s, had some clusters which may be due to poor solubilization of IBF-APTES while the CA90-SiO_2-$(CH_2)_3NH_2$-IBF(2) (light green) was casted with a solvent evaporation time of 15 s. The second sheet possesses an opaque white morphology with no apparent clusters. and seemed to be denser than first sheet. The variation in morphology of the two membrane sheets can explain the difference of Lp results values. The CA90-SiO_2-$(CH_2)_3NH_2$-IBF(1) with a higher Lp was chosen to be used in other permeation experiments (toxins clearance and albumin rejection).

In contrast to what was observed for the CA90-SiO_2-$(CH_2)_3NH_2$-IBF membranes, the CA95-IBF-SiO_2-$(CH_2)_3NH_2$ membranes (light, medium and dark blue data) Lp values were closer to each other. The first batch (CA95-IBF-SiO_2-$(CH_2)_3NH_2$.1, light and medium blue data) had solubilization problems. In both sheets, many clusters could be seen spread in membrane sheets. These clusters were IBF-TEOS compound that did not dissolve in casting solution. A new batch was fabricated to eliminate this problem. In second batch (CA95-IBF-SiO_2-$(CH_2)_3NH_2$.2, dark blue data), the solubilization was solved and two homogeneous sheets were fabricated. The CA95-IBF-SiO_2-$(CH_2)_3NH_2$(2).2 membrane was casted with a solvent evaporation time of 30 s, like other membranes, thus was chosen to be used for all permeation experiments because CA95-IBF-SiO_2-$(CH_2)_3NH_2$(2).1 was casted with a solvent evaporation time of 15 s. The first sheet from this second batch was not studied during this thesis timeline.

Two characteristics may have led to a decrease in Lp: steric hindrance and hydrophobicity. The steric crowding has two paths. When hindrance is still low but enough to open the membrane matrix, and enlarge pore sizes, the hydraulic permeability should be higher and comply with higher MWCO results. However, when the crowding starts to grow, it instigates a greater interaction of this bigger functional groups, IBF in this case, with polymer matrix which makes a more dense and compact

membrane. This produces a lower Lp and MWCO results. On the other side, hydrophobicity and hydrophilicity of pores is not a clear feature because it depends on quantities, for instance, CA, IBF and propylamine group from APTES provides hydrophobicity and TEOS hydrophilicity. The study of this property was done until APTES incorporation which showed that in a 5% mass content of silica membrane (the case of CA95-IBF-SiO_2-$(CH_2)_3NH_2$), until 10% molar addition of APTES, the Lp would increase. And, assuming TEOS add hydrophilicity and APTES hydrophobicity, with the incorporation of IBF to TEOS, the hydrophobicity increases significantly which is showed by the quick detachment of the membrane when contacts water from immersion precipitation. These two features combined can induce to these results.

Current hemodialysis equipment should deliver ultrafiltration rates between 10–13 mL $h^{-1}kg^{-1}$ [81], under an operating TMP of between 100 and 150 mmHg. Hence, for a 70 kg adult, the expected ultrafiltration rate in a clinical scenario should not be lower than 700 mL h^{-1} [57]. Typical hemodialyzers have an effective permeation area between 0,8 and 2,2 m^2 [82]. Considering Lp values for the membranes synthesized and an average TMP of 125 mmHg, in order to achieve a 700 mL h^{-1} threshold, the total membrane surface area is below the typical hemodialyzers effective permeation area for all synthesized membranes, especially for the lowest values for CA95-SiO_2-$(CH_2)_3NH_2$, CA90-SiO_2-$(CH_2)_3NH_2$-IBF (1) and CA95-IBF-SiO_2-$(CH_2)_3NH_2$(2).1 as shown in Table 11.

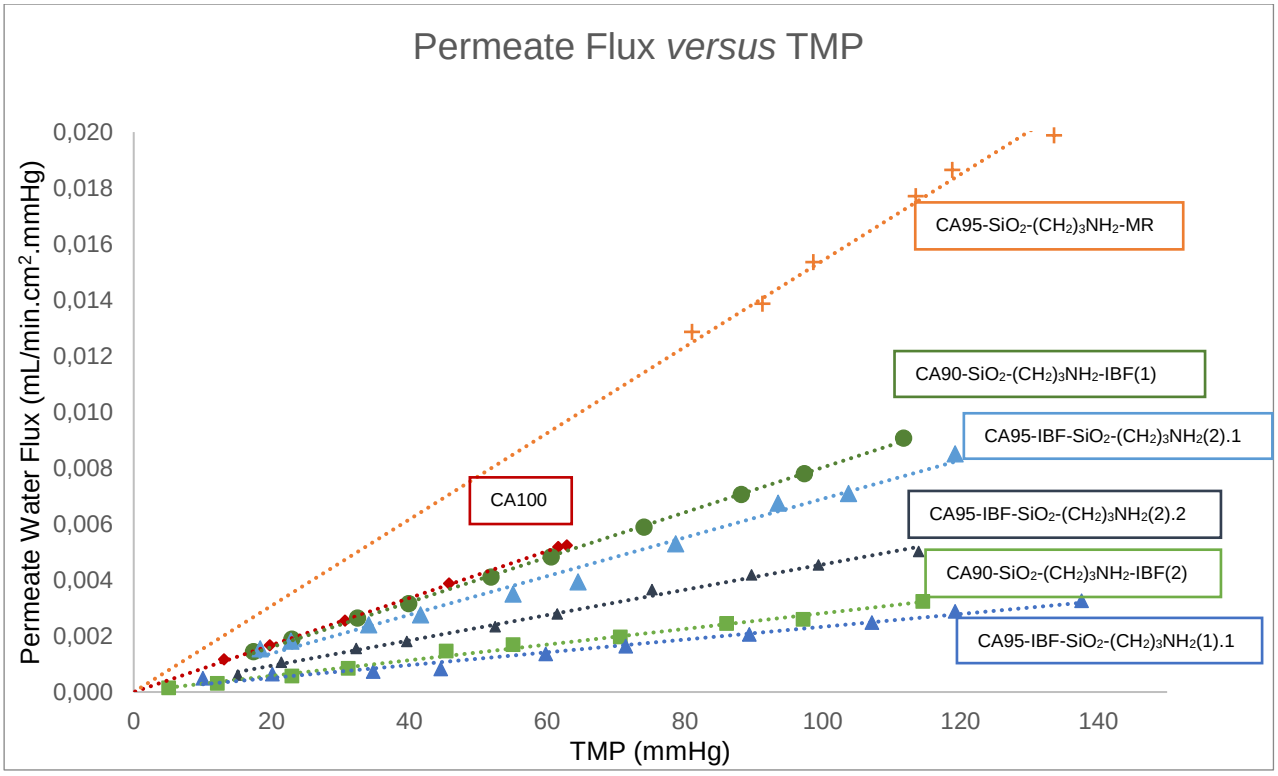

Figure 26: Lp results for all membranes synthesized.

Table 11: Hydraulic permeabilities, effective permeation area of the fabricated membranes at 37ºC and corresponding color for Figure 26 and Figure 27.

Membrane	Graph Color	Lp (kg h^{-1} m^{-2} bar^{-1})	Lp (mL h^{-1} m^{-2} $mmHg^{-1}$)	$A_{effective}$ (m^2)
CA100	Red	37,5	50,3	0,11
CA95-SiO_2-$(CH_2)_3NH_2$-MR	Orange	68,9	92,4	0,06
CA95-SiO_2-$(CH_2)_3NH_2$	Grey	66,6	89,4	0,06
CA90-SiO_2-$(CH_2)_3NH_2$-IBF (1)	Light Green	35,9	48,1	0,12
CA90-SiO_2-$(CH_2)_3NH_2$-IBF (2)	Green	12,6	16,9	0,33
CA95-IBF-SiO_2-$(CH_2)_3NH_2$ (1).1	Light Blue	10,4	14,0	0,40
CA95-IBF-SiO_2-$(CH_2)_3NH_2$ (2).1	Medium Blue	30,9	41,4	0,14
CA95-IBF-SiO_2-$(CH_2)_3NH_2$(2).2	Dark Blue	20,4	27,4	0,20

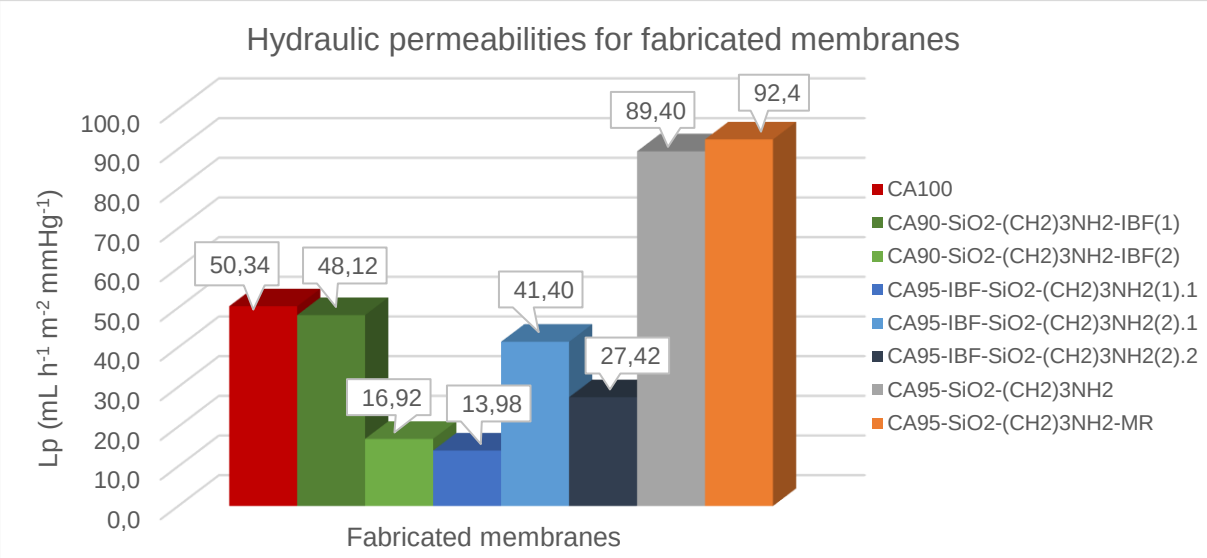

Figure 27: Hydraulic permeabilities for the fabricated membranes.

5.3. MWCO

Figure 28, Figure 29 and Figure 30 show the data obtained for the determination of the MWCO of the CA100, CA95-SiO_2-$(CH_2)_3NH_2$ [57], [58], and CA95-IBF-SiO_2-$(CH_2)_3NH_2$(2).2 membranes, respectively. The data was obtained by measuring the rejection coefficient to a series of PEGs with increasing MW: 3000, 6000, 10000, 20000 and 35000 Da.

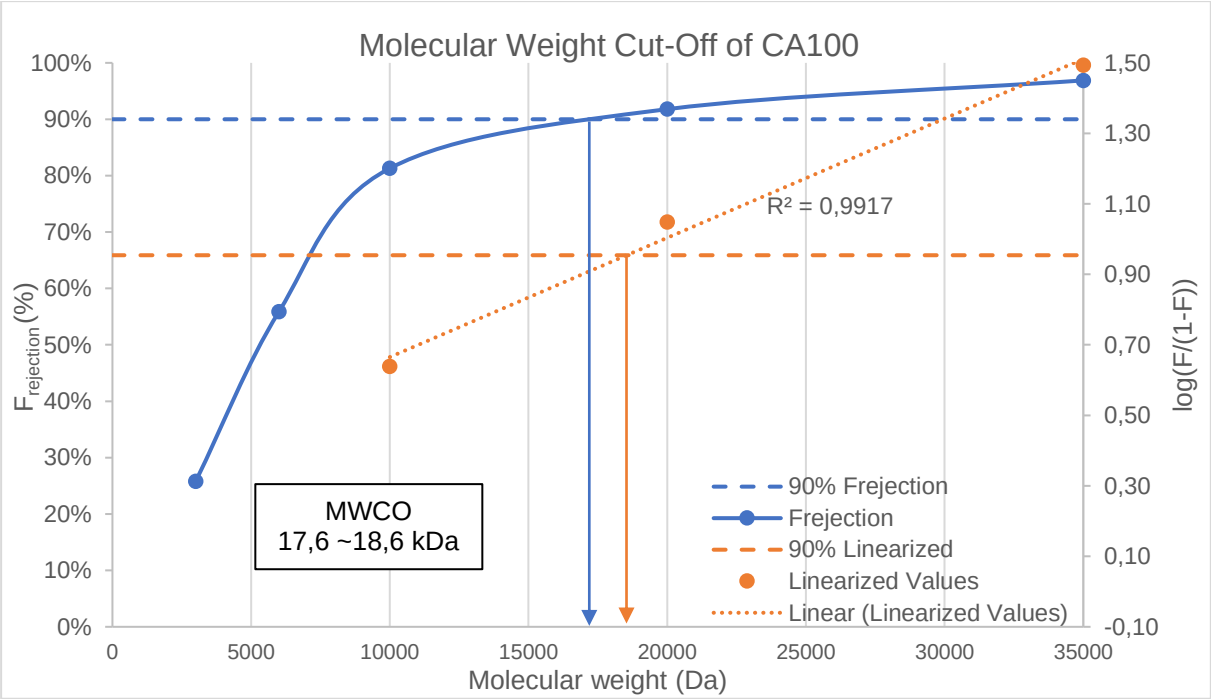

Figure 28: Rejection factor profile for CA100 membrane to PEG of increasing molecular weight. The horizontal dashed lines indicate a rejection of 90% (blue) and log(f/(1-f))=0,954 (orange).

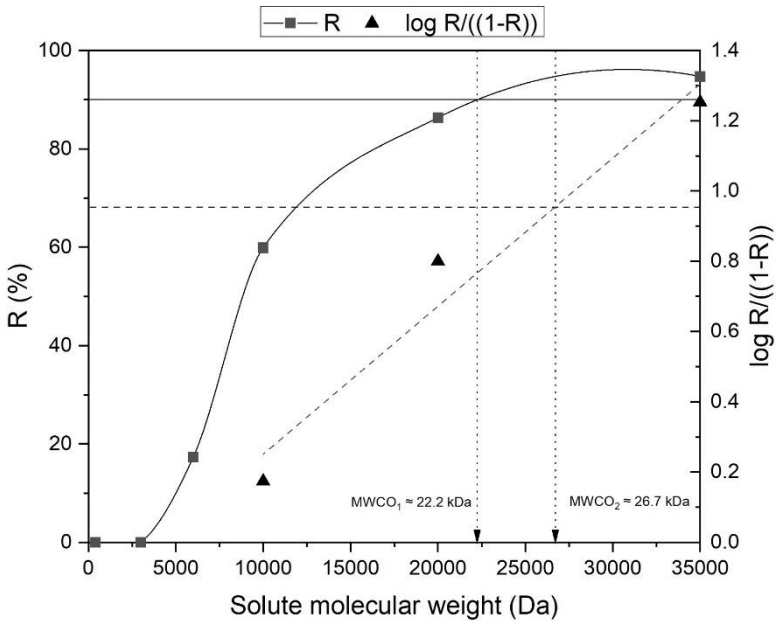

Figure 29: Rejection factor profile for CA95-SiO_2-$(CH_2)_3NH_2$ membrane to PEG of increasing molecular weight. The horizontal dashed line indicate a rejection of 90% and full line indicate log(f/(1-f))=0,954.[57].

The MWCO was estimated to range between 22,2 and 26,7 kDa for the CA95-SiO_2-$(CH_2)_3NH_2$ membrane, and between 17,6 and 18,6 kDa for the CA100 membrane. With the understanding that both membranes reject solutes with MWs greater than 20 kDa, it was predicted that vital blood components such as albumin, platelets, and blood cells would be rejected by both membranes. Furthermore, it is envisioned that molecules belonging to two different classes of uremic toxins proposed by EUTox - small

water-soluble compounds and middle molecules - can be removed, as they are able to cross the membrane.

Because there is evidence of leaching of IBF-TEOS the CA95-IBF-SiO_2-$(CH_2)_3NH_2$(2).2 membrane, prior to determining the MWCO using PEG solutions, pure water filtration was performed for approximately 2 h and samples of the feed and permeate streams were collected and analyzed in the TOC analyzer. The concentrations of the TOC were subtracted to all of the TOC values obtained for each of the PEG solution.

Results show that the highest rejection factor obtained, 77%, was for the largest PEG with MW of 35kDa. Due to the fact that it was below 90%, the rejection factor to Dextran T40 and T70 (40000 and 70000 Da, respectively) was evaluated, and the rejection factors were 76% and 74%, respectively.

Because the rejection coefficient values didn't reach the 90% threshold it is concluded that the MWCO of the CA95-IBF-SiO_2-$(CH_2)_3NH_2$(2).2 membrane could not be determined with high confidence and need to be repeated. To have an idea of a value, the linear function in the graph of Figure 30 was extended until the interception with the 90% value and a tentative MWCO value of 62,5 kDa was obtained.

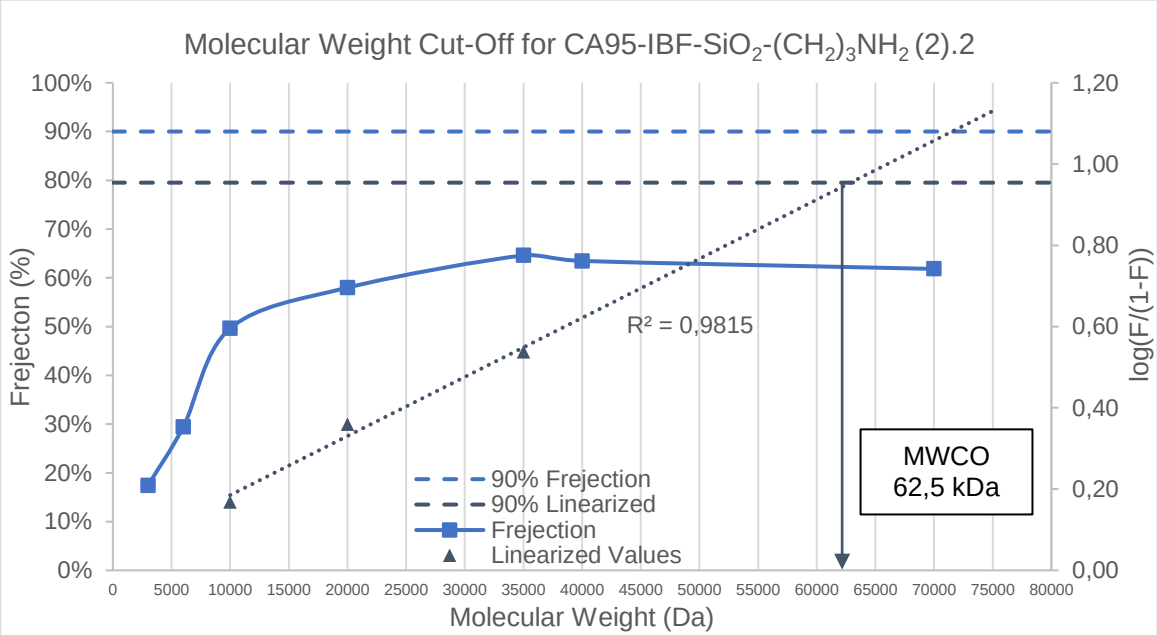

Figure 30: Rejection factor profile for CA95-IBF-SiO_2-$(CH_2)_3NH_2$ membrane to PEG increasing molecular weight. The horizontal dashed lines indicate a rejection of 90% (blue) and log(f/(1-f))=0,954 (orange).

5.4. Rejection coefficients to small water-soluble uremic toxins

The rejection coefficients to creatinine (initial feed solution with pathological concentration of 240 mg/L), uric acid (initial feed solution with pathological concentration of 60 mg/L), and urea (initial feed solution with pathological concentration of 4600 mg/L), were determined for the CA100 and CA95-SiO_2-$(CH_2)_3NH_2$ membrane. Figure 31 and Figure 32 show the evolution of the concentrations of creatinine, uric acid and urea in both feed and permeate solution throughout time for the CA100 and the and CA95-SiO_2-$(CH_2)_3NH_2$ membrane, respectively.

In general, for both the CA100 and CA95-SiO_2-$(CH_2)_3NH_2$ membranes, it was observed that, between 15 and approximately 50 min, the concentration of the solutes in the feed compartment increased, and this could be explained by the decrease of water in the system, which was constantly being removed by convection from the feed compartment through the membrane and into the permeate channel. Between ~50 and 90 min, the concentration of the feed solution tended to stabilize at values close to the ones of the initial feed solution.

Regarding the concentration of the permeate solution, at the beginning of the experiment (t= 0), the collecting permeate chamber was filled with water, and as expected, the solute concentration in the permeate chamber was zero. The concentrations of the permeate solution increased considerably between zero and approximately 50 min and, towards the end of the experiment (t> 80 min), they approached concentration values similar to those of the feed solution (at the corresponding time). This behavior clearly demonstrates that the membranes are permeable to the three low-molecular weight water-soluble uremic toxins evaluated - creatinine, uric acid, and urea. The rejection coefficients were calculated after 90 min of permeation.

The rejection coefficient towards creatinine, uric acid and urea for the CA100 membrane were 4,3%, 0,0% and 9,9%, respectively; and for CA95-SiO_2-$(CH_2)_3NH_2$ membrane, 6,5%, 4,2% and 5,8%, respectively. These results agree with what was discussed before in terms of MWCO, given that urea (MW 60 Da), creatinine (113 Da), and uric acid (168 Da) have much lower MWs than the CA95-SiO_2-$(CH_2)_3NH_2$ and CA100 membranes' MWCO.

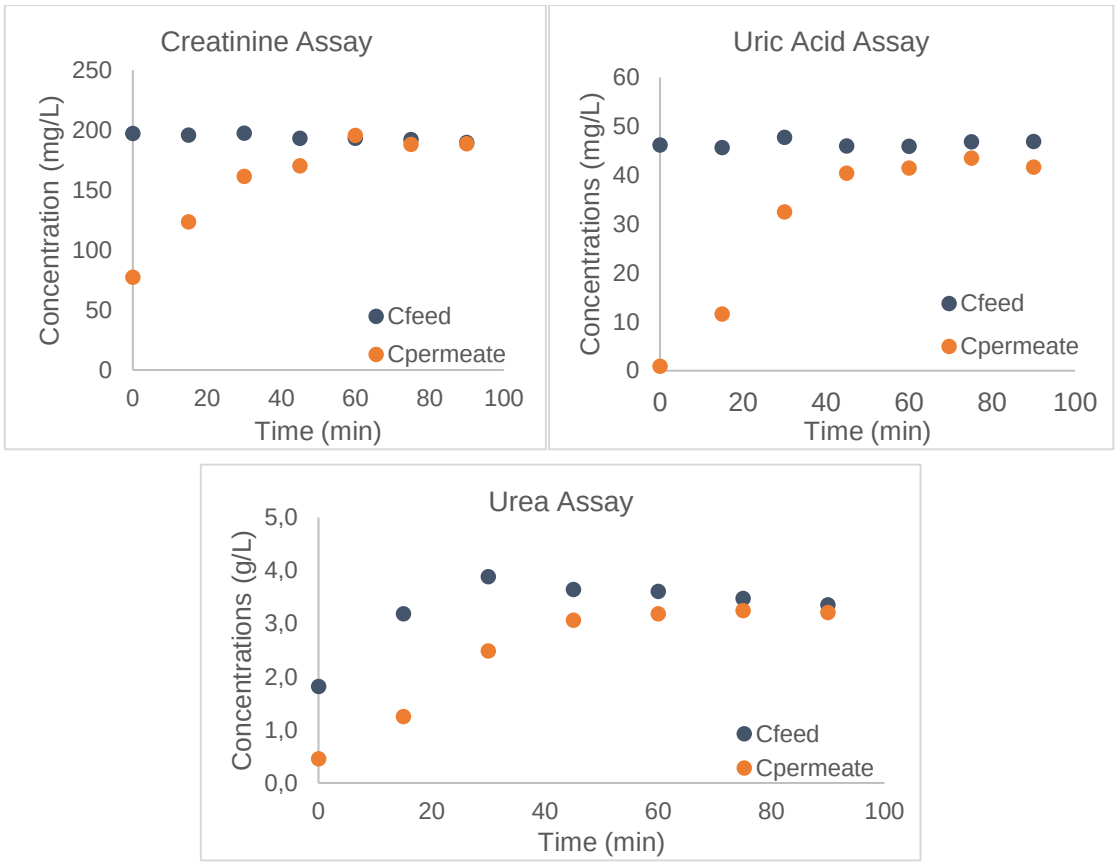

Figure 31: Values represented for rejection coefficient values of small water-soluble toxins for pathological concentrations for CA100 membrane.

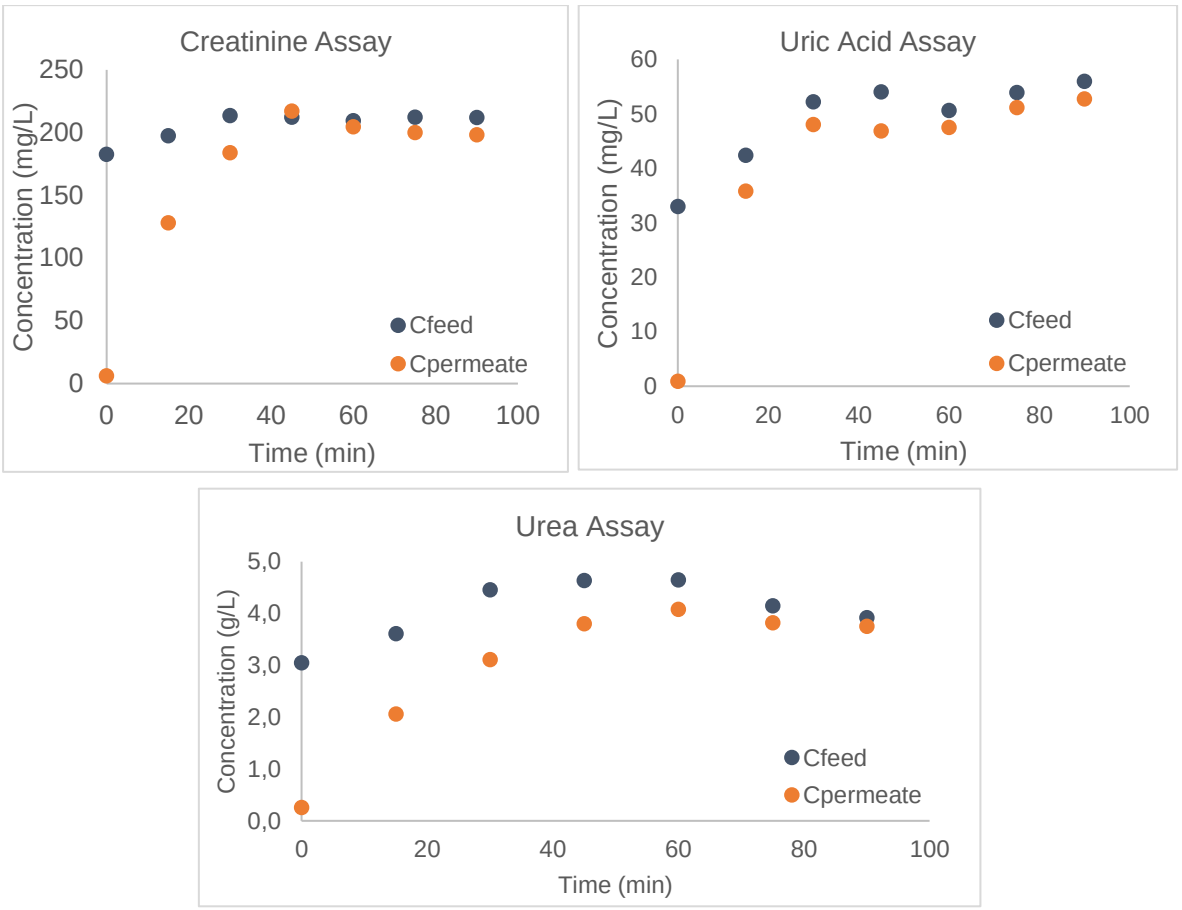

Figure 32: Values represented for rejection coefficient values of small water-soluble toxins for pathological concentrations for CA95-SiO_2-$(CH_2)_3NH_2$ membrane.

For the competitive binding CA90-SiO_2-$(CH_2)_3NH_2$-IBF and CA95-IBF-SiO_2-$(CH_2)_3NH_2$ membranes, it was possible to obtain the rejection coefficient to uric acid (initial feed solution with pathological concentration of 60 mg/L). For the CA90-SiO_2-$(CH_2)_3NH_2$-IBF(1) membrane permeation studies with creatinine (initial feed solution with healthy concentration of 12 mg/L) revealed unexpected results which compromised the evaluation of the rejection factor.

Figure 33 shows the evolution of the concentration of creatinine in both feed and permeate solutions throughout time for the CA90-SiO_2-$(CH_2)_3NH_2$-IBF(1) membrane. As shown in graph of Figure 33, the permeate concentrations, since the beginning of the experiment (t= 0), were higher or equal to the feed concentrations as represented. This outcome prompted a deeper analysis to explain why this happened.

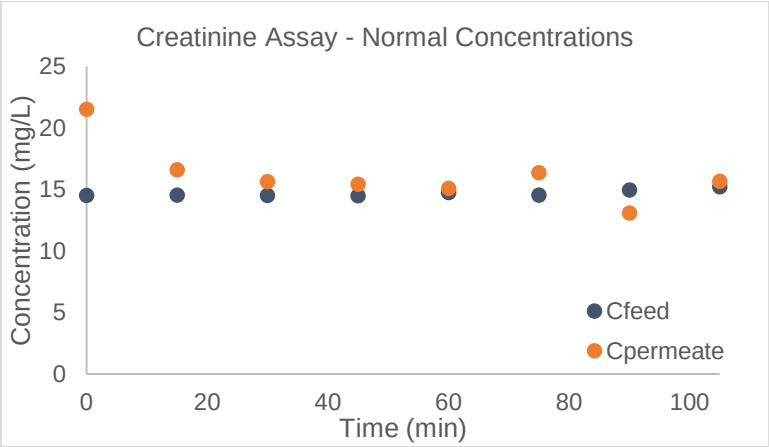

Figure 33: Creatinine assay for CA90-SiO_2-$(CH_2)_3NH_2$-IBF at normal concentrations.

The first interpretation was to assume that there is a presence in the permeate solution of another compound that is detected at the same wavelength as creatinine. To evaluate this hypothesis, pure deionized water was filtered through the membrane for 40 minutes for two days and samples of the permeate were collected every 10 minutes to detect possible leaching from the membrane to the permeate solution by UV-visible spectrophotometry at the same wavelengths used to read the samples containing the small water-soluble toxins, creatinine, urea, and uric acid (230, 200 and 293 nm, respectively) for a qualitative approach. Table 12 shows the values of absorbance obtained on two separate days.

Table 12: Values for experiment with deionized water detection in UV for CA90-SiO_2-$(CH_2)_3NH_2$-IBF.

Toxins Wavelength			
Time (min)	*Abs_{230}	**Abs_{200}	***Abs_{293}
Day 1			
0	0,944	2,529	0,002
10	0,782	2,096	-0,003
20	0,504	1,395	-0,004
30	0,411	1,165	-0,004
40	0,392	1,114	-0,004
Day 2			
0	0,058	0,255	-0,007
10	0,196	0,907	-0,012
20	0,171	0,834	-0,014
30	0,123	0,625	-0,018
40	0,086	0,472	-0,021

*Absorbance of creatinine; **Absorbance of urea; ***Absorbance of uric acid.

Results show that there is leaching of a certain compound from the membrane to the permeate which absorbs at the same wavelengths of creatinine and urea. Also, the fact that the values decrease throughout time suggests that the leaching tends to diminish with time. The only UT that seems to be able to be detected without interference of the molecule being leached from the CA90-SiO_2-$(CH_2)_3NH_2$-IBF(1) membrane is uric acid and therefore it was possible to determine its rejection coefficient. Graphs

from this assay are shown in Annex 7.4.1 and the rejection factor to uric acid for the CA90-SiO_2-$(CH_2)_3NH_2$-IBF(1) membrane was 0,0%.

Taking into account the leaching phenomena which occurred with the CA90-SiO_2-$(CH_2)_3NH_2$-IBF(1) membrane, the same pure water permeation experiment was performed with the CA95-IBF-SiO_2-$(CH_2)_3NH_2$(2).2 membrane where permeate and feed samples were collected and analyzed in the UV-visible spectrophotometer. Table 13 shows values of absorbance obtained on two separate days. Similar to what occurred for the CA90-SiO_2-$(CH_2)_3NH_2$-IBF(1) membrane, for the creatinine wavelength (230 nm) and urea wavelength (200 nm) absorbance values were higher than for the uric acid wavelength (293 nm). Again, the only UT that seems to be able to be detected without interference of the molecule being leached from the CA95-IBF-SiO_2-$(CH_2)_3NH_2$(2).2 membrane is uric acid and therefore was possible to determine the rejection coefficient. The result of this assay is a graph shown in Figure A 13 (Annex 7.4.1) and the rejection factor to uric acid for the CA95-IBF-SiO_2-$(CH_2)_3NH_2$(2).2 membrane was 4,4%.

Table 13: Absorbance values for deionized water experiments in CA95-IBF-SiO_2-$(CH_2)_3NH_2$(2).2.

Samples	Permeate			Feed		
	*Abs_{230}	**Abs_{200}	***Abs_{293}	*Abs_{230}	**Abs_{200}	***Abs_{293}
Feed flowrate (mL/min)	**Day 1******					
28,44	0,517	2,191	-0,007	0,051	0,120	0,023
51,66	0,743	2,677	-0,004	0,065	0,198	0,022
76,06	0,525	2,219	-0,009	0,080	0,268	0,023
98,98	0,512	2,219	0,015	0,087	0,298	0,024
122,49	0,510	2,219	0,015	0,091	0,315	0,024
130,82	0,502	2,125	0,019	0,096	0,332	0,025
146,72	0,494	2,069	0,022	0,104	0,368	0,025
177,73	0,455	1,963	0,019	0,096	0,334	0,025
194,01	0,428	1,824	0,017	0,103	0,363	0,027
214,24	0,378	1,641	0,013	0,095	0,325	0,025
Time (min)	**Day 2**					
0	0,217	0,896	0,034	0,08	0,270	0,019
60	0,230	0,998	0,011	0,063	0,227	0,012
90	0,211	0,934	0,008	0,063	0,233	0,011
120	0,209	0,888	0,012	0,077	0,251	0,017
150	0,191	0,830	0,008	0,073	0,243	0,014

*Absorbance of creatinine; **Absorbance of urea; ***Absorbance of uric acid; ****Assay performed simultaneously to hydraulic permeability assay for the CA95-IBF-SiO_2-$(CH_2)_3NH_2$(2).2 membrane.

Ibuprofen absorbs in the UV range between 200 and 250 nm [82,83]. This indicates that the compound being leached from the CA90-SiO_2-$(CH_2)_3NH_2$-IBF(1) and CA95-IBF-SiO_2-$(CH_2)_3NH_2$(2).2 membranes is IBF-APTES and IBF-TEOS, respectively.

Table 14 shows the summary of the rejection coefficients that were measured for the different membranes. Results show that the rejection factors to creatinine, uric acid and urea were 4,3%, 9,9% and 0,0% respectively for the CA100 membrane, and 6,5%, 4,2% and 5,8% for the CA95-SiO_2-

$(CH_2)_3NH_2$ membrane. The rejection factors towards uric acid was 0,0% and 4,4% for the CA90-SiO_2-$(CH_2)_3NH_2$-IBF(1) and CA95-IBF-SiO_2-$(CH_2)_3NH_2$(2).2 membranes, respectively.

Table 14: Rejection factors for small water-soluble molecules for membranes studied.

Membrane	Creatinine	Uric acid	Urea
CA100	4,3%	9,9%	0,0%
CA95-SiO_2-$(CH_2)_3NH_2$	6,5%	5,8%	4,2%
CA90-SiO_2-$(CH_2)_3NH_2$-IBF(1)	-	0,0%	-
CA95-IBF-SiO_2-$(CH_2)_3NH_2$(2).2	-	4,4%	-

5.5. BSA rejection

The BSA permeation experiments were carried out for over 8 h with initial concentration of 900 mg/L of BSA for CA100, CA95-SiO_2-$(CH_2)_3NH_2$, CA90-SiO_2-$(CH_2)_3NH_2$-IBF(1) and CA95-IBF-SiO_2-$(CH_2)_3NH_2$(2).2 membranes. The rejection coefficient to BSA were also determined for the four membranes and the evidence of membrane fouling was evaluated. Figure 34, Figure 35, Figure 36 and Figure 37 show the concentration profiles in the feed and permeate streams as for TMP throughout time for the CA100, CA95-SiO_2-$(CH_2)_3NH_2$, CA90-SiO_2-$(CH_2)_3NH_2$-IBF(1) and CA95-IBF-SiO_2-$(CH_2)_3NH_2$(2).2 membranes, respectively.

Throughout the entire experiment for CA100 and CA95-SiO_2-$(CH_2)_3NH_2$ membranes, the highest concentration of BSA detected in the permeate was 4,1 and 12,0 mg/L, respectively. Furthermore, there seems to be no clear evidence of fouling events, as the TMP remained approximately constant throughout the experiment, at 47 mmHg and 57 mmHg for the CA100 and CA95-SiO_2-$(CH_2)_3NH_2$ membrane, respectively. The rejection coefficient towards BSA was calculated with the BSA concentrations measured at the end of the experiment (after 480 min of filtration) and was 99,2% and 99,4% for CA100 and the CA95-SiO_2-$(CH_2)_3NH_2$ membranes, respectively. These results were expected given that BSA has a MW of 66,5 kDa which is similar to human serum albumin (HSA) [85], and the MWCO of the CA95-SiO_2-$(CH_2)_3NH_2$ and CA100 membranes is approximately 27 kDa and 19 kDa, respectively.

Regarding the BSA filtration experiment for the competitive binding CA95-IBF-SiO_2-$(CH_2)_3NH_2$(2).2 membranes, prior to BSA filtration, pure deionized water was filtered through the membranes and samples from the feed and permeate streams were read in UV-visible spectrophotometer to evaluate whether there was leaching of any compound which could interfere with the absorbance reading of BSA performed at 595, 450 and 590 nm as described in section 4.6. The results are shown in Table A 15 (in Annex 7.4.2) and it is concluded there is no interference for this wavelength.

For CA90-SiO_2-$(CH_2)_3NH_2$-IBF(1) and CA95-IBF-SiO_2-$(CH_2)_3NH_2$(2).2 membranes, the rejection factor for BSA were 93,6% and 89,5% respectively. This is concordant to the enlargement of pore sizes from the membranes but not with MWCO values for the CA95-IBF-SiO_2-$(CH_2)_3NH_2$(2).2

membrane. BSA has a molecular weight of 66,5 kDa and after 8 h of assay, the rejection factor was 89,5%. Dextran T70, has a MW of 70 kDa and after two hours of experiment, the rejection factor was 75%. These results can lead to two conclusions: the IBF in the membrane interact more with BSA which makes them to not pass through the membrane or the Dextran assay went wrong for some unknown reason.

However, the high rejection coefficient of BSA reveal good results for all membranes studied, since the objective is to retain as much as possible. Also, there seems to be no clear evidence of fouling events since TMP was constant during all 8 h assay as shown in Figure 34, Figure 35, Figure 36 and Figure 37.

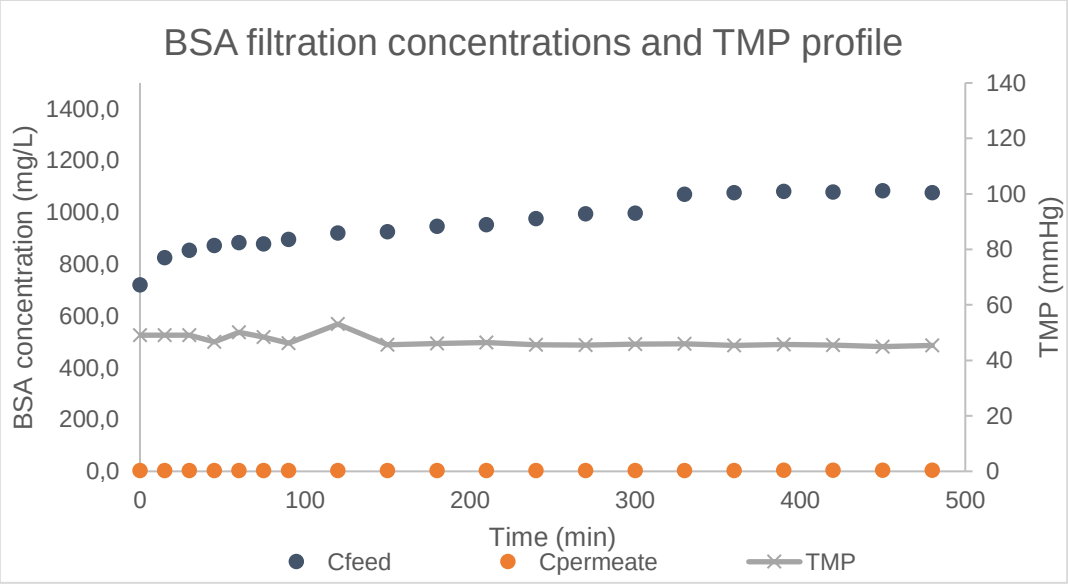

Figure 34: BSA concentration and TMP profile for BSA long-term filtration for CA100 membrane.

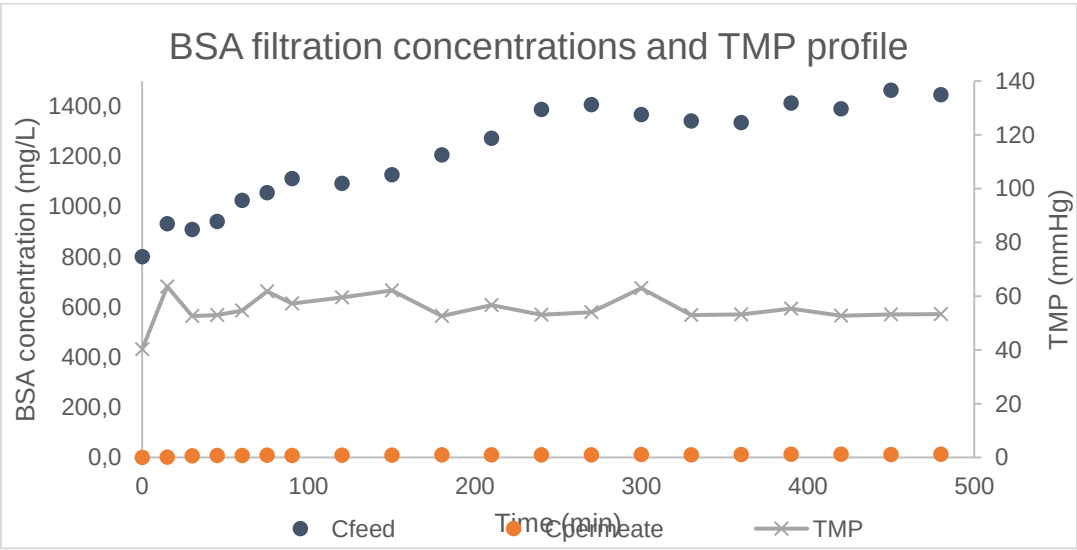

Figure 35: BSA concentration and TMP profile for BSA long-term filtration for CA95-SiO_2-$(CH_2)_3NH_2$ membrane.

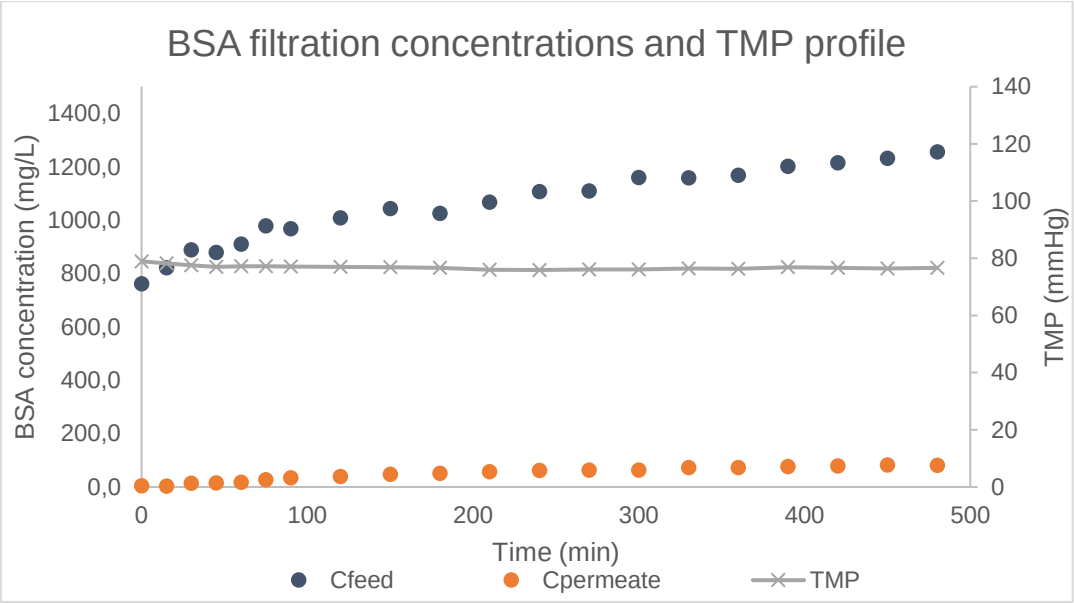

Figure 36: BSA concentration and TMP profile for BSA long-term filtration for CA90-SiO_2-$(CH_2)_3NH_2$-IBF(1) membrane.

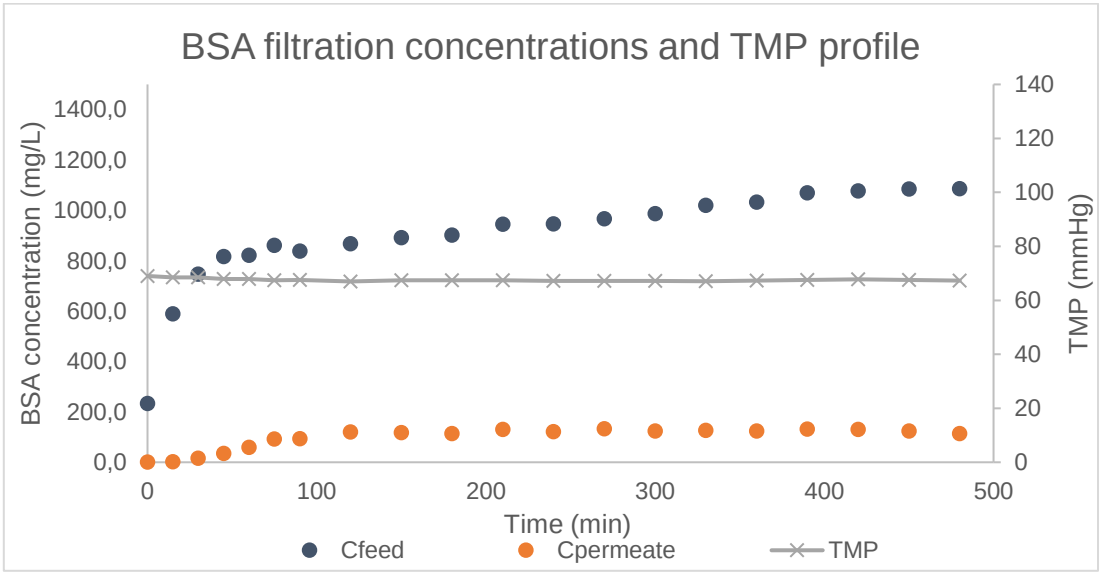

Figure 37: BSA concentration and TMP profile for BSA long-term filtration for CA95-IBF-SiO_2-$(CH_2)_3NH_2$(2).2 membrane.

Another parameter to support the absence of membrane fouling, is the microchannel height of SHDMM that was followed throughout the entire experiment to check for BSA deposition. The values are shown in Figure 38 and comparing with the values measured initially with pure water (shown in Table 8), the results show no evidence of narrowing the microchannel indicating the molecule deposition is negligible.

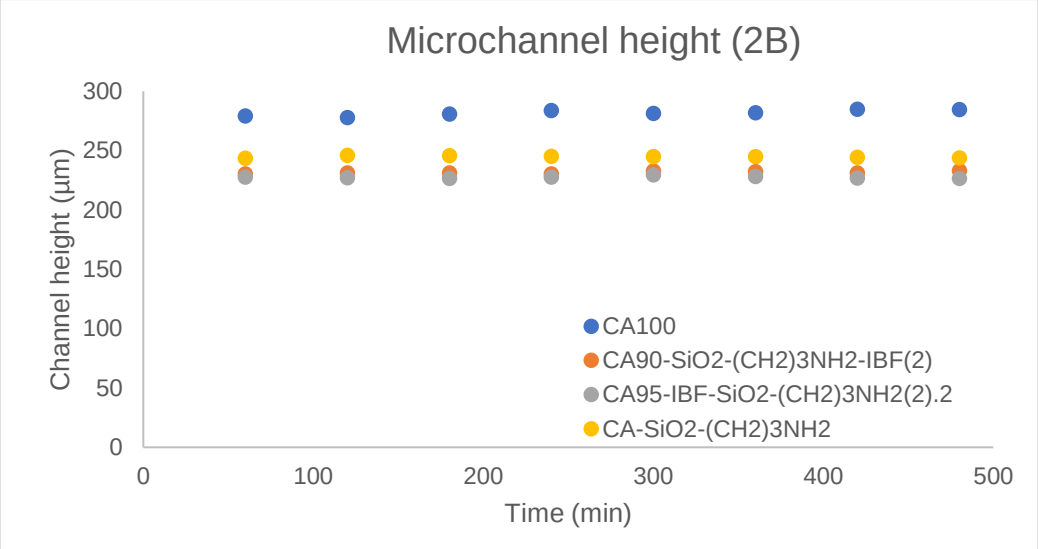

Figure 38: Microchannel height throughout BSA assay for 480 minutes for CA100, CA95-SiO_2-$(CH_2)_3NH_2$, CA90-SiO_2-$(CH_2)_3NH_2$-IBF(1) and CA95-IBF-SiO_2-$(CH_2)_3NH_2$(2).2.

5.6. Conclusions and Future Work

The integral asymmetric, hybrid monophasic cellulose acetate/silica and mixed matrix membranes were characterized and incorporated with novel compounds to enhance PBUT's removal. A $PURE_{G4}$ dendrimer was functionalized with IBF and selected dyes, rose bengal (RB) and methyl red (MR). Also, silica precursors were conjugated with IBF or MR for direct incorporation into the membranes. Membranes with MR and RB, CA99-RB-$PURE_{G4}$ and CA95-SiO_2-$(CH_2)_3NH_2$-MR, stayed colored after the running experiments, proving their incorporation in the CA polymer matrix.

Membranes with 5% and 10% silica content showed similar permeation studies. Hydraulic permeabilities were lower than pristine CA membrane due to steric hindrance and hydrophobicity conferred by the incorporation of IBF. Rejection factors for uric acid were low evidencing efficient removal of small water-soluble molecules. MWCO showed a significantly increase in pore sizes which led to lower BSA rejection.

Overall, the obtained results are very promising since the incorporation of target molecules (*e.g.* ibuprofen, a BSA binding competitor) in these HD especially designed membranes was confirmed to occur using silicon precursors, prepared following simple synthetic protocols. The incorporation of IBF changes some of the membrane properties but the physical properties are maintained.

In future work, further membrane characterization should include information from Scanning Electron Microscope (SEM) and Fourier-Transform Infrared Spectroscopy (FT-IR). Since permeation performance assays for mixed matrix membranes using $PURE_{G4}$ dendrimers were not performed due to time constrains, this data should be acquired. Also, repeating experiments with different concentrations and different approaches should help to achieve more conclusive results on these novel HD systems.

6 References

[1] N. R. Hill *et al.*, “Global prevalence of chronic kidney disease - A systematic review and meta-analysis,” *PLoS One*, vol. 11, no. 7, pp. 1–18, 2016, doi: 10.1371/journal.pone.0158765.

[2] B. Bikbov *et al.*, “Global, regional, and national burden of chronic kidney disease, 1990–2017: a systematic analysis for the Global Burden of Disease Study 2017,” *Lancet*, vol. 395, no. 10225, pp. 709–733, 2020, doi: 10.1016/S0140-6736(20)30045-3.

[3] M. Faria and M. N. de Pinho, “Challenges of reducing protein-bound uremic toxin levels in chronic kidney disease and end stage renal disease,” *Transl. Res.*, pp. 1–20, 2020, doi: 10.1016/j.trsl.2020.09.001.

[4] J. Himmelfarb, R. Vanholder, R. Mehrotra, and M. Tonelli, “The current and future landscape of dialysis,” *Nat. Rev. Nephrol.*, vol. 16, no. 10, pp. 573–585, 2020, doi: 10.1038/s41581-020-0315-4.

[5] M. Faria, C. Moreira, T. Eusébio, P. Brogueira, and M. N. de Pinho, “Hybrid flat sheet cellulose acetate/silicon dioxide ultrafiltration membranes for uremic blood purification,” *Cellulose*, vol. 27, no. 7, pp. 3847–3869, 2020, doi: 10.1007/s10570-020-02985-2.

[6] A. of Achievement, “Willem J. Kolff,” *4 October*, 2021. https://achievement.org/achiever/willem-j-kolff/ (accessed Oct. 27, 2021).

[7] F. M. Canals, “Convection versus diffusion: Is it time to make a change?,” *Nefrologia*, vol. 29, no. 6, pp. 589–58993, 2009, doi: 10.3265/Nefrologia.2009.29.6.5665.en.full.

[8] W. L. Henrich, *Principles and Practice of Dialysis*, Fourth edi. Lippincott Williams & Wilkins, 2009.

[9] R. Vanholder *et al.*, “The role of EUTox in uremic toxin research,” *Semin. Dial.*, vol. 22, no. 4, pp. 323–328, 2009, doi: 10.1111/j.1525-139X.2009.00574.x.

[10] R. Vanholder, R. De Smet, G. Glorieux, and A. Argilés, “Review on uremic toxins: Classification , concentration , and interindividual variability,” *Kidney Int.*, vol. 63, pp. 1934–1943, 2003, doi: 10.1046/j.1523-1755.2003.00924.x.

[11] J. F. Winchester and P. F. Audia, “Extracorporeal strategies for the removal of middle molecules,” *Semin. Dial.*, vol. 19, no. 2, pp. 110–114, 2006, doi: 10.1111/j.1525-139X.2006.00135.x.

[12] G. Glorieux and R. Vanholder, “New uremic toxins -Which solutes should be removed?,” *Hemodiafiltration - A New Era*, vol. 168, pp. 117–128, 2010, doi: 10.1002/9783805595612.ch12.

[13] S. Lekawanvijit, A. R. Kompa, and H. Krum, “Protein-bound uremic toxins: A long overlooked culprit in cardiorenal syndrome,” *Am. J. Physiol. - Ren. Physiol.*, vol. 311, no. 1, pp. F52–F62, 2016, doi: 10.1152/ajprenal.00348.2015.

[14] S. Daneshamouz, U. Eduok, A. Abdelrasoul, and A. Shoker, “Protein-bound uremic toxins (PBUTs) in chronic kidney disease (CKD) patients: Production pathway, challenges and recent

advances in renal PBUTs clearance," *NanoImpact*, vol. 21, no. January, p. 100299, 2021, doi: 10.1016/j.impact.2021.100299.

[15] N. Neirynck, G. Glorieux, E. Schepers, A. Pletinck, A. Dhondt, and R. Vanholder, "Review of Protein-Bound Toxins, Possibility for Blood Purification Therapy," *Blood Purif.*, vol. 35, no. suppl 1, pp. 45–50, 2013, doi: 10.1159/000346223.

[16] F. C. Barreto *et al.*, "Serum indoxyl sulfate is associated with vascular disease and mortality in chronic kidney disease patients," *Clin. J. Am. Soc. Nephrol.*, vol. 4, no. 10, pp. 1551–1558, 2009, doi: 10.2215/CJN.03980609.

[17] L. Sultatos, "Drug reservoirs," *xPharm Compr. Pharmacol. Ref.*, pp. 1–2, 2007, doi: 10.1016/B978-008055232-3.60026-1.

[18] V. Maheshwari, X. Tao, S. Thijssen, and P. Kotanko, "Removal of protein-bound uremic toxins using binding competitors in hemodialysis: A narrative review," *Toxins (Basel).*, vol. 13, no. 9, 2021, doi: 10.3390/toxins13090622.

[19] Y. Itoh, A. Ezawa, K. Kikuchi, Y. Tsuruta, and T. Niwa, "Protein-bound uremic toxins in hemodialysis patients measured by liquid chromatography/tandem mass spectrometry and their effects on endothelial ROS production," *Anal. Bioanal. Chem.*, vol. 403, no. 7, pp. 1841–1850, 2012, doi: 10.1007/s00216-012-5929-3.

[20] C. Basile *et al.*, "Frontiers in hemodialysis: Innovations and technological advances," *Artif. Organs*, vol. 45, no. 2, pp. 175–182, 2021, doi: 10.1111/aor.13798.

[21] T. Shafi and A. S. Levey, "Measurement and Estimation of Residual Kidney Function in Patients on Dialysis," *Adv. Chronic Kidney Dis.*, vol. 25, no. 1, pp. 93–104, Jan. 2018, doi: 10.1053/j.ackd.2017.09.001.

[22] M. K. van Gelder *et al.*, "Protein-bound uremic toxins in hemodialysis patients relate to residual kidney function, are not influenced by convective transport, and do not relate to outcome," *Toxins (Basel).*, vol. 12, no. 4, 2020, doi: 10.3390/toxins12040234.

[23] Y. Obi *et al.*, "Incremental Hemodialysis, Residual Kidney Function, and Mortality Risk in Incident Dialysis Patients: A Cohort Study," *Am. J. Kidney Dis.*, vol. 68, no. 2, pp. 256–265, Aug. 2016, doi: 10.1053/j.ajkd.2016.01.008.

[24] D. Shemin, A. G. Bostom, P. Laliberty, and L. D. Dworkin, "Residual renal function and mortality risk in hemodialysis patients," *Am. J. Kidney Dis.*, vol. 38, no. 1, pp. 85–90, 2001, doi: 10.1053/ajkd.2001.25198.

[25] W. C. Liu, Y. Tomino, and K. C. Lu, "Impacts of indoxyl sulfate and p-Cresol sulfate on chronic kidney disease and mitigating effects of AST-120," *Toxins (Basel).*, vol. 10, no. 9, pp. 1–22, 2018, doi: 10.3390/toxins10090367.

[26] N. Jourde-Chiche and S. Burtey, "Accumulation of protein-bound uremic toxins: the kidney

remains the leading culprit in the gut-liver-kidney axis," *Kidney Int.*, vol. 97, no. 6, pp. 1102–1104, 2020, doi: 10.1016/j.kint.2020.02.026.

[27] W. Van Biesen and S. Eloot, "Enhanced removal of protein-bound uremic toxins using displacers: Road to success?," *Clin. J. Am. Soc. Nephrol.*, vol. 14, no. 3, pp. 324–326, 2019, doi: 10.2215/CJN.00500119.

[28] S. Yamamoto *et al.*, "Continuous Reduction of Protein-Bound Uraemic Toxins with Improved Oxidative Stress by Using the Oral Charcoal Adsorbent AST-120 in Haemodialysis Patients," *Sci. Rep.*, vol. 5, no. August, pp. 3–10, 2015, doi: 10.1038/srep14381.

[29] R. H. Cha *et al.*, "A randomized, controlled trial of oral intestinal sorbent AST-120 on renal function deterioration in patients with advanced renal dysfunction," *Clin. J. Am. Soc. Nephrol.*, vol. 11, no. 4, pp. 559–567, 2016, doi: 10.2215/CJN.12011214.

[30] M. Asai, S. Kumakura, and M. Kikuchi, "Review of the efficacy of AST-120 (KREMEZIN®) on renal function in chronic kidney disease patients," *Ren. Fail.*, vol. 41, no. 1, pp. 47–56, 2019, doi: 10.1080/0886022X.2018.1561376.

[31] Y. K. Kee *et al.*, "Comparison of different types of oral adsorbent therapy in patients with chronic kidney disease: A multicenter, randomized, phase iv clinical trial," *Yonsei Med. J.*, vol. 62, no. 1, pp. 41–49, 2021, doi: 10.3349/ymj.2021.62.1.41.

[32] J. Li, L. Han, J. Xie, S. Liu, and L. Jia, "Multi-sites polycyclodextrin adsorbents for removal of protein-bound uremic toxins combining with hemodialysis," *Carbohydr. Polym.*, vol. 247, no. March, p. 116665, 2020, doi: 10.1016/j.carbpol.2020.116665.

[33] S. R. Sandeman *et al.*, "An adsorbent monolith device to augment the removal of uraemic toxins during haemodialysis," *J. Mater. Sci. Mater. Med.*, vol. 25, no. 6, pp. 1589–1597, 2014, doi: 10.1007/s10856-014-5173-9.

[34] S. Yamamoto *et al.*, "Adsorption of Protein-Bound Uremic Toxins Through Direct Hemoperfusion With Hexadecyl-Immobilized Cellulose Beads in Patients Undergoing Hemodialysis," *Artif. Organs*, vol. 42, no. 1, pp. 88–93, 2018, doi: 10.1111/aor.12961.

[35] Z. Chao *et al.*, "Hemocompatible MOF-decorated pollen hemoperfusion absorbents for rapid and highly efficient removal of protein-bound uremic toxins," *Mater. Chem. Front.*, vol. 5, no. 20, pp. 7617–7627, 2021, doi: 10.1039/D1QM01071A.

[36] D. Pavlenko *et al.*, "New low-flux mixed matrix membranes that offer superior removal of protein-bound toxins from human plasma," *Sci. Rep.*, vol. 6, no. June, pp. 1–9, 2016, doi: 10.1038/srep34429.

[37] I. Geremia, R. Bansal, and D. Stamatialis, "In vitro assessment of mixed matrix hemodialysis membrane for achieving endotoxin-free dialysate combined with high removal of uremic toxins from human plasma," *Acta Biomater.*, vol. 90, pp. 100–111, 2019, doi:

10.1016/j.actbio.2019.04.009.

[38] C. Legallais *et al.*, “Bioengineering Organs for Blood Detoxification,” *Adv. Healthc. Mater.*, vol. 7, no. 21, pp. 1–32, 2018, doi: 10.1002/adhm.201800430.

[39] C. M. S. Schophuizen *et al.*, “Development of a living membrane comprising a functional human renal proximal tubule cell monolayer on polyethersulfone polymeric membrane,” *Acta Biomater.*, vol. 14, pp. 22–32, 2015, doi: 10.1016/j.actbio.2014.12.002.

[40] H. Watanabe *et al.*, “Interaction between two sulfate-conjugated uremic toxins, p-cresyl sulfate and indoxyl sulfate, during binding with human serum albumin,” *Drug Metab. Dispos.*, vol. 40, no. 7, pp. 1423–1428, 2012, doi: 10.1124/dmd.112.045617.

[41] N. A. Kratochwil, W. Huber, F. Müller, M. Kansy, and P. R. Gerber, “Predicting plasma protein binding of drugs: A new approach,” *Biochem. Pharmacol.*, vol. 64, no. 9, pp. 1355–1374, 2002, doi: 10.1016/S0006-2952(02)01074-2.

[42] I. Petitpas, A. A. Bhattacharya, S. Twine, M. East, and S. Curry, “Crystal structure analysis of warfarin binding to human serum albumin. Anatomy of drug site I,” *J. Biol. Chem.*, vol. 276, no. 25, pp. 22804–22809, 2001, doi: 10.1074/jbc.M100575200.

[43] X. Tao, S. Thijssen, N. Levin, P. Kotanko, and G. Handelman, “Enhanced Indoxyl Sulfate Dialyzer Clearance with the Use of Binding Competitors,” *Blood Purif.*, vol. 39, no. 4, pp. 323–330, 2015, doi: 10.1159/000381008.

[44] X. Tao *et al.*, “Improved dialytic removal of protein-bound uraemic toxins with use of albumin binding competitors: An in vitro human whole blood study,” *Sci. Rep.*, vol. 6, no. December 2015, pp. 2–10, 2016, doi: 10.1038/srep23389.

[45] M. Madero *et al.*, “Removal of protein-bound uremic toxins during hemodialysis using a binding competitor,” *Clin. J. Am. Soc. Nephrol.*, vol. 14, no. 3, pp. 394–402, 2019, doi: 10.2215/CJN.05240418.

[46] J. Li *et al.*, “Improved dialysis removal of protein-bound uremic toxins by salvianolic acids,” *Phytomedicine*, vol. 57, pp. 166–173, 2019, doi: 10.1016/j.phymed.2018.12.018.

[47] V. Maheshwari, S. Thijssen, X. Tao, D. H. Fuertinger, F. Kappel, and P. Kotanko, “In silico comparison of protein-bound uremic toxin removal by hemodialysis, hemodiafiltration, membrane adsorption, and binding competition,” *Sci. Rep.*, vol. 9, no. 1, pp. 1–13, 2019, doi: 10.1038/s41598-018-37195-1.

[48] Y. Shi, H. Tian, Y. Wang, Y. Shen, Q. Zhu, and F. Ding, “Improved Dialysis Removal of Protein-Bound Uraemic Toxins with a Combined Displacement and Adsorption Technique,” *Blood Purif.*, 2021, doi: 10.1159/000518065.

[49] G. Mendes, M. Faria, A. Carvalho, M. C. Gonçalves, and M. N. de Pinho, “Structure of water in hybrid cellulose acetate-silica ultrafiltration membranes and permeation properties,” *Carbohydr.*

Polym., vol. 189, pp. 342–351, 2018, doi: 10.1016/j.carbpol.2018.02.030.

[50] M. C. Andrade, J. C. Pereira, N. de Almeida, P. Marques, M. Faria, and M. C. Gonçalves, "Improving hydraulic permeability, mechanical properties, and chemical functionality of cellulose acetate-based membranes by co-polymerization with tetraethyl orthosilicate and 3-(aminopropyl)triethoxysilane," *Carbohydrate Polymers*, vol. 261. 2021, doi: 10.1016/j.carbpol.2021.117813.

[51] R. B. Restani, P. I. Morgado, M. P. Ribeiro, I. J. Correia, A. Aguiar-Ricardo, and V. D. B. Bonifácio, "Biocompatible polyurea dendrimers with pH-dependent fluorescence," *Angew. Chemie - Int. Ed.*, vol. 51, no. 21, pp. 5162–5165, 2012, doi: 10.1002/anie.201200362.

[52] R. B. Restani *et al.*, "Nano-in-Micro POxylated Polyurea Dendrimers and Chitosan Dry Powder Formulations for Pulmonary Delivery," *Part. Part. Syst. Charact.*, vol. 33, no. 11, pp. 851–858, 2016, doi: 10.1002/ppsc.201600123.

[53] P. Mota, R. F. Pires, J. Serpa, and V. D. B. Bonifácio, "L-Buthionine sulfoximine detection and quantification in polyurea dendrimer nanoformulations," *Molecules*, vol. 24, no. 17, pp. 2–9, 2019, doi: 10.3390/molecules24173111.

[54] R. Tacke, C. Burschka, I. Richter, B. Wagner, and R. Willeke, "Pentacoordinate silicon compounds with SiO5 skeletons containing SiOH or SiOSi groups: Derivatives of the pentahydroxosilicate(1-) anion [Si(OH)5]- and its anhydride [(HO)4Si-O-Si(OH)4]2-," *J. Am. Chem. Soc.*, vol. 122, no. 35, pp. 8480–8485, 2000, doi: 10.1021/ja000637i.

[55] A. J. Rastegar, M. Vosgueritchian, J. C. Doll, J. R. Mallon, and B. L. Pruitt, "Nanomechanical actuation of a silicon cantilever using an azo dye, self-assembled monolayer," *Langmuir*, vol. 29, no. 23, pp. 7118–7124, 2013, doi: 10.1021/la3034676.

[56] J. Shang, S. Liu, X. Ma, L. Liujin, and Y. Deng, "S.I. A new route of CO2 catalytic activation," *Green Chem.*, no. November, 2012.

[57] A. Janeca, F. S. C. Rodrigues, M. C. Gonçalves, and M. Faria, "Novel Cellulose Acetate-Based Monophasic Hybrid Membranes for Improved Blood Purification Devices: Characterization under Dynamic Conditions," *Membranes (Basel).*, vol. 11, no. 11, p. 825, Oct. 2021, doi: 10.3390/membranes11110825.

[58] A. Janeca, "Characterization of a cellulose acetate-based monophasic hybrid membrane in a single hemodialysis membrane module for blood purification," Instituto Superior Técnico, 2021.

[59] M. Smaïhi, T. Jermoumi, J. Marignan, and R. D. Noble, "Organic-inorganic gas separation membranes: Preparation and characterization," *J. Memb. Sci.*, vol. 116, no. 2, pp. 211–220, 1996, doi: 10.1016/0376-7388(96)00042-7.

[60] M. Guglielmi, "Sol-gel science," *Materials Chemistry and Physics*, vol. 26, no. 2. pp. 211–212, 1990, doi: 10.1016/0254-0584(90)90039-d.

[61] A. Kumari, A. Choudhury, and G. Sarkhel, “Effect of tetraethyl orthosilicate on the structural, thermal, and morphological properties of a cellulose acetate membrane,” *Prog. Rubber, Plast. Recycl. Technol.*, vol. 28, no. 3, pp. 111–126, 2012, doi: 10.1177/147776061202800302.

[62] S. Loeb and S. Sourirjan, “Sea Water Demineralization by Means of an Osmotic Membrane,” in *Sea Water Demineralization by Means of an Osmotic Membrane*, 1963, pp. 117–132.

[63] L. Pageau and S. Sourirajan, “Improvement of porous cellulose acetate reverse osmosis membranes by change of casting conditions,” *J. Appl. Polym. Sci.*, vol. 16, no. 12, pp. 3185–3206, Dec. 1972, doi: 10.1002/app.1972.070161212.

[64] B. Kunst and S. Sourirajan, “An approach to the development of cellulose acetate ultrafiltration membranes,” *J. Appl. Polym. Sci.*, vol. 18, no. 11, pp. 3423–3434, 1974, doi: 10.1002/app.1974.070181121.

[65] H. Strathmann and K. Kock, “The formation mechanism of phase inversion membranes,” *Desalination*, vol. 21, no. 3, pp. 241–255, 1977, doi: 10.1016/S0011-9164(00)88244-2.

[66] S. Zare and A. Kargari, “Membrane properties in membrane distillation,” in *Emerging Technologies for Sustainable Desalination Handbook*, Elsevier, 2018, pp. 107–156.

[67] SigmaAldrich, “Sigma Aldrich - Methyl Red.” https://www.sigmaaldrich.com/PT/en/product/sial/250198 (accessed Aug. 11, 2021).

[68] F. Pichot, “Characterization of hybrid flat sheet cellulose acetate/silicon dioxide ultrafiltration membranes for uremic blood purification,” Lisbon, 2018.

[69] N. KRISHNAN, “Transmembrane Pressure,” *Yale University School of Medicine*. https://hemodialysiskinetics.coursepress.yale.edu/the-basics-tmp/ (accessed Sep. 18, 2021).

[70] L. I. Amar *et al.*, “Erythrocyte fouling on micro-engineered membranes,” *Biomed. Microdevices*, vol. 20, no. 3, pp. 1–11, 2018, doi: 10.1007/s10544-018-0297-1.

[71] R. B. Bird, W. E. Stewart, and E. N. Lightfoot, *Transport Phenomena - 2nd Edition*, vol. 52, no. 3. University of Wiscousin-Madison: John Wiley & Sons, Inc., 2002.

[72] B. Blood, Q. Lu, Q. Lu, B. V Hofferbert, G. Koo, and R. A. Malinauskas, “In Vitro Shear Stress-Induced Platelet Activation : Sensitivity of Human and In Vitro Shear Stress-Induced Platelet Activation : Sensitivity of Human and Bovine Blood,” no. June 2013, 2020, doi: 10.1111/aor.12099.

[73] S. S. Lee, M. R. Hardeman, A. Medisch, and C. Universiteit, “Shear induced damage of red blood cells monitored by the decrease of their deformability,” no. January 2014, 2004.

[74] L. S. Araujo, F. R. M. Laurindo, D. C. Fernandes, and L. Y. Tanaka, “Hemodynamic Forces in the Endothelium: From Mechanotransduction to Implications on Development of Atherosclerosis,” in *Endothelium and Cardiovascular Diseases*, Elsevier Inc., 2018, pp. 85–95.

[75] A. S. Michaels and H. Strathmann, “Preparation and Characterization of Ion-Exchange Membranes,” in *Journal of Membrane Science*, vol. 15, no. 1, Elsevier, 2004, pp. 89–146.

[76] S. De and A. Roy, *Hemodialysis Membranes, For Engineers to Medical Practitioners*. 2017.

[77] S. Filtration, “Definition of Molecular Weight Cut-Off.” https://synderfiltration.com/learning-center/articles/membranes/molecular-weight-cut-off/ (accessed Oct. 01, 2021).

[78] F. Duranton *et al.*, “Normal and Pathologic Concentrations of Uremic Toxins,” *J. Am. Soc. Nephrol.*, vol. 23, no. 7, pp. 1258–1270, Jul. 2012, doi: 10.1681/ASN.2011121175.

[79] M. M. Bradford, “A Rapid and Sensitive Method for the Quantitation of Microgram Quantities of Protein Utilizing the Principle of Protein-Dye Binding,” *Anal. Biochem.*, no. 72, pp. 248–254, 1976.

[80] T. Zor and Z. Selinger, “Linearization of the Bradford protein assay increases its sensitivity: Theoretical and experimental studies,” *Anal. Biochem.*, vol. 236, no. 2, pp. 302–308, 1996, doi: 10.1006/abio.1996.0171.

[81] J. E. Flythe, S. E. Kimmel, and S. M. Brunelli, “Rapid fluid removal during dialysis is associated with cardiovascular morbidity and mortality,” *Kidney Int.*, vol. 79, no. 2, pp. 250–257, 2011, doi: 10.1038/ki.2010.383.

[82] C. C. Magee, J. K. Tucker, and A. K. Singh, *Core Concepts in Dialysis and Continuous Therapies*. Boston, MA: Springer US, 2016.

[83] V. D. Hoang, D. T. H. Ly, N. H. Tho, and H. Minh Thi Nguyen, “UV spectrophotometric simultaneous determination of paracetamol and ibuprofen in combined tablets by derivative and wavelet transforms,” *Sci. World J.*, vol. 2014, 2014, doi: 10.1155/2014/313609.

[84] H. H. Jasim and N. K. Abed, “Determination of Ibuprpfen in Aqueaus Solutions and Pharmacetical Preparations by UV-VIS Spectrophotometric,” *J. Al-Nahrain Univ.*, vol. 18, no. 2, pp. 1–9, 2015, doi: 10.22401/jnus.18.2.01.

[85] D. A. Belinskaia, P. A. Voronina, A. A. Batalova, and N. V Goncharov, “Serum Albumin,” *Encyclopedia*, vol. 1, no. 1, pp. 65–75, Dec. 2020, doi: 10.3390/encyclopedia1010009.

[86] T. Scientific, “Type 1 Ultrapure Water Systems.” https://www.thermofisher.com/pt/en/home/life-science/lab-equipment/lab-water-purification/type-1-ultrapure-water-systems.html (accessed Oct. 01, 2021).

7 Annex

7.1. Reaction Mechanisms

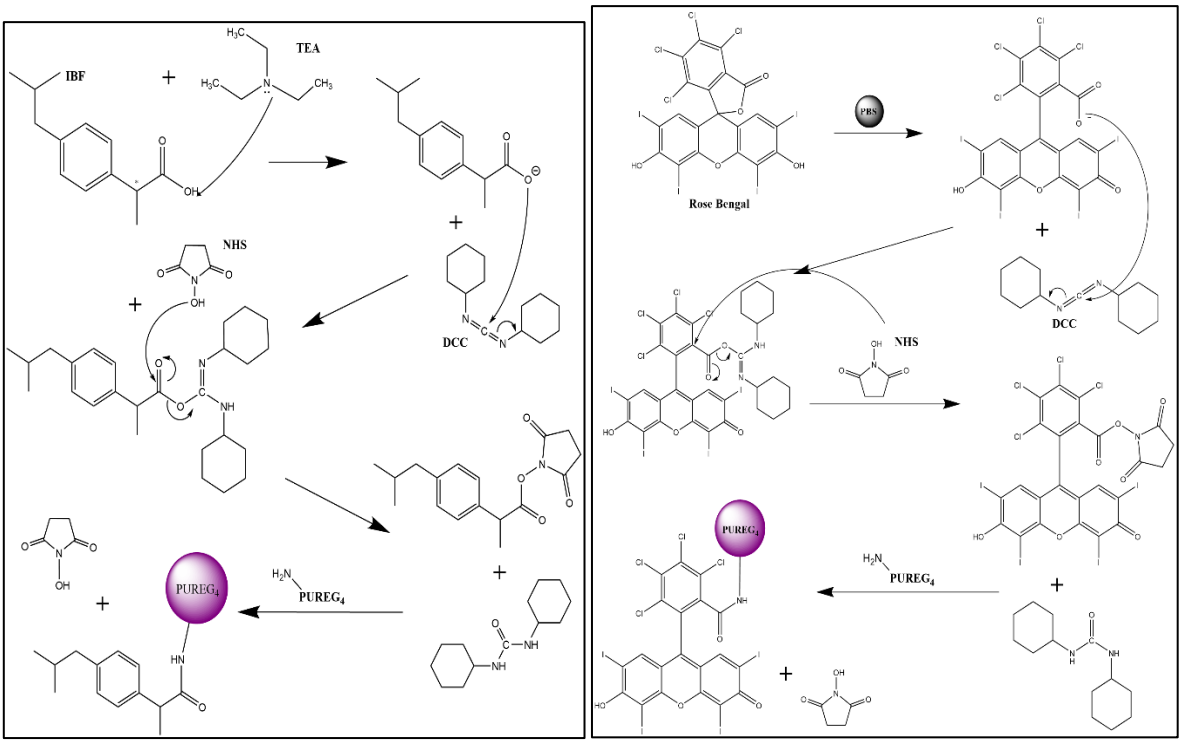

Figure A 1: Mechanisms of synthesis of IBF-PURE$_{G4}$ (left) and RB-PURE$_{G4}$ (right).

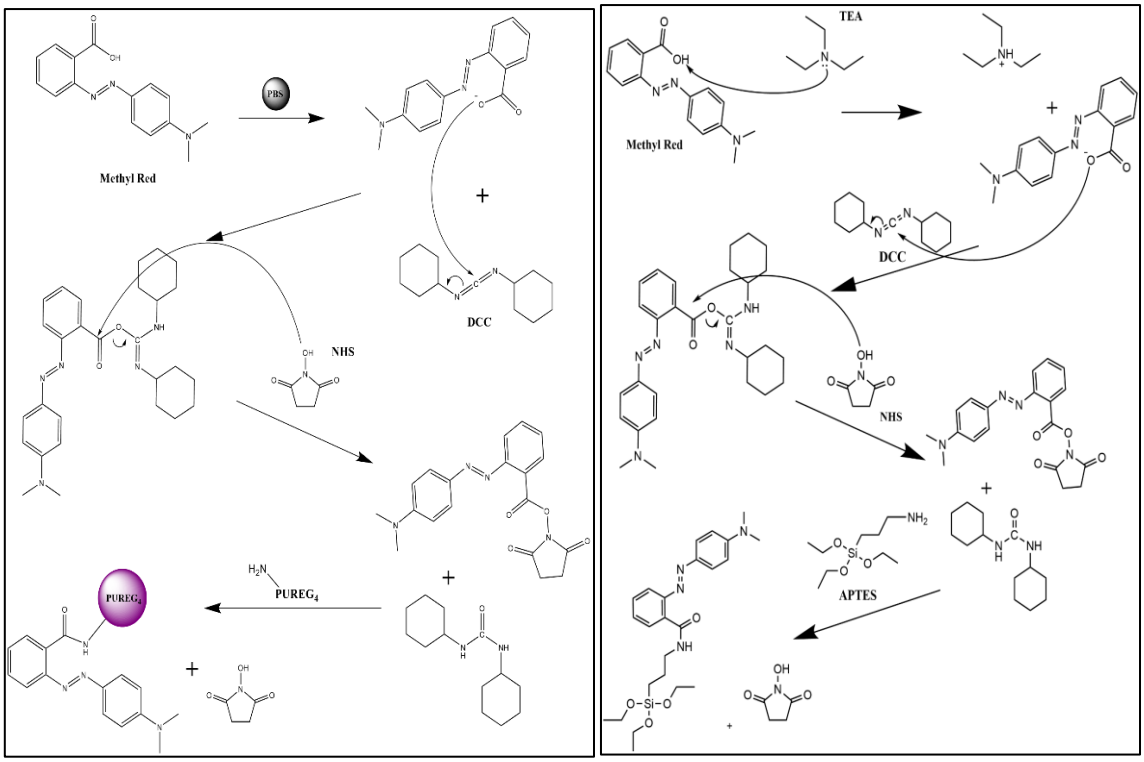

Figure A 2: Mechanisms of synthesis of MR-PURE$_{G4}$ (left) and MR-APTES (right).

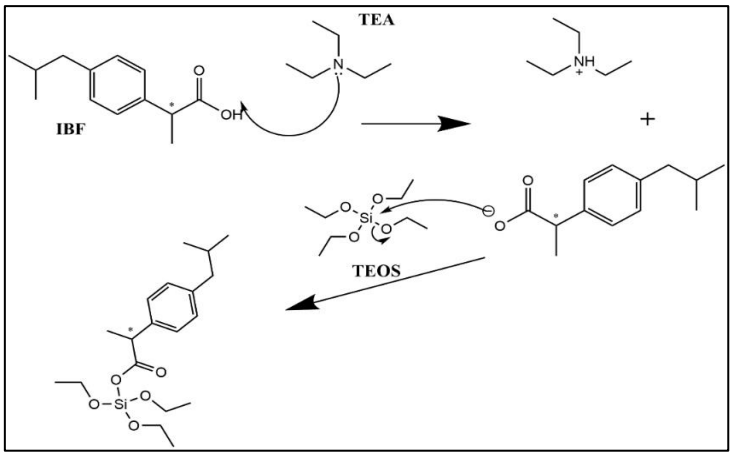

Figure A 3: Mechanism of synthesis of IBF-TEOS.

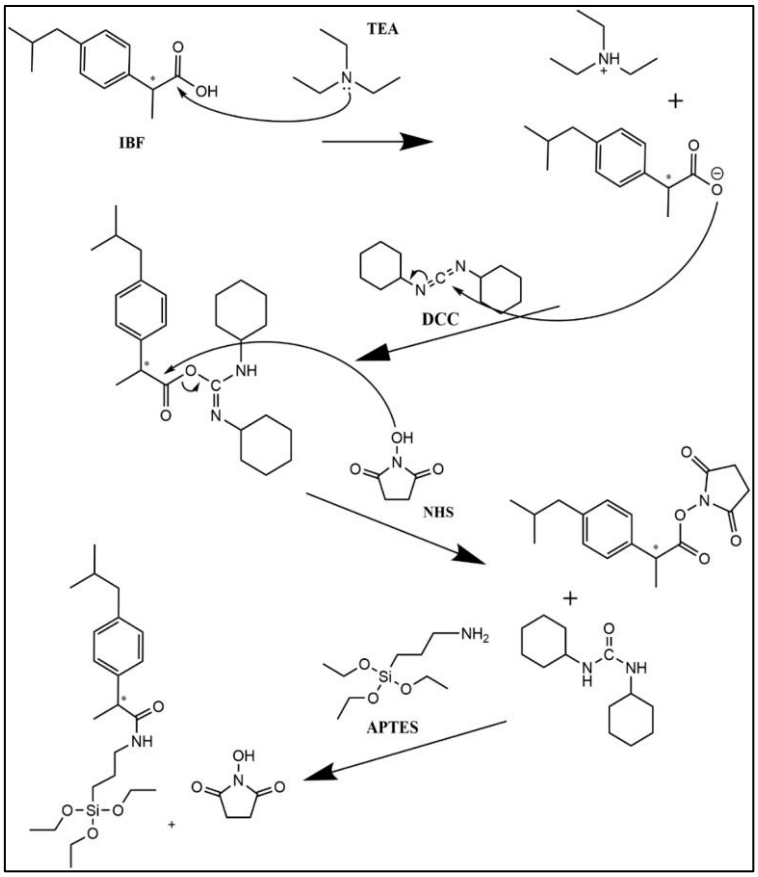

Figure A 4: Mechanism of synthesis of IBF-APTES.

7.2. Hydraulic Permeability

Feed flowrates with corresponding permeate flowrate, permeate flux, TMP and pressure drop for all membranes and sheets tested are tabled below.

Table A 1: Hydraulic permeability values described values for CA100 membrane.

CA100					
Feed Flowrate (mL/min)	**Permeate Flowrate (mL/min)**	**Flux (mL/min.cm^2)**	**TMP (mmHg)**	**ΔP**	**Lp**
28,44	0,290	0,0028	13,1	12,5	1,17E-04
51,66	0,343	0,0033	19,8	24,0	
76,06	0,435	0,0041	30,7	41,1	mL/min.cm^2.mmHg
98,98	0,575	0,0055	45,8	52,0	70,20
122,49	0,712	0,0068	61,6	69,5	
130,82	0,717	0,0068	62,9	82,0	mL/h.m^2.mmHg

Table A 2: Hydraulic permeability values described values for CA95-SiO_2-$(CH_2)_3NH_2$-MR membrane.

CA95-SiO_2-$(CH_2)_3NH_2$-MR					
Feed Flowrate (mL/min)	**Permeate Flowrate (mL/min)**	**Flux (mL/min.cm2)**	**TMP (mmHg)**	**ΔP**	**Lp**
28,44	0,869	0,0140	16,1	4,4	1,85E-04
51,66	0,863	0,0139	16,8	7,7	
76,06	0,977	0,0157	22,3	13,6	mL/min.cm^2.mmHg
98,98	0,986	0,0159	26,9	18,0	
122,49	0,990	0,0159	34,5	24,9	
130,82	0,988	0,0159	40,4	30,1	111,00
146,72	0,830	0,0134	47,8	38,7	
177,73	0,770	0,0124	55,6	47,2	mL/h.m^2.mmHg
194,01	0,951	0,0153	61,8	52,1	
214,24	0,828	0,0133	74,0	62,7	
231,17	0,798	0,0129	81,0	68,5	
255,67	0,861	0,0139	91,3	77,9	
269,38	0,953	0,0153	98,6	84,6	
283,53	1,100	0,0177	113,5	94,0	
304,15	1,158	0,0186	118,8	102,1	
321,65	1,235	0,0199	133,6	107,9	

Table A 3: Hydraulic permeability values described values for CA90-SiO_2-$(CH_2)_3NH_2$-IBF membrane both sheets.

CA90-SiO_2-$(CH_2)_3NH_2$-IBF(1)					
Feed Flowrate (mL/min)	**Permeate Flowrate (mL/min)**	**Flux (mL/min.cm2)**	**TMP (mmHg)**	**ΔP**	**Lp**
28,44	0,245	0,0023	17,4	11,5	1,00E-04
51,66	0,292	0,0028	23,0	22,3	

76,06	0,372	0,0035	32,5	38,7	mL/min.cm^2.mmHg
98,98	0,425	0,0041	39,9	49,9	
122,49	0,525	0,0050	51,8	67,5	
130,82	0,601	0,0057	60,6	80,1	60,00
146,72	0,713	0,0068	74,1	98,6	
177,73	0,835	0,0080	88,2	117,1	mL/h.m^2.mmHg
194,01	0,913	0,0087	97,4	128,9	
214,24	1,046	0,0100	111,8	147,1	
CA90-SiO_2-$(CH_2)_3NH_2$-IBF(2)					
Feed Flowrate (mL/min)	**Permeate Flowrate (mL/min)**	**Flux (mL/min.cm2)**	**TMP (mmHg)**	**ΔP**	**Lp**
28,44	0,068	0,0006	5,1	10,9	4,28E-05
51,66	0,084	0,0008	12,1	23,1	
76,06	0,113	0,0011	22,9	41,1	mL/min.cm^2.mmHg
98,98	0,141	0,0013	31,1	53,7	
122,49	0,206	0,0020	45,4	74,7	
130,82	0,230	0,0022	55,1	88,5	25,68
146,72	0,259	0,0025	70,7	109,0	
177,73	0,309	0,0029	86,1	128,6	mL/h.m^2.mmHg
194,01	0,325	0,0031	97,2	141,5	
214,24	0,392	0,0037	114,5	161,5	

Table A 4: Hydraulic permeability values described values for CA-5-SiO_2-IBF membrane for both batches.

CA95-IBF-SiO_2-$(CH_2)_3NH_2$(1).1					
Feed Flowrate (mL/min)	**Permeate Flowrate (mL/min)**	**Flux (mL/min.cm2)**	**TMP (mmHg)**	**ΔP**	**Lp**
28,44	0,219	0,0021	10,1	17,4	5,35E-05
51,66	0,235	0,0022	20,1	35,1	
76,06	0,245	0,0023	34,8	60,3	mL/min.cm^2.mmHg
98,98	0,254	0,0024	44,6	76,9	
122,49	0,310	0,0030	59,8	102,0	
130,82	0,340	0,0032	71,4	120,0	32,10
146,72	0,384	0,0037	89,4	145,6	
177,73	0,428	0,0041	107,2	171,8	mL/h.m^2.mmHg
194,01	0,470	0,0045	119,2	188,4	
214,24	0,510	0,0049	137,6	213,3	
CA95-IBF-SiO_2-$(CH_2)_3NH_2$(2).1					
Feed Flowrate (mL/min)	**Permeate Flowrate (mL/min)**	**Flux (mL/min.cm2)**	**TMP (mmHg)**	**ΔP**	**Lp**
28,44	0,120	0,0011	18,4	13,7	5,64E-05
51,66	0,148	0,0014	22,8	25,8	
76,06	0,210	0,0020	34,1	44,4	mL/min.cm^2.mmHg

98,98	0,247	0,0024	41,6	56,8	
122,49	0,325	0,0031	55,1	76,6	
130,82	0,370	0,0035	64,5	90,4	33,84
146,72	0,514	0,0049	78,7	110,0	
177,73	0,666	0,0063	93,5	130,0	
194,01	0,702	0,0067	103,8	143,4	mL/h.m^2.mmHg
214,24	0,851	0,0081	119,2	163,2	
CA95-IBF-SiO_2-$(CH_2)_3NH_2$(2).2					
Feed Flowrate (mL/min)	**Permeate Flowrate (mL/min)**	**Flux (mL/min.cm2)**	**TMP (mmHg)**	**ΔP**	**Lp**
28,44	0,084	0,0008	15,1	11,9	4,99E-05
51,66	0,132	0,0013	21,4	23,6	
76,06	0,184	0,0018	32,3	41,1	
98,98	0,210	0,0020	39,7	53,0	mL/min.cm^2.mmHg
122,49	0,265	0,0025	52,5	71,7	
130,82	0,314	0,0030	61,5	84,7	29,94
146,72	0,404	0,0039	75,2	103,4	
177,73	0,460	0,0044	89,7	122,3	
194,01	0,497	0,0047	99,4	134,3	mL/h.m^2.mmHg
214,24	0,548	0,0052	114,0	152,0	

7.3. Calibration Curves

7.3.1. Pump Calibration

Table A 5: Pump calibration values used in Artificial Kidney installation.

Pump Position	Feed Flowrate (mL/min)
1	28,44
2	51,66
3	76,06
4	98,98
5	122,49
6	130,82
7	146,72
8	177,73
9	194,01
10	214,24
11	231,17
12	255,67
13	269,38
14	283,53
15	304,15
16	321,65

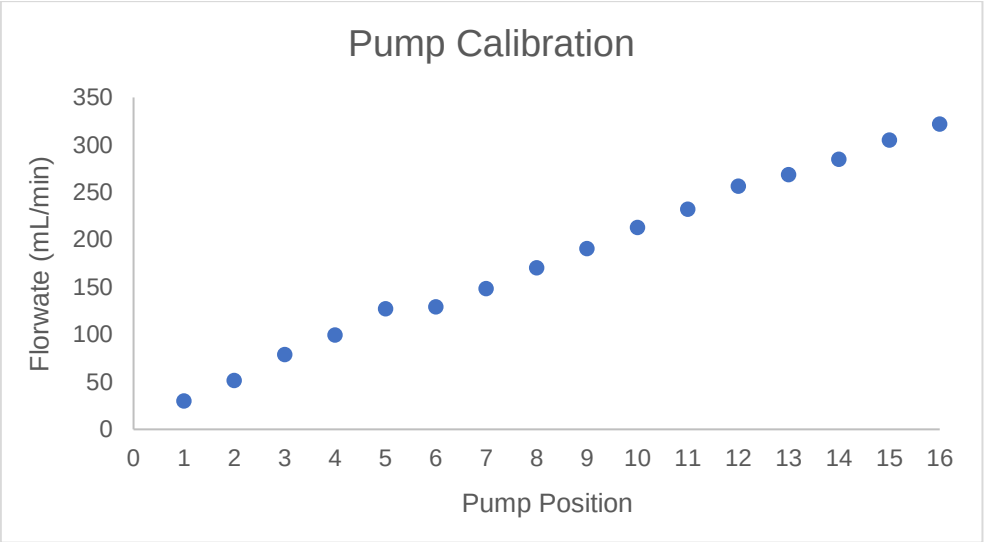

Figure A 5: Calibration Line for pump used in laboratory set-up.

7.3.2. Small Water-Soluble Toxins

Calibration curves for small water-soluble toxins used in this study: creatinine (13), urea (14) and uric acid (15). Detection was made in UV-visible spectrophotometer at corresponding wavelength with quartz cells with pure deionized water as the blank cell.

$$C_{creatinine}\left(\frac{mg}{L}\right) = 16{,}53 * ABS_{230} \quad (13)$$

Table A 6: Creatinine absorbance calibration values.

λ (nm)	**230**
C (mg/L)	**Abs**
2,5	0,187
5,0	0,342
10,0	0,691
15,0	1,055
25,0	1,762
50,0	2,834

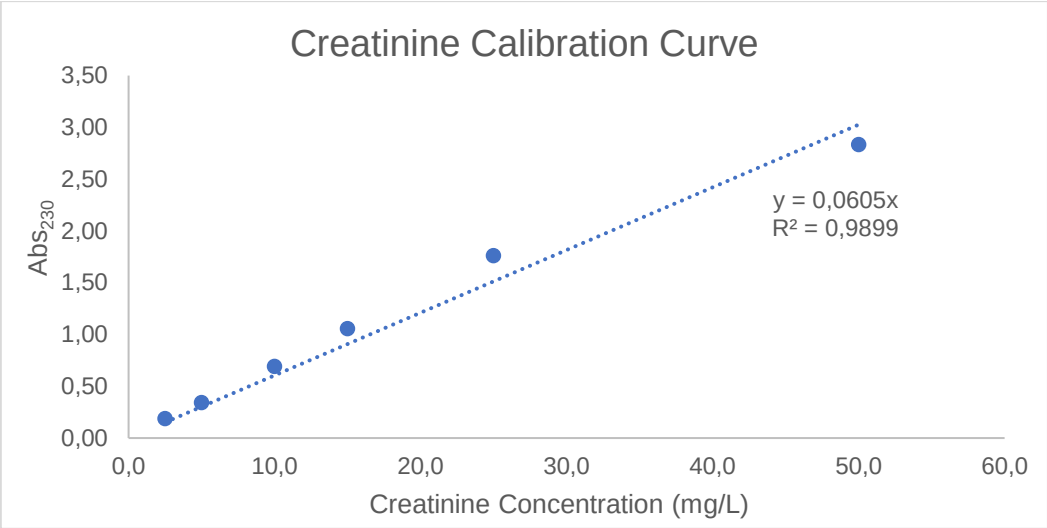

Figure A 6: Calibration curve for creatinine.

$$C_{urea}\left(\frac{g}{L}\right) = 0{,}739 * ABS_{200} \quad (14)$$

Table A 7: Urea absorbance calibration values.

λ (nm)	200
C (g/L)	Abs
0,1	0,192
0,2	0,301
0,4	0,549
0,6	0,797
0,8	1,160
1	1,285

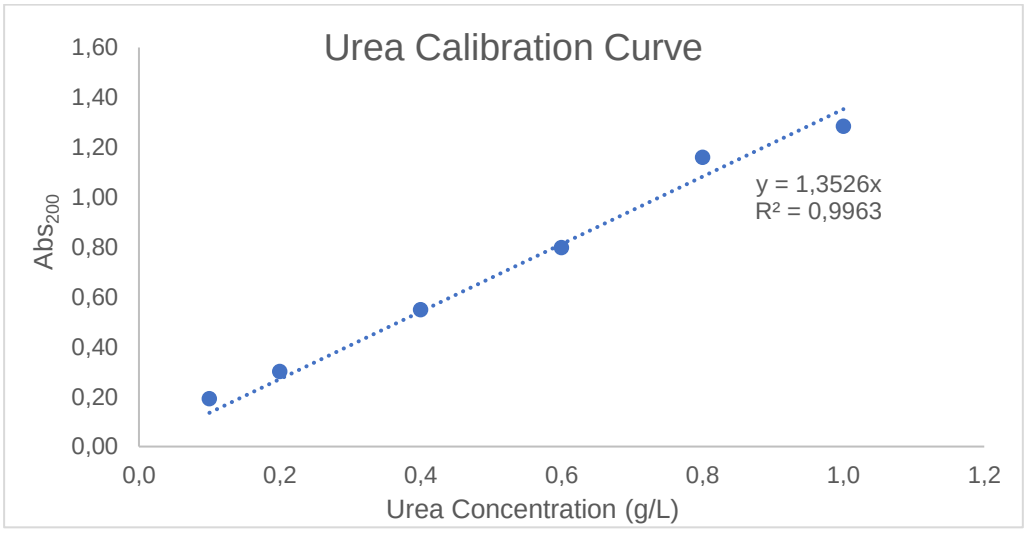

Figure A 7: Urea Calibration curve.

$$C_{uric\ acid}\left(\frac{mg}{L}\right) = 16{,}08 * ABS_{293} \quad (15)$$

Table A 8: Uric Acid absorbance calibration values.

λ (nm)	293
C (mg/L)	ABS
1,5	0,116
3,0	0,203
6,0	0,393
15,0	0,933
25,0	1,545

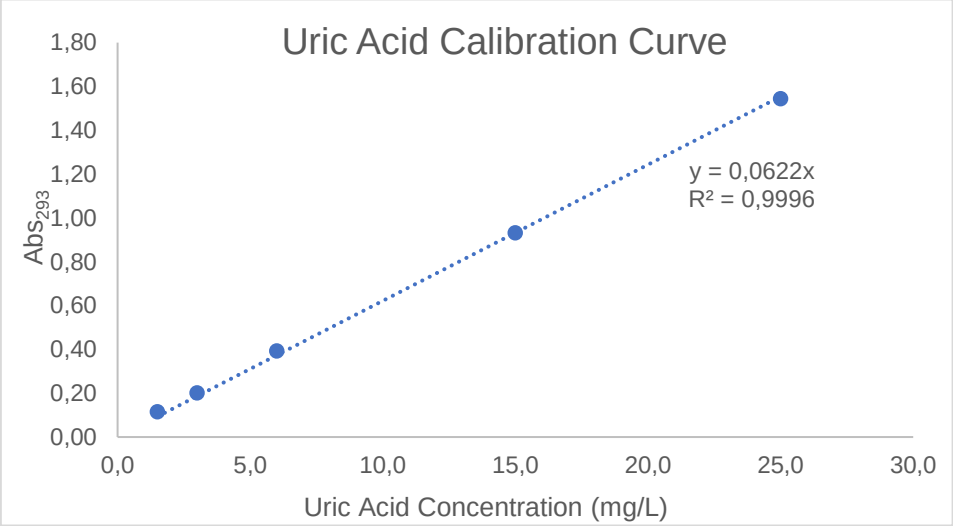

Figure A 8: Uric Acid calibration curve.

7.3.3. PEG's and DEXTRAN's Calibration Line

For Molecular Weight Cut-Off (MWCO) determination, calibration curves for all polyethylenglycol (3000, 6000, 10000, 20000, 35000) and Dextran (T40 and T70) were needed. For that, Total Organic Carbon (TOC) equipment was used, and all concentrations and the blank cell prepared with Mili-Q water (Only Type1 – Ultrapure water can be used, with a resistivity of 18,2 MΩ.cm at 25ºC [86], to eliminate the risks of costly equipment damage and incorrect research data due to contaminating impurities.).

Table A 9: Calibration curves values for PEG polymers with Total Organic Carbon.

Concentration (mg/L)	Polyethylenglycol Total Organic Carbon (mg/L)				
	3000	6000	10000	20000	35000
1000	525,0	583,6	525,3	574,6	571,8

500	247,5	278,2	247,8	301,3	267,5
400	198,0	222,9	215,2	219,6	215,2
300	152,5	167,6	166,0	164,1	160,8
200	96,9	111,5	110,0	109,8	109,3
100	47,1	55,7	51,9	54,1	53,7
50	24,2	35,1	26,3	25,4	25,5
25	11,5	10,3	12,6	13,2	12,0

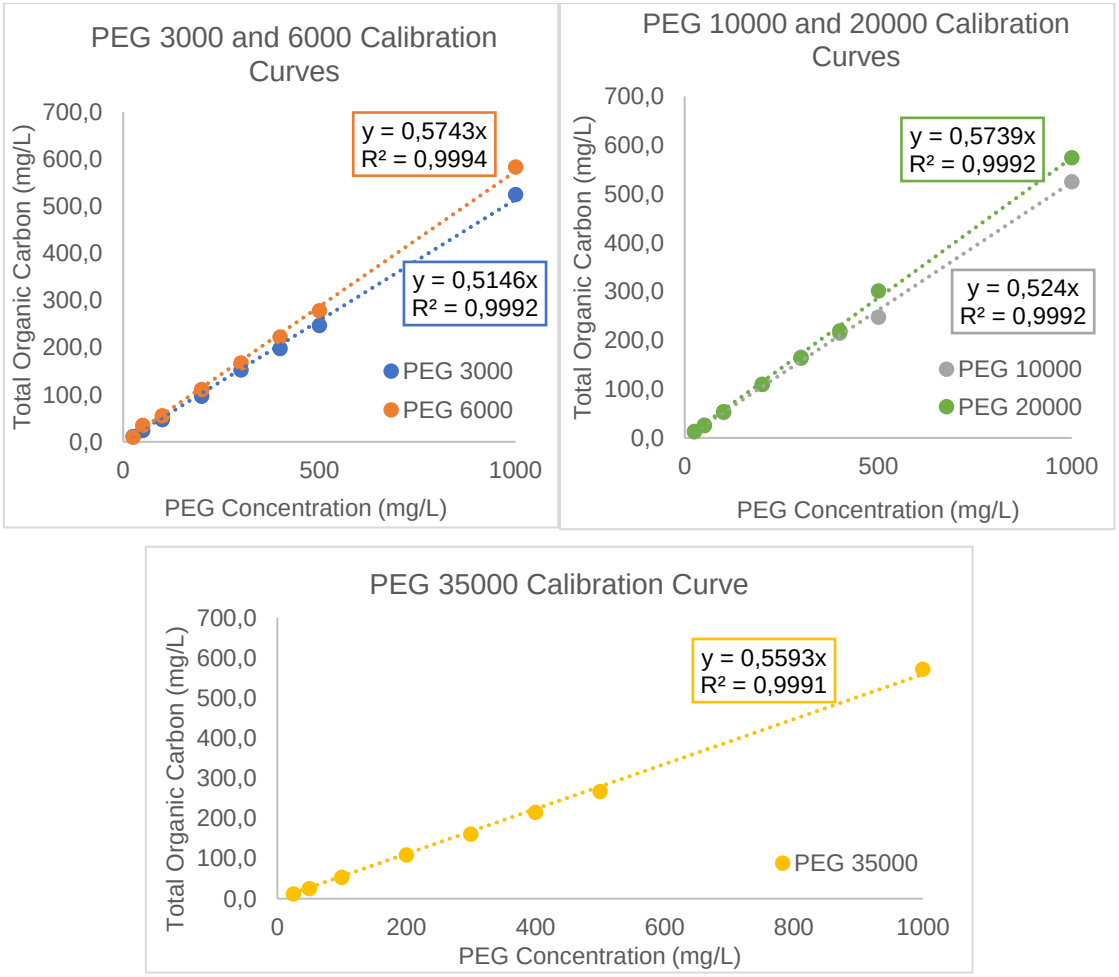

Figure A 9: Calibration curves for PEG's.

Table A 10: Calibration curve values for Dextran T40 and T70 with Total Organic Carbon.

Concentration (mg/L)	Dextran T40	Concentration (mg/L)	Dextran T70
1000	408,8	1017	490,0
500	189,9	750	350,6
400	150,9	500	230,3
300	117,5	250	121,4
200	76,2	100	46,6

100	38,0	50	23,5
50	19,5	25	11,6
25	8,7	-	-

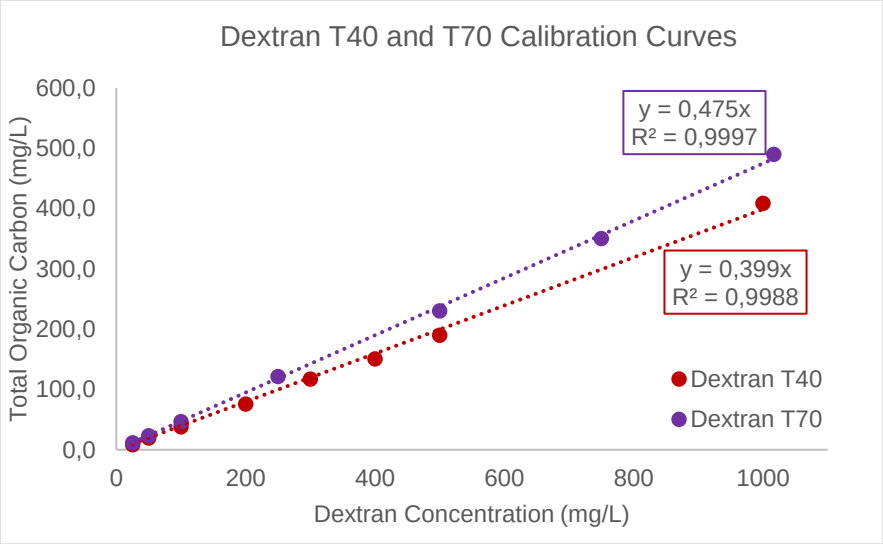

Figure A 10: Calibration Lines for Dextran's.

7.3.4. BSA Calibration Line

The Blue Coomassie reagent, also called Bradford reagent, is used for the detection of proteins which forms complexes with them, and it's prepared as described as [30]. The detection is made by UV spectrophotometry. Concentrations higher than 100 mg/L have a linear behavior in 595 nm with a proportion of 1: 50 of sample and Bradford reagent. In this case, in a 3 mL cell, the volumes of sample (deionized water for blank) and Bradford reagent are 0,059 and 2,941 mL, respectively.

For lower concentrations (< 100 mg/L), linearization is made with different peaks and proportions [31]. The ratio of two peaks, 590 and 450 nm, and a proportion of 1:4 sample/Bradford are described to give a calibration line. The blank cell was only deionized water therefore zero concentration of BSA is not at the origin.

For this measurement, duplicated samples are read in UV spectrophotometer and the average value is the result.

Table A 11: Calibration Values for high concentrations of BSA.

BSA Calibration Line - High Concentrations			
[BSA] (mg/L)	**Abs595**		**Average Abs595**
	1	**2**	
100	0,124	0,125	0,125
250	0,254	0,238	0,246
500	0,436	0,442	0,439

750	0,561	0,576	0,569
1000	0,722	0,734	0,728
1250	0,805	0,828	0,816
1510	0,932	0,921	0,926

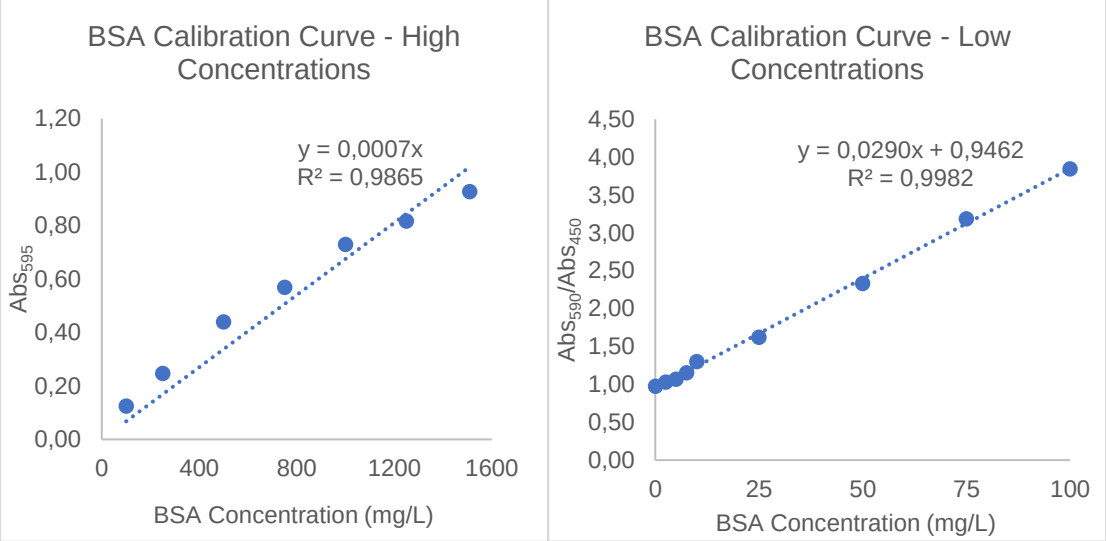

Figure A 11: Calibrations curves for low and high BSA concentrations.

Table A 12: Calibration values for low concentrations of BSA.

BSA Calibration Line – Low Concentrations							
[BSA] (mg/L)	Abs450		Avg Abs450	Abs590		Avg Abs590	Abs590/Abs450
	1	2		1	2		
0	0,564	0,590	0,577	0,541	0,581	0,561	0,972
2,5	0,574	0,563	0,569	0,587	0,583	0,585	1,029
5	0,568	0,575	0,572	0,606	0,615	0,611	1,068
7,5	0,582	0,578	0,580	0,664	0,670	0,667	1,150
10	0,531	0,526	0,529	0,686	0,686	0,686	1,298
25	0,5	0,492	0,496	0,795	0,811	0,803	1,619
50	0,414	0,417	0,416	0,965	0,973	0,969	2,332
75	0,365	0,356	0,361	1,143	1,154	1,149	3,186
100	0,332	0,328	0,330	1,265	1,272	1,269	3,844

7.3.5. Methyl Red Calibration

Methyl Red calibration curve was made with UV-visible spectrophotometer at 410 nm [67]. The calibration was performed with ethanol since MR is not soluble in water. The concentration range was prepared by dilution from mother solution with 24 mg/L. The absorbance at 410 nm for ethanol and water is the same, thus it doesn't interfere when reading samples with water. The values are described in Table A 13 and calibration curve is showed in Figure A 12.

Table A 13: Absorbance calibration values for methyl red at 410 nm.

Abs_{410} (1)	Abs_{410} (2)	Abs_{410} Average	C_{real} (mg/L)
0,0000	0,0000	0,0000	0,00
0,0124	0,0135	0,0129	0,24
0,024	0,0229	0,0235	0,48
0,0454	0,0431	0,0448	0,96
0,0809	0,0797	0,0804	1,92
0,1601	0,1598	0,1603	4,80
0,3482	0,3513	0,3486	9,60
0,5211	0,5189	0,5201	14,40
0,6756	0,6773	0,6756	19,20
0,8509	0,8528	0,8211	24,00

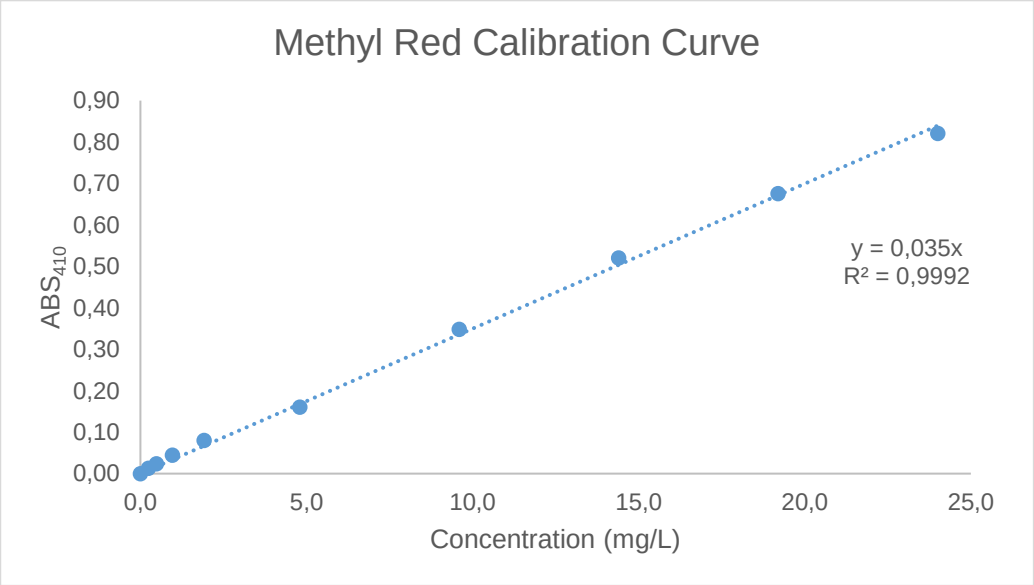

Figure A 12: Calibration curve for methyl red in UV spectrophotometer.

7.4. Permeation Assays

7.4.1. Uric Acid Assay

Uric acid experiments with initial feed solution of 60 mg/L for pathological concentrations results are described here. When the first feed time is not zero it means that, initially, the dilution problem is big enough, thus the value used to calculate the rejection factor was from the sample at the time after.

Table A 14: Pathological concentrations of uric acid assay (60 mg/L) for CA90-SiO_2-$(CH_2)_3NH_2$-IBF(1) and CA95-IBF-SiO_2-$(CH_2)_3NH_2$(2).2 membranes.

URIC ACID for CA90-SiO_2-$(CH_2)_3NH_2$-IBF(1)				
Time (min)	ABS_{293}	ABS_{293} corr.	C (mg/L)	$F_{rejection}$
Feed				
15	0,4758	0,4754	30,57	
90	0,7006	0,7002	45,03	-0,412

Permeate				
0	0,1028	0,1024	6,59	-41,2%
90	0,6717	0,6713	43,17	
URIC ACID for CA95-IBF-SiO_2-$(CH_2)_3NH_2$(2).2				
Time (min)	**ABS_{293}**	**ABS_{293} corr.**	**C (mg/L)**	**$F_{rejection}$**
Feed				
15	0,2454	0,2449	39,37	
90	0,2922	0,2917	46,90	0,044
Permeate				
0	0,0005	0	0,00	4,4%
90	0,2347	0,2342	37,65	

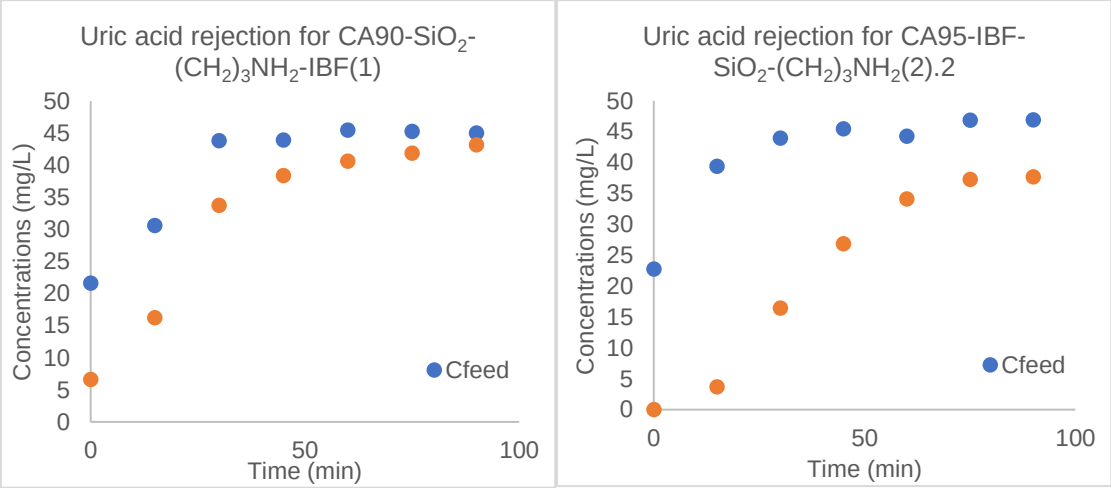

Figure A 13: Graphs corresponded to pathological concentrations of uric acid assay for CA90-SiO_2-$(CH_2)_3NH_2$-IBF(1) (left) and CA95-IBF-SiO_2-$(CH_2)_3NH_2$(2).2 (right) membranes.

7.4.2. Water Experiments

Pure deionized water experiments were done to realize if compound leaching interfered in absorbances of albumin detection for CA95-IBF-SiO_2-$(CH_2)_3NH_2$(2).2 membrane.

Table A 15: Pure water experiments for BSA detection UV wavelengths.

Pump Position	Permeate			Feed		
	*ABS_{595}	**ABS_{450}	**ABS_{590}	*ABS_{595}	**ABS_{450}	**ABS_{590}
1	0,000	0,001	0,000	0,010	0,011	0,010
2	0,001	0,001	0,001	0,009	0,010	0,009
3	0,004	0,000	0,004	0,009	0,010	0,009
4	0,000	0,000	0,000	0,009	0,010	0,009
5	0,001	0,005	0,000	0,009	0,010	0,009
6	0,003	0,003	0,003	0,009	0,011	0,009
7	0,005	0,007	0,008	0,009	0,011	0,009
8	0,007	0,008	0,005	0,009	0,011	0,009
9	0,005	0,004	0,002	0,010	0,011	0,010
10	0,000	0,000	-0,001	0,009	0,010	0,007

*absorbance for detection of high concentrations of BSA; **absorbances for detection of low concentrations of BSA.